NANYANG
TECHNOLOGICAL
UNIVERSITY

SKIN-INSPIRED FLEXIBLE TACTILE SENSING DEVICES

ZHU BOWEN

School of Materials Science and Engineering

2015

SKIN-INSPIRED FLEXIBLE TACTILE SENSING DEVICES

ZHU BOWEN

School of Materials Science and Engineering

A thesis submitted to the Nanyang Technological University

in partial fulfillment of the requirement for the degree of Doctor of Philosophy

2015

Acknowledgement

First of all, I would like to express my deepest appreciation to my supervisor, Prof. Chen Xiaodong, for his continuous guidance, inspiration and encouragement throughout my PhD study. I am inspired by his insight into science, motivation to address research challenges, creative and critical thinking, as well as energetic and efficient working style. Without his persistent support this dissertation would have not been possible.

In addition, I would like to thank Prof. Huo Fengwei, Prof. Christian Kloc and Prof. Lee Pooi See for their invaluable guidance, suggestions and cooperation to my research work.

Also, I would like to give sincere appreciation to my colleagues Dr. Cai Yurong, Dr. Du Jianjun, Dr. Dong Haibo, Dr. Hu Benhui, Dr. Jiang Lin, Dr. Jiang Yueyue, Dr. Lang Xianjun, Dr Li Yongqiang, Dr. Li Yuangang, Dr. Liu Yaqing, Dr. Meng Fanben, Dr. Niu Zhiqiang, Dr. Peng Tai, Dr. Qi Dianpeng, Dr. Shao Qi, Dr. Sun Yinghui, Dr. Tang Yuxin, Dr. Wang Hong, Dr. Wang Hua, Dr. Wang Wei, Dr. Wang Xiaotian, Dr. Wang Yi, Dr. Wu Yunlong, Dr. Yang Hui, Dr. Yin Shengyan, Dr. Yu Jiancan, Dr. Zhang Chenguang, Dr. Zhang Yanyan, Dr. Zheng Kaihong, Dr. Zheng Liyan, Mr. Cai Pingqiang, Mr. Deng Jiyang, Mr. Liu Zhiyuan, Mr. Xu Cai, Ms. Bu Jing, Ms. Chen Geng, Ms. Leow Wan Ru, Ms. Li Zhuyun, Ms. Liu Yuanjun, Ms. Wang Yu, Ms. Wei Chen, Ms. Zhang Xiaoqian, and Ms. Guo Xintong, for their inspiration, share of experience and warm supports.

I am also grateful to Dr. Li Shaozhou and Dr. Wu Jin for their kind instruction and cooperation in conducting experiments.

Finally, I thank my beloved family members and Ms. Yang Dan, and all my friends for their unfailing understanding and accompany through my study.

Table of Contents

List of Figures

List of Tables

Abstract

The human body is covered in skin which contains a variety of sensory receptors accounting for one's ability to sense objects physical properties. Receptors in skin respond to external stimuli and thus allow humans to perceive the sensations so as to recognize the surrounding environment and conduct daily activities. The exquisite sensations of the natural skin have inspired the rise of highly sensitive tactile sensing devices that could emulate the tactile sensation of natural skin. Herein, this thesis is engaged in developing materials and engineering ways to design and integrate high performance tactile sensing devices to mimic and emulate the sense of touch in human.

To devise high performance tactile sensors capable of emulating the exquisite tactile sensation of natural skin, anisotropic microstructures are introduced to pressure-response layers, which could serve as a universal approach to improve the sensitivity of tactile sensors. Two kinds of microstructured pressure-sensitive layers, namely graphene/PDMS and AgNWs/PDMS, are developed and applied in resistive tactile sensors. Both of the pressure-sensitive layers can be obtained by facile methods with high uniformity of patterns and large-scale fabrication capability. By virtue of anisotropic effect, the microstructured tactile sensors demonstrate high sensitivity in low pressure range, fast response time, and great stability, which are important parameters for mimicking tactile sensing in natural skin. The sensitivity of sensors can be tuned by modifying the parameters of microstructure patterns, shedding light on the application of the sensors in diverse sensing environments that require different tactile sensitivities. Also, the microstructured sensor illustrates remarkable capability of encoding tactile sensations and measuring pulse wave, demonstrating great potential for applications in information transmission and health monitoring.

With the achievement of highly sensitive tactile sensors, a further attempt is to mimic the sensory memory of human. Electrically configurable memory devices are integrated with resistive tactile sensors to address the retention of sensations after stimuli cease. External pressure can be detected and transduced to the different resistance states of the memory devices. Applied pressure distribution can be detected and retained in the memory device arrays for a long time by virtue of the nonvolatile memory performance. The integrated device can be programmed by the touch of a finger, showing great potential in sensing and retaining the tactile sensations for mimicking the human sensory memory.

To develop interactive tactile sensing devices for next-generation sensory memory devices, electrochromic devices are integrated with resistive tactile sensors to produce human-readable outputs. The low operation voltage for color switching of the electrochromic material renders it possible to transduce applied pressure into visible color change. Electrodeposited WO_3 films are selected as the electrochromic material to integrate with pressure sensors because of their great color memory effect. The integrated device can retain the tactile sensation information without power supply after stimuli ceased.

1. Introduction

This chapter introduces the background of human skin, followed by the varieties and functions of sensory receptors in skin. The role of skin in tactile sensation and perception is illustrated. Tactile sensing performance for sensing devices to emulate the tactile sensation of naturals is elucidated. Finally, the research motivation and objectives, as well as the organization of the thesis are presented.

1.1 Background—Tactile Sensing of Human

The human body is covered in skin—the largest organ in the human body—which accounts for ones ability to sense and cognize physical quantities in the surrounding environment. Skin comprises a variety of sensory receptors and provides significant sensation information, such as force, pain, temperature, shape and texture, when it contacts with objects, allowing the formation of human "sense of touch".[1-6] Sensory receptors of human can be attributed into four types, namely mechanoreceptors, proprioceptors, nociceptors and thermoreceptors, responsible for the sense of force/pressure, motion/position, pain/damage and hot/cold, respectively.[5] Mechanorecptors, comprises of four types with specific functions, are innervated by neural afferents and distributed in the skin with variable density, this result in the difference in sensitivity of different body parts.[4,7] For example, in adult humans, the number of mechanoreceptors per square centimeter area in the fingertips (~241) is four times higher than that in the palm (~58), rendering fingertips highly sensitive while palm insensitive. Due to the different responsive extent and adaptation rates, mechanoreceptors can be split into fast-adapting (FA) receptors and slow-adapting (SA) receptors. FA receptors, insensitive to static force, respond with action potentials only at the onset and offset of a stimulus, while SA receptors remain active as long as they interact with a stimulus. According to varied sensory response to stimuli, both FA and SA receptors can be further divided into two types, FA I (Meissner's corpuscle), FA II (Pacinian corpuscle), SA I (Merkel cells), and SA II (Ruffini corpuscle) (**Figure 1.1**).[1,5]

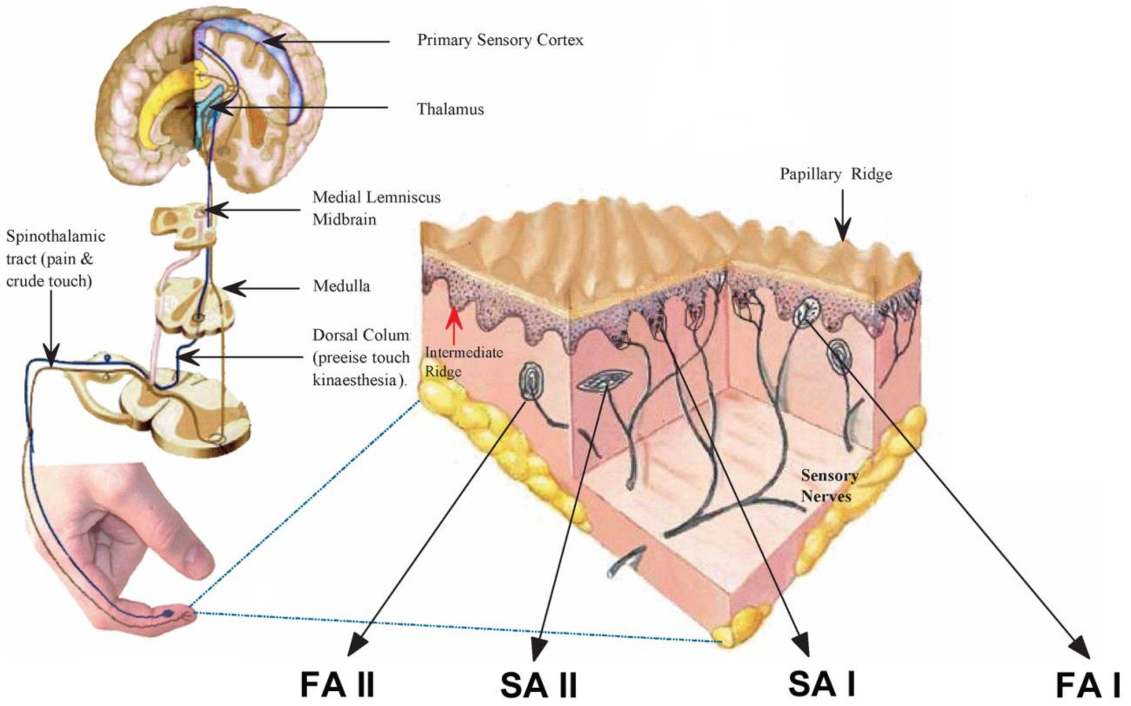

Figure 1.1. Schematic illustration of the sensory receptors embedded in skin for tactile sensing and perception. (Reprinted with permission from reference [1].)

FA I receptors are sensitive to dynamic deformation of skin with low frequency (5-50 Hz) and are responsible for slight touch of skin. FA II receptors are sensitive to transient mechanical stimuli with high frequency vibrations (40-400 Hz). SA I receptors accounts for the perception of shape and texture of an object that contacts with the skin. SA II receptors are sensitive to tangential force and respond to skin stretch. A summary of the four types of mechanoreceptors is illustrated in **Table 1.1**.

Table 1.1. Sensory responses of mechanoreceptors.

Type	**FA I**	**FA II**	**SA I**	**SA II**
Receptor	Meissner's corpuscle	Pacinian corpuscle	Merkel cells	Ruffini corpuscle
Location	Dermal papillae	Dermis and deeper tissues	Tip of epidermal sweat ridges	Dermis
Effective stimulus	Skin motion	Vibration	Edges, points, corners, curvature	Skin stretch
Static sensing	None	None	Yes	Yes
Frequency range	1–300 Hz	5–1000 Hz	0–100 Hz	0–? Hz
Peak sensitivity	50 Hz	200 Hz	5 Hz	0.5 Hz
Innervation density (finger pad)	150/cm^2	20/cm^2	100/cm^2	10/cm^2
Spatial acuity	3 mm	10 mm	0.5 mm	7 mm

1.2 Motivation

Skin deforms at the contact place and conforms to an object's surface when it contacts with an object, inducing the deformation of the mechanoreceptors, which encode and transmit the spatiotemporal tactile information, in the form of spikes of action potentials, to brain through tactile afferents for perception and cognition (Figure 1.2). The perception of the contact information allows us to keep the impression of the mechanical stimuli, and then to conduct corresponding activities.

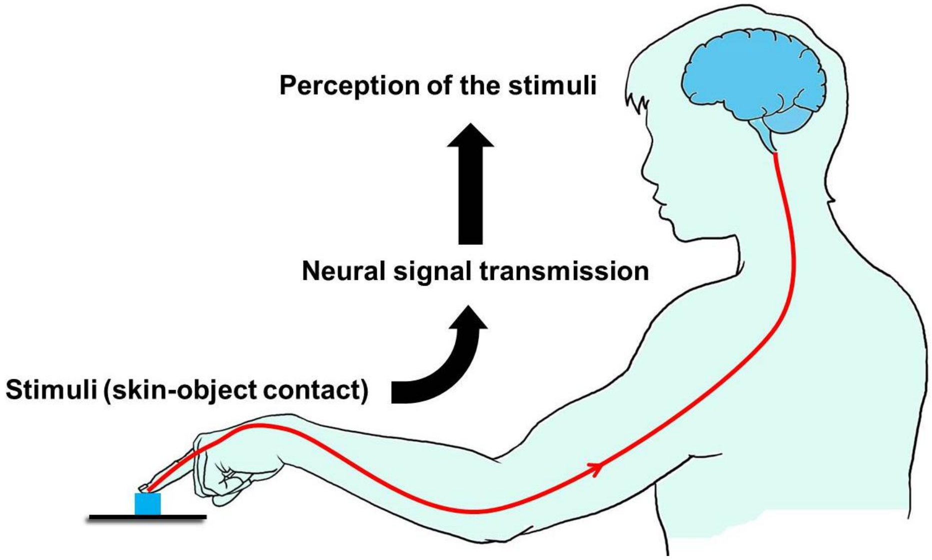

Figure 1.2. Schematic illustration of tactile signal transmission. Skin contacts with an object and transmits the sensation information to somatosensory area of brain through afferent nerves.

Biological systems have inspired the advancements of science and engineering for centuries.[8-10] Still, human sense of touch inspires the development of electronic tactile sensing devices and systems for applications in humanoid robotics, electronic skin, prosthetics, as well as human-machine interfaces.[11-14] The last decade has witnessed tremendous advances in the design and integration of skin-like tactile sensing devices for the mimicry of human skin. In order to emulate the exquisite sensation of natural skin, tactile sensing devices should be able to address the following criteria:

1) High sensitivity in low pressure regime. Skin has high tactile sensitivity with a broad response range. It can detect pressure stimuli with both high value (>10 kPa) and low value (<100 Pa). Traditional tactile sensors suffer low sensitivity in responding to tiny pressure loadings.
2) Fast response time. Skin can response to a temporal stimulus of about 1.4 ms. The response time of tactile sensors should be fast enough in order to allow signal

processing and task control in future applications such as smart screens and humanoid robotics.

3) Detection of both dynamic and static mechanical stimuli. Skin comprises of FA and SA mechanoreceptors that are responsible for dynamic and static contact events, respectively. Tactile sensing devices should be able to transduce both dynamic and static stimuli to signals.
4) Retention of the sensory information. Skin perceives touch sensations and transmits tactile information to brain for analyzing and processing, allowing humans possess the impressions of the contact and external stimuli. Tactile sensing devices should not only transduce mechanical stimuli into signals, but retain the tactile information after the external stimuli ceased.
5) Interactive signal output. Interactive tactile sensing devices visible and human-readable output could reduce the complexity of fabrication and signal-processing processes. More significantly, it is possible to re-establish the tactile sensation to people who lost the sense of touch by transducing the tactile information to optical signals that can be perceived by the sensory modality of vision.

1.3 Objectives and Scope

The ultimate goal of this thesis is to design and develop high performance tactile sensors for the mimicry of human sense of touch. Tactile sensors are defined as devices that can detect and measure a given property of an object through contact. In this thesis, tactile sensing was emphasized on the detection of external pressure. To emulate the exquisite tactile sensation and perception of natural skin, the main objectives of this thesis are summarized in the following:

1) To design and develop flexible tactile sensors with high pressure sensing performance, such as high sensitivity, fast response time, low detection limit, stable output, ease of fabrication, as well as low cost. Natural skin demonstrates excellent tactile sensation. To emulate the function of skin, high performance flexible tactile sensors should be firstly addressed. Because the sensitive layer of a tactile sensor responds to external stimuli with geometry deformation, rationale selection of sensitive material and configuration is of paramount importance to achieve high sensitivity. This thesis is engaged in developing and applying microstructured pressure sensitive layers with pyramidal pattern arrays to deliver high sensitivity to tactile sensors.

2) To integrate highly sensitive pressure sensors with memory devices for the mimicry of human sensory memory. Natural skin accounts for not only tactile sensation, but for transmitting sensation information to brain to form sensory memory. To mimic this, sensing devices should be able to retain the sensing information after external stimuli cease. It is possible to achieve this by programming memory devices with external pressure. The study in this thesis is aim to integrate electrically reconfigurable resistive witching memory devices with highly sensitive pressure sensors to retain the pressure distribution after external stimuli vanish.

3) To develop interactive tactile sensing devices with human-readable outputs. Interactive tactile sensing devices that respond external stimuli with visible outputs are of significance for next-generation smart electronics. This can be addressed by integrating light-emitting or chromic units with pressure sensor. This thesis is aim to develop interactive tactile sensors that provide human-readable color changes in response to external pressure.

1.4 Dissertation Overview

The thesis can be attributed to the following seven sections:

Chapter 1 begins with an introduction to the tactile sensation and perception of human. The role of skin in tactile sensation and perception provides inspiration and establishes a benchmark for developing tactile sensing devices. The objective and scope of this thesis are elucidated by aiming at emulating the tactile sensing of natural skin. Several important parameters of high performance tactile sensors are discussed.

Chapter 2 introduces the state-of-the-art tactile sensing techniques and mechanism. Sensors are attributed to five main categories according to different transducing principle. Sensor prototypes and sensing performance of different types are discussed. Advancements of the tactile sensing sensors in the last decade are summarized. Limits of current tactile sensors and perspectives are presented.

Chapter 3 illustrates the experimental methodology. The role of fingerprints in human tactile sensing is introduced, followed by the rationale of the applying microstructure patterns in pressure sensitive layers. Fabrication processes of microstructures patterned silicon masters are illustrated. Methods to prepare conductive pressure sensitive layers based on patterned silicon masters are presented. Experimental setup for performing electrical measurement of sensors is illustrated.

Chapter 4 provides a highly sensitive pressure sensor based on graphene films with pyramidal microstructure arrays. Similar to the role of fingerprints to skin, the microstructure pattern arrays endow the sensor with high performance in tactile sensing. The pressure response of the sensor is characterized in detail, and potentials for applications in information transmission and health monitoring are demonstrated.

Chapter 5 demonstrates the rational integration of resistive switching memory devices with resistive pressure sensors for the mimicry of human sensory memory. Rationale of the integrating these two kinds of devices are discussed. Performance of the integrated device in sensing and retaining applied pressure is elucidated. Device arrays are fabricated to detect and retain pressure distribution.

Chapter 6 depicts an interactive tactile sensing device with visible outputs and memory. A summary of current interactive pressure sensors with human-readable outputs is firstly provided. Subsequently, the rationale of design and integration of electrochromic materials with tactile sensors is elaborated. Performance of as-prepared electrochromic materials and integrated devices is demonstrated at last.

Chapter 7 summarizes the conclusions of this thesis and provides perspectives and recommendation to future attempts for the mimicry of the five senses of human.

2. Literature Review

In this chapter, the state-of-the-art tactile sensing techniques and sensor prototypes are reviewed and discussed. Flexible tactile sensors can be attributed to five main categories based on different sensing mechanism, namely resistive sensors, capacitive sensors, optical sensors, piezoelectric and triboelectric sensors. The sensing mechanism and typical examples are introduced. A summary of the advancements and perspective are presented at last.

2.1 Tactile Sensing Techniques

Various designs and configurations have been adopted in flexible tactile sensing devices to emulate the tactile sensation of natural skin. A tactile sensor device can be attributed to a transducer that transduces mechanical stimuli into electrical signals. Based on sensing principles, we can divide the current flexible pressure devices into the following five species: resistive sensors, capacitive sensors, optical sensors, piezoelectric sensors and triboelectric sensors.[1,5,6,8,15-17] The operations of these devices originate from the exploitation of transduction effects and materials capable of mechano-electric and mechano-optical conversion. In the past decade, we have witnessed great development in these kinds of sensors for tactile sensing, and we will discuss the state-of-the-art sensor systems specifically in the following parts.

2.1.1 Resistive Tactile Sensors

Resistive tactile sensors change their resistance in a predictable way when pressure is applied. They translate the pressure change into resistance change which can be easily measured. Typically, the resistance value of a resistive sensor reduces with the addition of pressure loadings, and *vice versa*. According to different pressure sensitive materials and sensor configurations, resistive tactile sensors can be attributed to two main categories: sensors responding to pressure by 1) changes of conductive particle density, and by 2) changes of contact resistance of conductive micro-/nano-structures.[18] A schematic of the two kinds of sensing mechanism is illustrated in **Figure 2.1**.

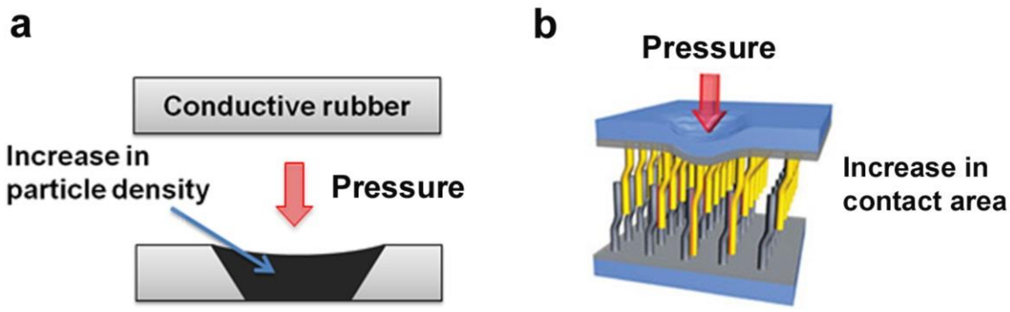

Figure 2.1. Typical sensing mechanisms of resistive tactile sensors. a) Sensors with conductive rubber as sensitive layer. b) Pressure response of micro-/nano-structured resistive sensors result from contact area change. (Figure 2.1b, reprinted with permission from reference [18].)

Conductive rubber, comprises of a conducting phase of particles and an insulating elastomeric polymer matrix, is widely used in flexible electronics as pressure sensing elements because of their stability, good mechanical strength, and commercially availability. When pressure is applied to the sensor, the conductive rubber is compressed and the paths among the conductive particles shorten, resulting in a reduction of resistance. Carbon black is one of the best candidates to serve as the conductive fillers. However, it suffers poor conductivity, low sensitivity and hysteresis. To conquer these disadvantages and to achieve measuring pressure distribution, several research groups have developed active sensor matrix by integration of conductive rubbers with control units like field-effect transistors (FETs).[19-21] In this way, the gate and drain bias of FETs can be used for addressing the word lines and bit lines of the matrix.

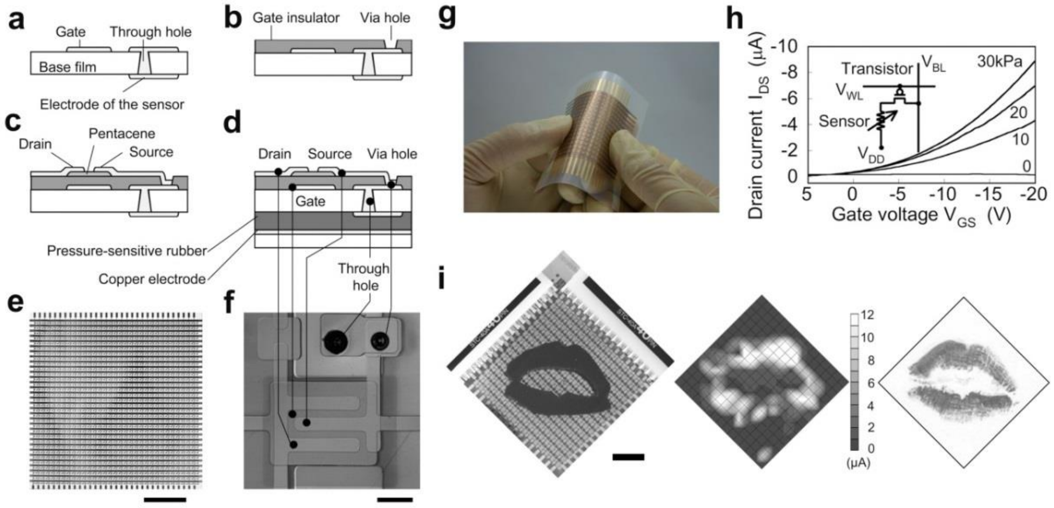

Figure 2.2. A flexible electronic skin device fabricated by integrating conductive rubber with OFETs matrix. a-d) Schematic of the fabrication process. e) A picture of sensor matrix with 32 × 32 pixels, with a resolution of 2.54 mm. Scale bar: 2 cm. f) An optical image of an individual sensor pixel. Scale bar: 0.5 mm. g) A photo of the sensor matrix. h) Transfer curves of the OFET under different pressures at V_{DS} = -20 V. i) Demonstration of the sensor matrix in mapping pressure distribution applied through a rubber lip. (Reprinted with permission from reference [19].)

In 2004, Someya's group in Tokyo University integrated conductive rubber into organic transistors and fabricated a flexible electronic skin device (Figure 2.2).[19] The conductive rubber layer, acting as pressure sensitive layer, is Polydimethylsiloxane (PDMS) films embedded with graphite particles. The conductive rubber is connected with the source of organic FETs via holes. In this respect, no patterning of the conductive rubber is required, allowing large scale fabrication of sensor matrix. When pressure is applied to the device, the resistance of the graphite/PDMS layer decreases, leading to an increased drain current I_{DS} (Figure 2.2h). All parts of the device except for the electrodes are made of organic materials, which make it feasible for the application as artificial skin. The pitch of the sensor matrix is 2.54 mm, which endows it enough spatial resolution, though not high, to image a human lips mark. However, the sensor needs high operation voltage (-20 V), which limits its realistic application.

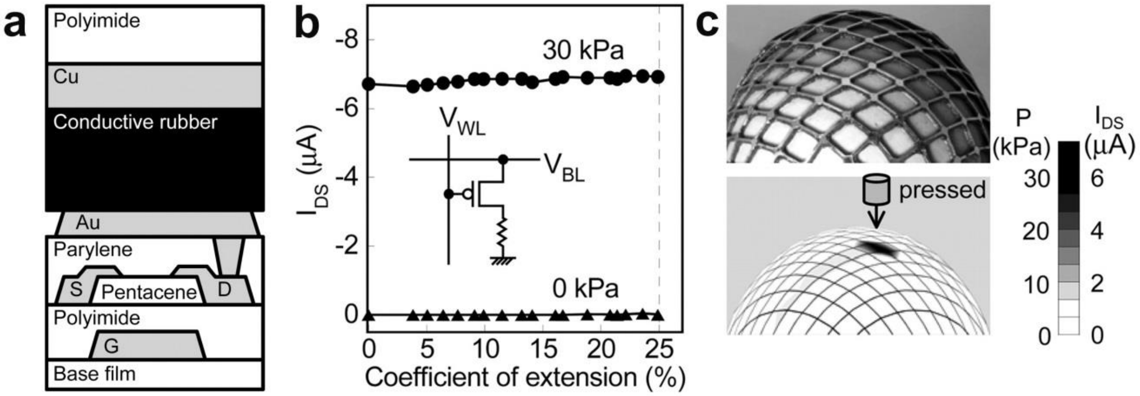

Figure 2.3. A conformable and stretchable pressure sensor matrix. a) The structure of the pressure sensor. b) The sensor has a stable increase in I_{DS} at applied pressure under stretching up to 25%. c) Pressure distribution applied on an egg can be obtained. (Reprinted with permission from reference [20].)

In a following work, by applying a net-shaped structure to the OFET matrix, Someya's group reported conformable, flexible and large-area skin-like sensing matrix based on organic semiconductors (Figure 2.3).[20] By the implementation of both pressure and thermal sensors, the sensor network can detect and map pressure and heat distributions simultaneously. The pressure sensor has the same configuration with their previous work. Besides, because of the special net-shaped structure, the sensor array is conformable and can be extended by 25%. The multi-functionality of the sensor provides great improvement in mimicking natural human skin. However, because the use of conductive rubber, the sensor needs relatively high voltage (-40V) to operate, and can only detect relatively high pressure (30 kPa).

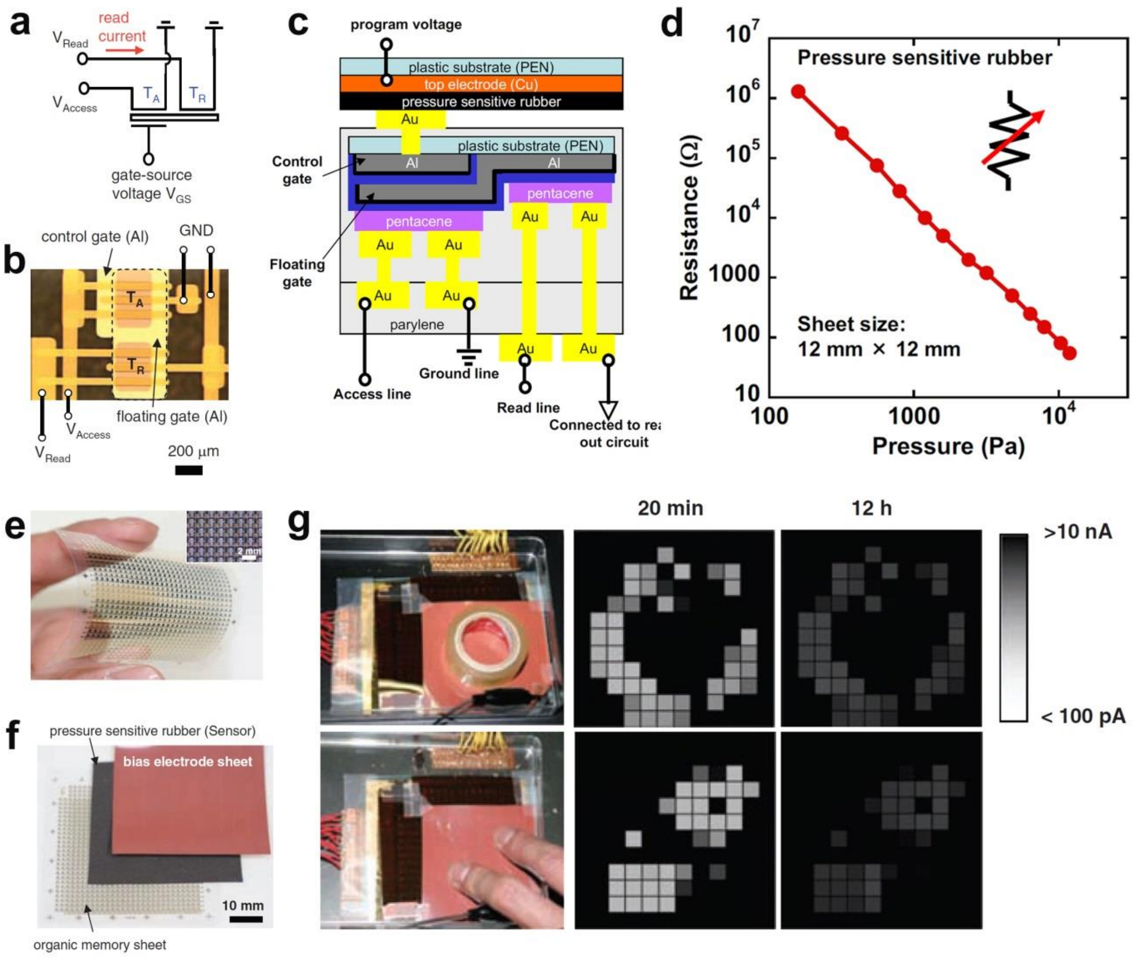

Figure 2.4. Flexible pressure sensor matrixes with floating-gate memory. a-b) Circuit diagram and optical image of the floating-gate memory cell, connecting with an access transistor and a read-out transistor. c) Schematic of the configuration of the integrated device. d) The pressure response of the conductive rubber. e) A photo of the floating-gate transistor matrix with 26 × 26 cells. f) Photo of the three parts of the integrated pressure sensing matrix. g) The sensor matrix shows non-volatile behaviors towards applied pressure distribution. (Reprinted with permission from reference [22].)

Later in 2009, the same group integrated a conductive rubber sheet to flexible organic floating-gate transistors, and the sensor matrix can not only detect the spatial distribution of applied pressure through OFET arrays, but also store the analog sensor input by the floating-gate memory devices over a long time (Figure 2.4).[22] The floating-gate transistor uses thin layer of dielectric materials to isolate the charge states in a floating gate which can be tuned by applied pressure, and the operation voltage bias is reduced to < 6 V.

The combination of conductive rubber and OFET presents a promising strategy for sensing devices to achieve spatial resolution. Nevertheless, organic semiconductors used in OFETs have relatively low carrier mobility and require high voltages to operate. Thus, OFET based pressure sensing matrix can only produce effective response to pressure in high ranges. In contrast, inorganic semiconductors provide a merit due to their high carrier mobility. In addition, by miniaturizing to micro-/nano-meter dimensions, superior mechanical flexibility can be achieved.

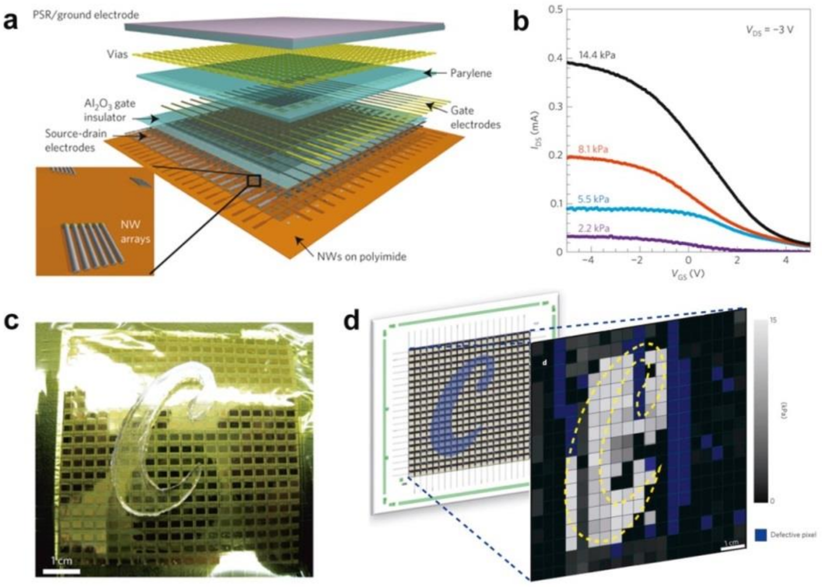

Figure 2.5. Inorganic nanowires FETs integrated with conductive rubber for pressure sensing. a) Schematic of the device with conductive rubber as pressure sensing unit and nanowire transistors as control unit. b) I_{DS} of the transistors increase with the addition of pressure loadings at a V_{DS} of -3 V. c) A photo of the sensing arrays for mapping pressure distributions applied through a letter "C". d) The transducing of pressure distributions into electrical profile by the sensor arrays. (Reprinted with permission from reference [23].)

Ali Javey's group integrated transistor based on Ge/Si core/shell semiconductor nanowires (NW) with conductive rubber to achieve low operation voltage and high spatial resolution (Figure 2.5).[23] The conductive rubber was connected with the source electrode of the FETs. The I_{DS} increases when conductive rubber is compressed and the conductance changes could be used to measure pressure value. Because of the higher carrier mobility of the NW array FETs compared to that of their organic counterparts, the sensor array can be operated at low voltage. Besides, the mechanical robustness of NW array allows the sensor to bend at small radii of curvature for over 2, 000 cycles without performance degradation. Still, the pressure response also arises from resistance change of conductive rubber. By virtue of the better performance of NW FET, the sensor exhibits high sensitivity to applied pressure in the range of 0-15 kPa at a low working voltage of -3 V. In addition to inorganic nanowire FETs, Ali Javey's group also fabricated flexible active matrix sensor array based on single-walled carbon nanotube (SWNT) thin film transistors. The use of SWNTs furbishes the transistor with superb electrical properties compared to organic materials. More noteworthy is the fact that the laser-cut honeycomb mesh structure enables the sensor capable of being unidirectionally stretched and intimately covered on curved surfaces.

Though conductive rubber based tactile sensing devices demonstrated great capability in detecting pressure distribution with large scale fabrication, the low conductivity of the film and hysteresis effect make it difficult for sensing pressure in low regime. To improve the sensitivity of pressure sensing devices, electrode patterns and three-dimensional pressure sensitive micro-/nano-structures have been widely adopted.

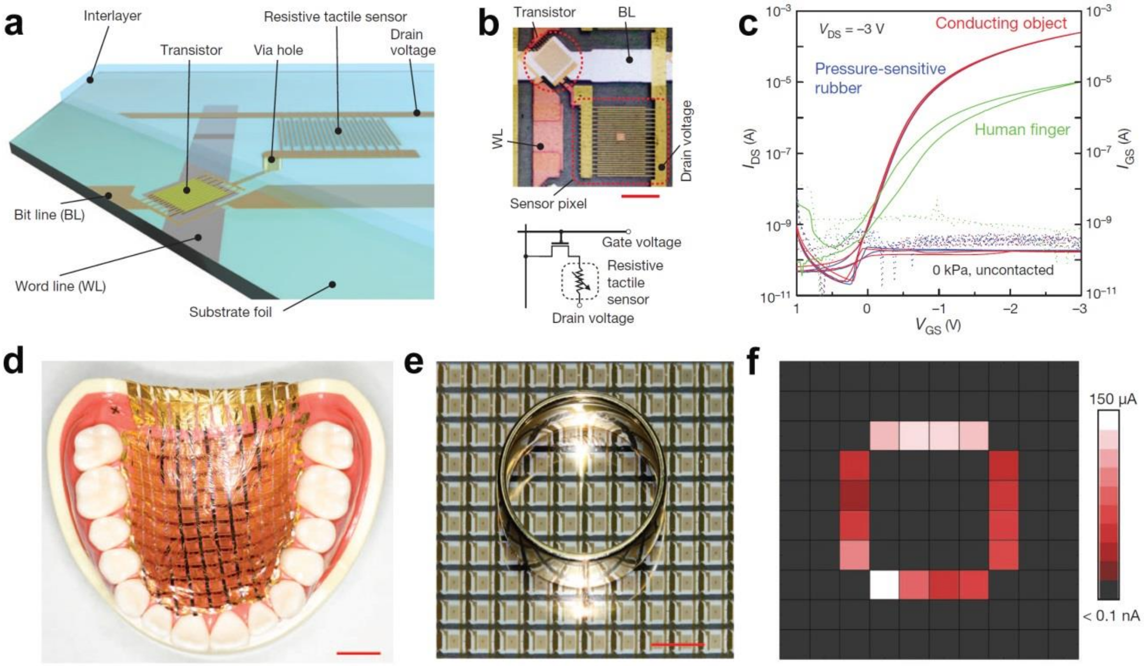

Figure 2.6. An ultrathin and lightweight pressure sensing array. a) Schematic configuration of tactile sensor composed by a transistor and a tactile sensor. b) Photo and circuit diagram of a tactile sensing pixel. c) The I_{DS} of a transistor has a discernable increase when the device contacts with a finger. d) Photo of a sensing array put on a jaw model. Scale bar: 1 cm. e) Photo of a sensing array with a metal ring on top. f) Current mapping of the sensing array responding to the pressure distribution of the ring in (e). (Reprinted with permission from reference [24].)

By patterning contact electrodes with interdigitated structures, pressure sensors can response to a touch of a finger at a low working voltage (Figure 2.6).[24] Due to the ultrathin and lightweight, the sensors can be put onto a human upper jaw model with conformal contact, demonstrating potential for health monitoring. The sensor arrays also exhibit high resolution to detect pressure distribution. However, because no deformable material is applied, the sensors can only respond to pressure applied through conductive materials. Also, it is difficult to distinguish pressure stimuli from highly conductive objects.

Nevertheless, interdigitated electrode could be applied to obtain high pressure sensitivity to both conductive and non-conductive objects by laminating deformable pressure sensitive layer onto it. Tissue paper with gold nanowires was placed on interdigitated electrodes by W. Cheng's group to serve as pressure sensitive layer.[25] Applied pressure will lead to improved contact among AuNWs and the bottom electrode, reducing the resistance of the sensor. By virtue of the excellent conductivity of AuNWs grafted tissue paper, the tactile sensor exhibits a high sensitivity in low pressure range of <5 kPa, a fast response time of <17 ms, as well as a detection limit of 13 Pa.

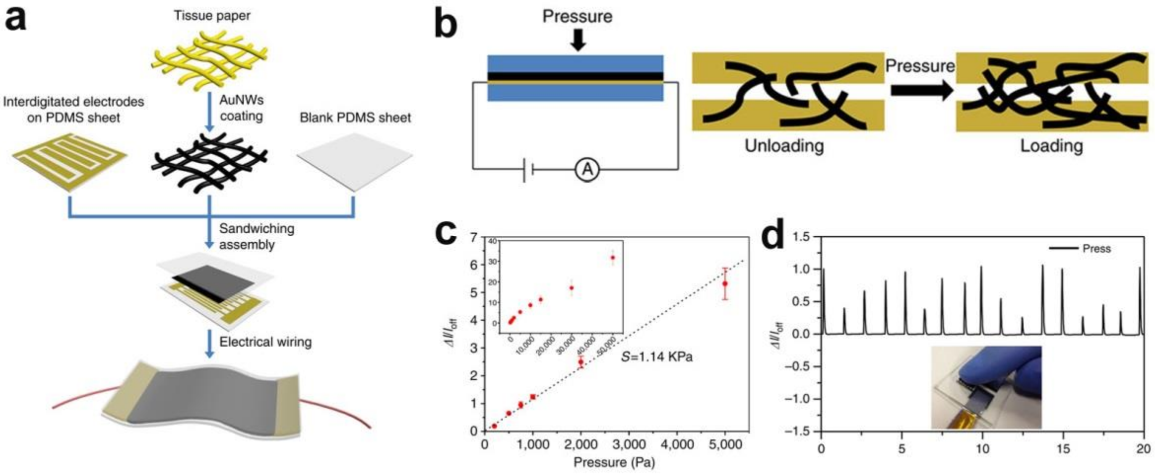

Figure 2.7. AuNWs on paper matrix as sensitive layers for tactile sensors. a) Schematic illustration of the fabrication process. b) Pressure sensing mechanism. c) Sensitivity of the sensor at pressure range of <5 kPa. d) Application of the sensor for tactile sensing. (Reprinted with permission from reference [25].)

In order to further improve the sensitivity of a resistive sensor, pressure sensitive layers with three-dimensional (3D) structures were developed. K. Y. Suh's group developed a flexible strain sensor based on two interlocked arrays of Pt-coated polymeric fibers embedded in PDMS films, which can detect pressure, shear and torsion with the same device.[18] When different mechanical stimuli are applied, the sensor responds with exclusive resistance changes by different contact states of interconnection formed by the two layers of fiber arrays. The sensor showed good cycle stability and repeatability, and the measurement of spatial distribution of pressure can be achieved by fabricating a network sensor array. However, the sensor uses noble metal, Pt, coated polymer nanopillar arrays as sensitive materials. After a number of sensing cycles, permanent and irreversible contacts between the two fiber array layers may be formed, leading to deterioration of performance.

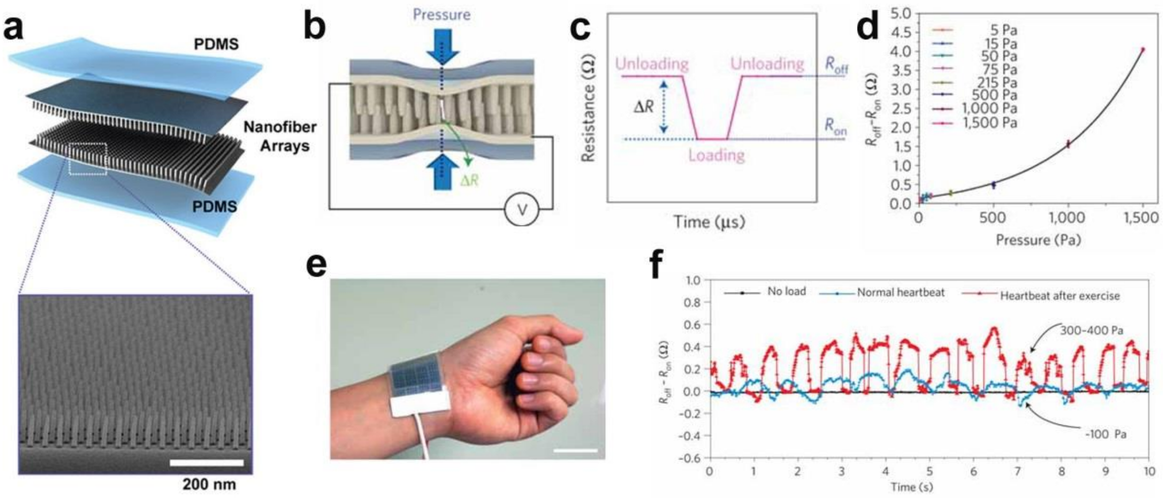

Figure 2.8. A highly sensitive resistive tactile sensor based on interlocked Pt coated polymer nanofibers. a) Schematic of the sensor configuration. b) Schematic of the sensing mechanism. The contact area of the conductive nanofibers increases with the applied pressure. c) Typical resistance change of a sensor with loading or unloading of a pressure. d) The sensor shows high sensitivity to pressure in low regime (<1.5 kPa). e) Sensor placed on wrist for measuring pulse waves. f) The sensor is capable of discerning pulse wave signals of under different conditions (normal/exercise). (Reprinted with permission from reference [18].)

Compared with metal nanowires and nanofibers, conducting polymers and carbon based material have attracted more attention for being shaped into micro-/nano-structured films to serve as sensitive layers in flexible tactile sensors by virtue of their superior mechanical flexibility, good conductivity as well as ease of fabrication. Resistive pressure sensors with sensitive layers of polyurethane (PU) sponge wrapped with graphene have been reported by S. Yu's group (Figure 2.9).[26] The fractured microstructures of the PU sponge allows for a broad pressure response range. The fabrication process is simple and low-cost, with large area production capability. The sensor exhibits a sensitivity of 0.26 kPa^{-1} in pressure range of <2 kPa.

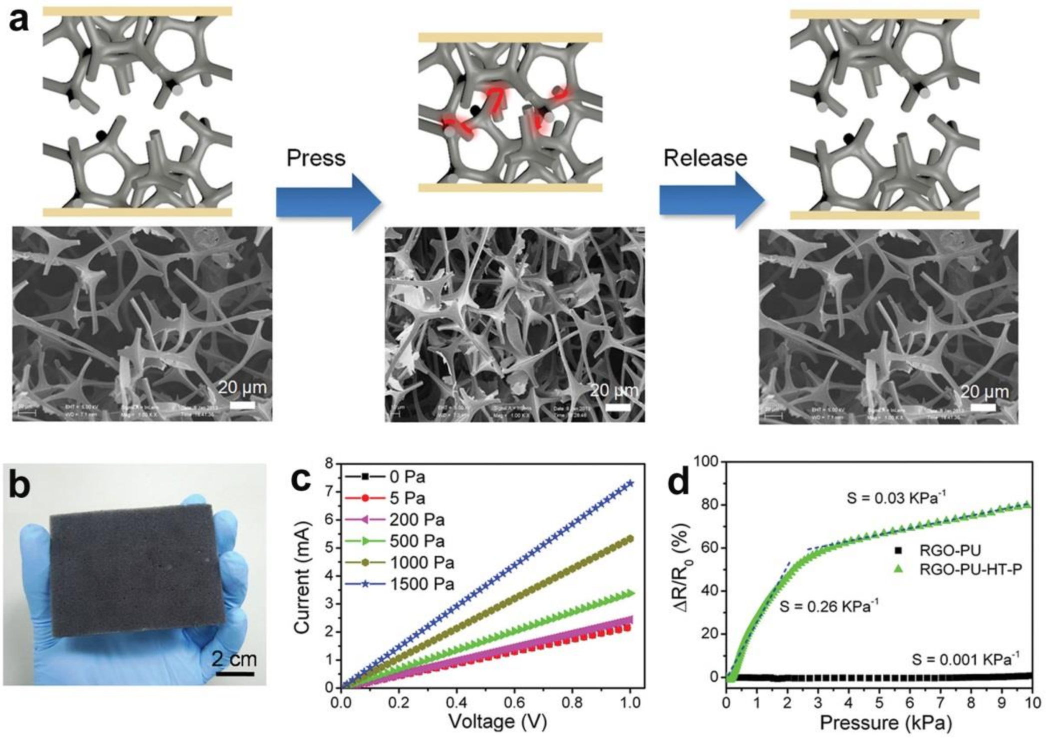

Figure 2.9. Resistive pressure sensor based on graphene-coated polyurethane sponge. a) Schematic illustration of the pressure sensing mechanism. The fractured microstructures of PU have large contact areas and thus have low resistance. b) A photo of the graphen/PU sponge. c) Current-voltage curves of a sensor under different applied pressures. d) Sensitivity of the sensor in the range of <10 kPa. (Reprinted with permission from reference [26].)

Microstructured carbon nanotubes/PDMS films have been introduced by T. Zhang's group to serve as sensitive layer in a resistive sensor with high sensitivity (Figure 2.10).[27] The microstructures are obtained by replicating the patterns in silk moulds with PDMS, and then carbon nanotubes films are placed on the microstructure PDMS films and annealed to form conformal contact. Two microstructured carbon nanotubes/PDMS films were laminated face-to-face to form a resistive pressure sensor. The deformation of PDMS films responding to applied pressure will lead to an increased contact area between the carbon nanotube films, thus the resistance decreases. The sensor demonstrated a good capability of detecting low pressure stimuli, such as the weight of an ant or a bee.

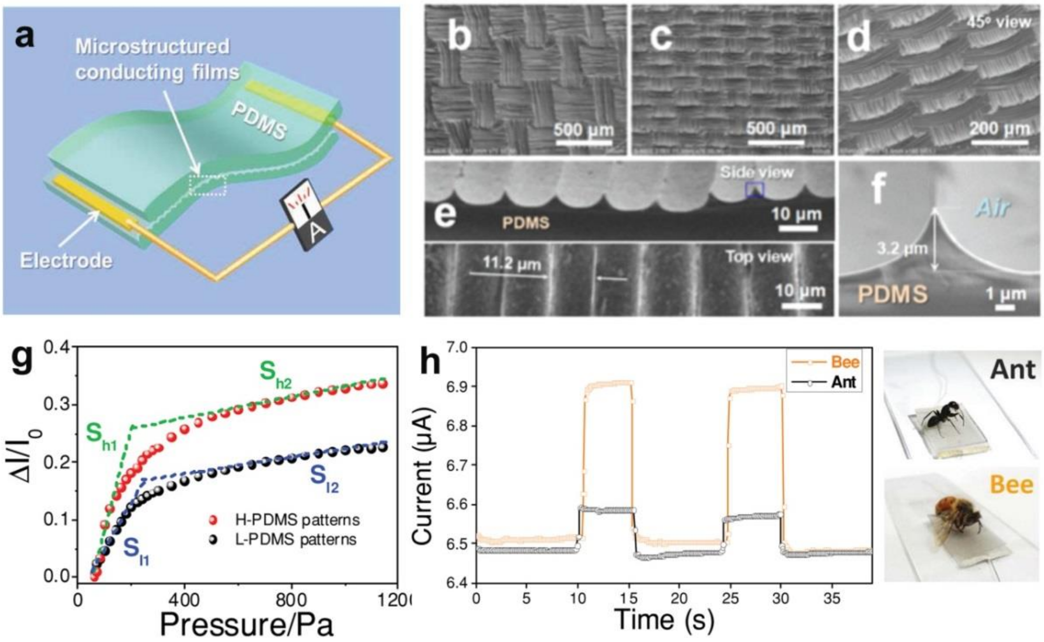

Figure 2.10. Microstructured carbon nanotubes/PDMS films based resistive pressure sensor. a) Schematic of the sensor configuration. b-f) SEM images of the silk-molded microstructures. g) Sensitivity of the sensors with different pattern density. h) Instant current-time of the sensors responding to the loading and unloading of tiny weights of an ant and a bee. (Reprinted with permission from reference [27].)

Using micro-patterned silicon masters is a more efficient way to produce microstructure patterns with perfect uniformity, which contributes a more stable and sensitive response to resistive pressure sensors. Z. Bao's group demonstrated a high sensitive pressure sensor based on PPy hydrogels with hollow-sphere microsturctures (Figure 2.11).[28] The PPy hydrogel film can be further modified with microstructured pattern arrays by molding with silicon master. The microstrucured pattern arrays benefit the sensor with an ultrahigh sensitivity of 133 kPa^{-1} in pressure of <30 Pa, and a low detection limit of 0.8 Pa.

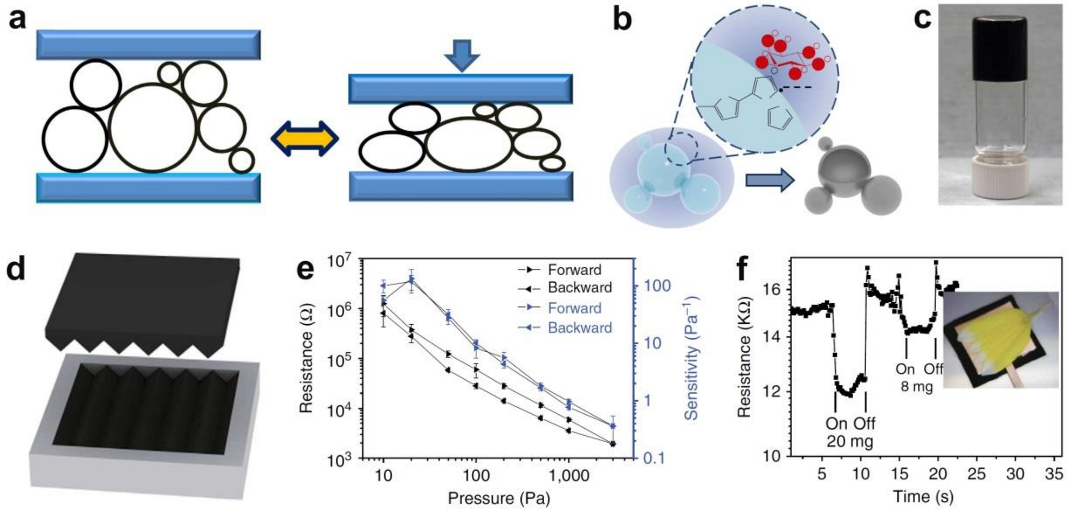

Figure 2.11. Microstructured PPy films based resistive pressure sensor. a) Schematic of the pressure sensing mechanism of the microstrutured PPy film. b) Schematic of the synthesis mechanism of PPy hydrogels. c) A photo of the hydrogel. d) Schematic of introducing microstructure patterns to the PPy films by molding with micro-patterned silicon master. e) The sensor shows a high sensitivity to pressure in low ranges. f) Instant resistance changes of the sensor responding to the loading/unloading of tiny weights. (Reprinted with permission from reference [28].)

Microstrutured pattern arrays with pyramid geometry are one of the most effective structures to enhance the sensitivity of a pressure sensor because of anisotropic effect. J. Park’s group coated a conductive layer of PEDOT:PSS onto the microstructured PDMS films to render the latter conductive so as to serve as the sensitive layer in a resistive pressure sensor.[29] Applied pressure will induce the pyramidal microstructure patterns deform in an anisotropic way, providing fast response time and high sensitivity. The employment of pyramidal microstructures endows the sensor with a high sensitivity of 4.88 kPa^{-1} in the pressure range of <8 kPa, and a detection limit of 23 Pa.

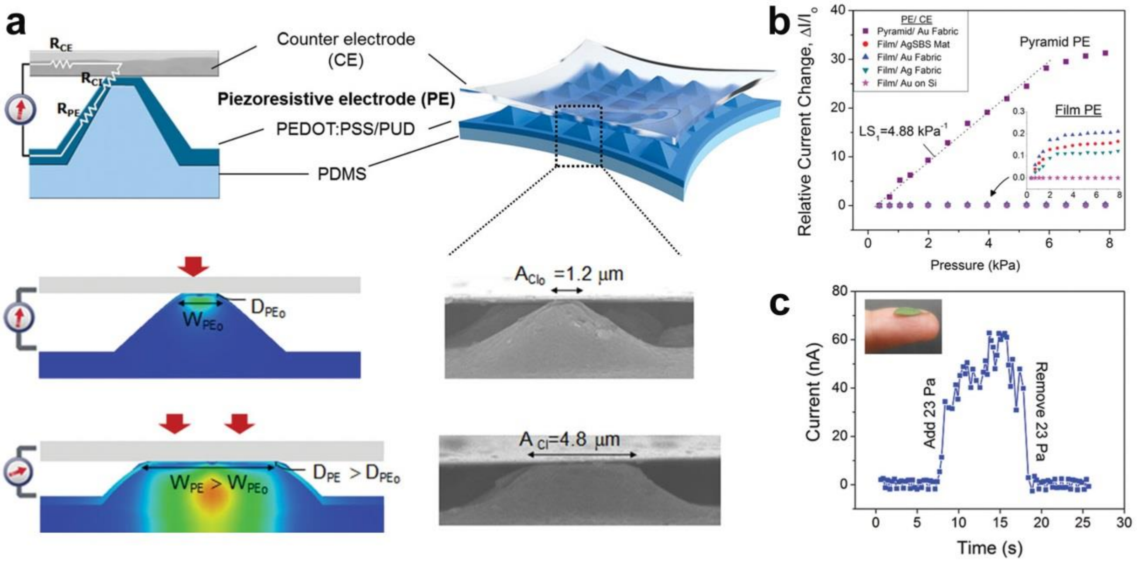

Figure 2.12. Resistive pressure sensor based on pyramidal microstructure patterns. a) Schematic illustration of the sensing mechanism. b) Sensitivity of the sensor in the range of <8 kPa. c) Instant current-time curve of the sensor for detecting a leaf of 93 mg, corresponding to 23 Pa. (Reprinted with permission from reference [29].)

2.1.2 Capacitive Tactile Sensors

A capacitive tactile sensor changes its capacitance under mechanical stimuli. It often takes a three-layer structure of a parallel plate capacitor, with a deformable dielectric layer (Figure 2.13).[30,31]

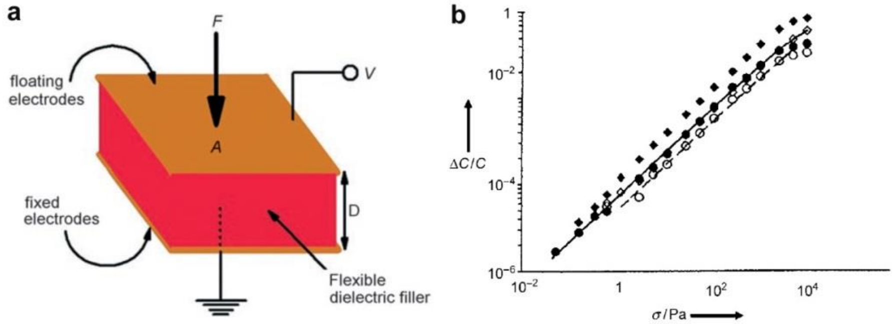

Figure 2.13 Pressure sensing mechanism of a capacitive tactile sensor. a) Schematic of a parallel plate capacitor. b) Typical capacitance change under applied pressure. (Reprinted with permission from reference [30].)

The capacitance of a parallel-plate capacitor is:

$$C= \varepsilon_0 \varepsilon_r A/d$$

Where A is the area of one of the plates, d is the distance between them, ε_r is relative permittivity, and ε_0 is permittivity of free space which a constant. Pressure applied on a capacitive sensor reduces the distance between the two electrodes, leading to an increase in capacitance.[8,31] Conventional capacitive pressure sensor, using air or polymer films as dielectric layers, usually showed poor sensitivity toward pressure in low range, and is susceptible to hysteresis.

By shaping PDMS films with microstructure arrays as dielectric layer, Z. Bao's group reported a flexible capacitive pressure sensor with high sensitivity and short response time. Different to the unstructured film, which showed little response even at high pressure values above 5 kPa, the pyramid-structured films exhibited a significant response at low pressure values below 2 kPa (Figure 2.14).[32] The sensor's good sensitivity and stability toward low pressure events enable it to meet the requirement of tactile sensing. In a following work, Z. Bao's group replaced the metal electrodes with carbon nanotubes to make a capacitive sensor stretchable and transparent.[33] The sensor can detect both strain and pressure stimuli by capacitance changes with different sensitivity. Pressure distribution can be detected by using cross-bar configurations. Because the whole device is made of flexible and stretchable materials, it shows great potential for applying as electronic skin devices.

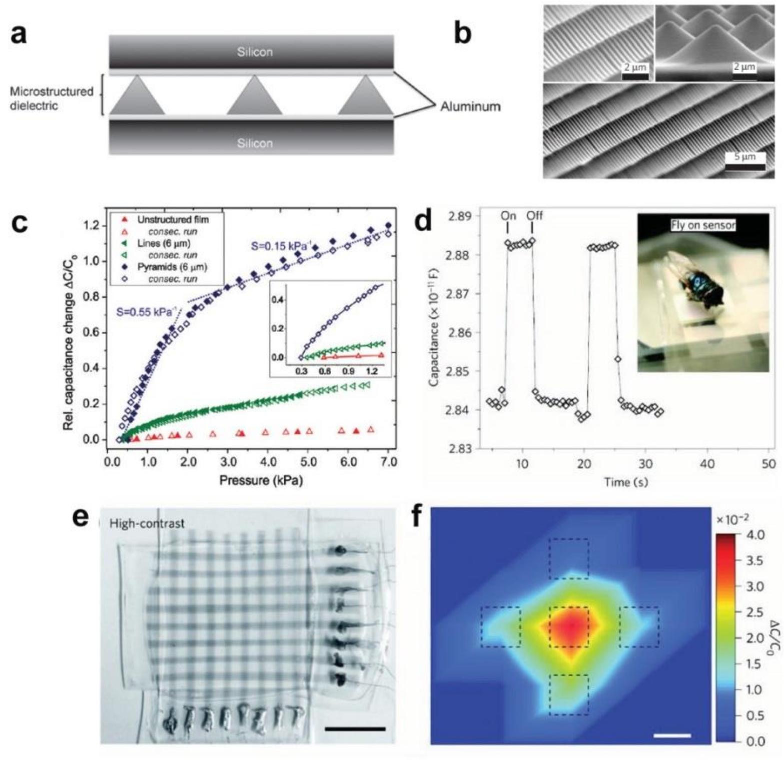

Figure 2.14 High performance capacitive tactile sensors. a) Schematic of the capacitive sensor using dielectric layer with microstructure patterns. b) SEM images of the pyramidal microstructures. c) Sensitivities of the sensors with different microstructures. d) Instant current-time curve of a sensor in response to the loading/unloading of a fly. e) A photo of nanotubes/PDMS based capacitive sensor array. Scale bar: 2 mm. f) Mapping of a pressure applied on the sensor array. (Reprinted with permission from reference [32,33].)

Because the pressure response of a capacitive sensor relies on the deformation of dielectric layer, it is rationale to use the microstructured PDMS film in an OFET device as the gate dielectric for building active pressure sensing matrix. Deformation of the PDMS gate affects the output current of an OFET device, thus external pressure can be detected by current change. The integration of microstructured PDMS in OFETs could provide capacitive sensors with fast response time because the capacitance change of the microstructured PDMS layer is directly transformed into the source-drain current change of the OFET.

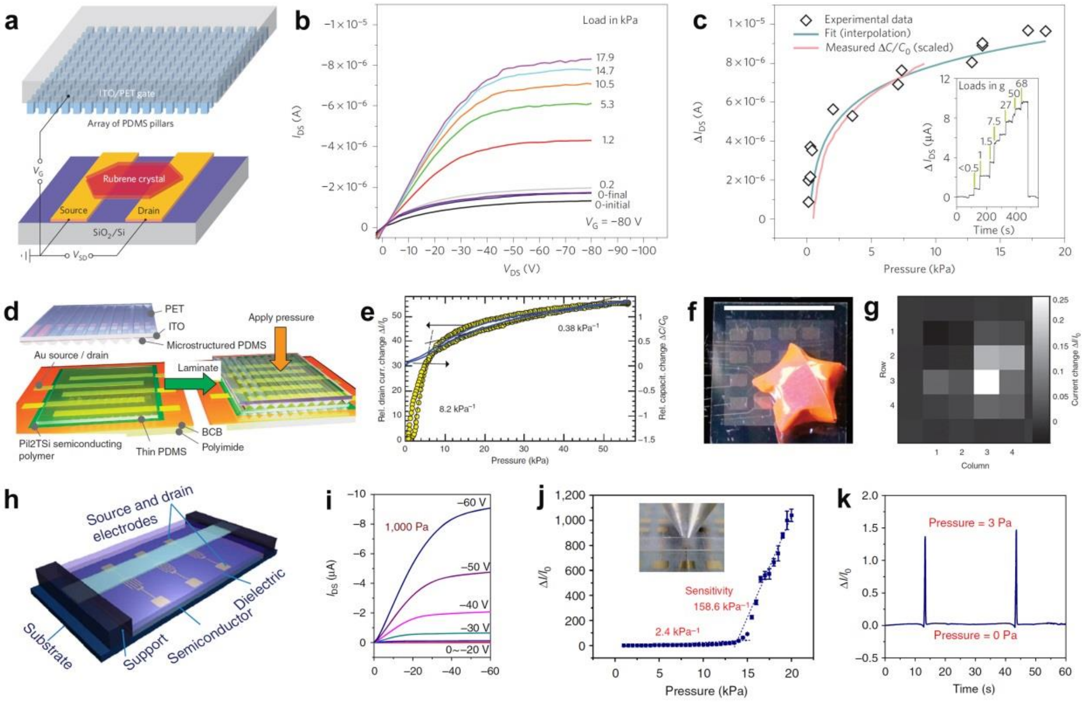

Figure 2.15. Capacitive pressure sensors based on OFETs. a) Schematic of a pressure sensing transistor with microstructured PDMS as gate dielectric layer. b) Pressure response of the sensor at different applied pressures. c) Drain-source current changes are in accordance with the capacitance change induced by different applied pressure. d) Schematic of an OFET basd on a polymer semiconductor with microstructured PDMS as gate dielectric. d) The sensor show a high sensitivity of 8.2 kPa^{-1} in <8 kPa. f) A photo of sensor arrays to detect pressure distribution and corresponding current mapping image (g). h) Schematic of the OFET with suspended gate. i) Output current curves of the transistor under a pressure of 1 kPa. j) The transistor using ITO/PET as gate shows a high sensitivity. k) Response of the sensor to a tiny load of 3 Pa. (Reprinted with permission from reference [32,34,35].)

Several capacitive pressure sensor prototypes applying microstructured PDMS as gate dielectric in OFETs have been reported by Z. Bao's group. By using the PDMS dielectric layer in a single crystal organic transistor, a fast response in millisecond ranges can be achieved (Figure 2.15a). The sensor demonstrates a stable response to pressure in <20 kPa range at a voltage bias of -20 V.[32] In a subsequent report, to improve the pressure sensitivity of the transistors, semiconducting polymer with high mobility was used to replace the organic single crystal as the semiconductor layer (Figure 2.15d). The sensor demonstrates a high sensitivity of 8.2 kPa^{-1} in pressure range of <8 kPa, a fast response time of <10 ms, as well as good stability.[34]

In addition to the pressure sensing OFETs using microstructured PDMS as gate dielectric, D. Zhu's group reported a suspended gate OFET for pressure sensing (Figure 2.15h).[35] The gate electrode is suspended by supports to form air gaps as dielectric layer, and applied pressure will affect the distance of the gap, resulting in an output current change of the transistor. Because thin conductive films can be applied as the gate electrodes which are easy to vibrate, the sensor exhibits an ultrahigh sensitivity of 158.6 kPa^{-1} in pressure ranges of 15 ~ 20 kPa, and a fast response time of <10 ms.

2.1.3 Optical Tactile Sensors

Optical tactile sensors are insensitive to electromagnetic radiation and electrical discharges. Because of their stable performance, they are suitable for large area human-computer interface applications such as touch screens and displays.

Plastic optical fibers are commonly used in optical pressure sensors, and they provide several advantages such as low cost, flexibility and ease of operation. Though two kinds of sensor devices have been utilized, the sensing principles of both are dependent on the change in light intensity transduced from pressure change. In one kind of sensor, light goes through a transparent elastomer. The deformation of elastomer rising from the external pressure will generate a change in its optical properties. By measuring the correspondent change in optical intensity, the applied pressure can be detected.[36] In the other kind, silicone fibers are directly integrated into a pressure sensitive matrix. Applied pressure results in cross-sectional change of fibers textile, which leads to a simultaneous change in light density.[37]

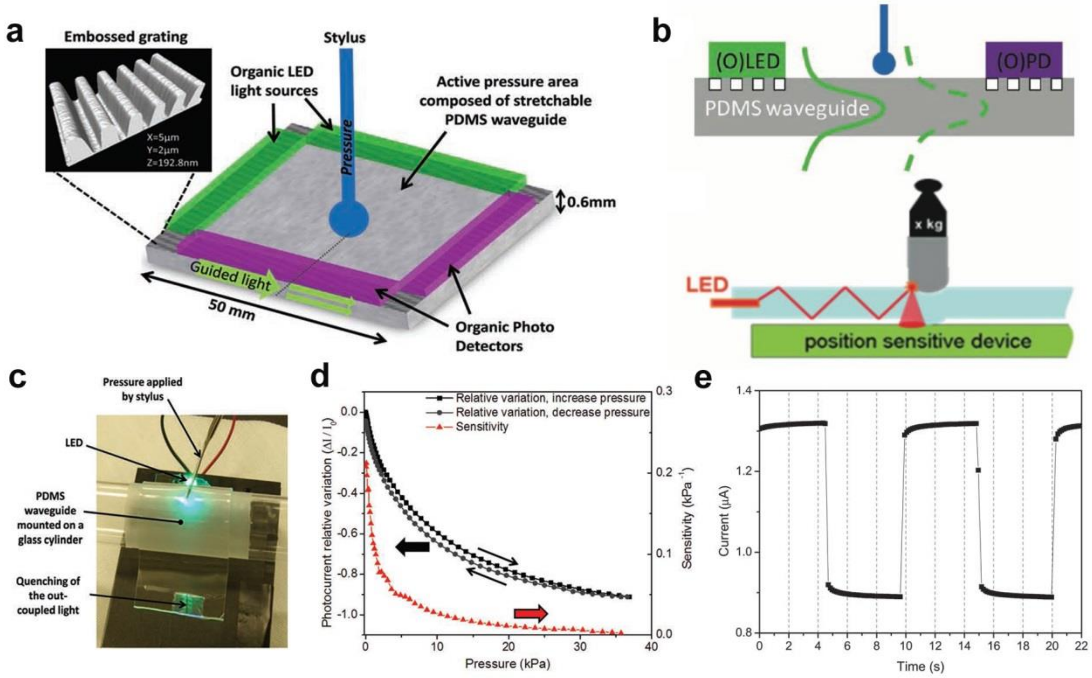

Figure 2.16. Optical pressure sensor based on PDMS waveguide. a) Schematic of the sensor. b) Schematic of the pressure sensing mechanism. Light density received by detector decreases when pressure is applied on the waveguide. c) A photo of the sensor coated on a cylinder in response to a pressure applied through a stylus. d) Light density changes with applied pressure. e) Instant current-time curve of the sensor with the loading/unloading a pressure of 40 kPa. (Reprinted with permission from reference [38].)

Besides optical fiber, optical waveguide based pressure sensors have also been reported. The sensor system is based on the waveguide's optical evanescent field, and pressure applied to the waveguide will cause variations in refractive index of the top transparent polymer film, which subsequently changes the effective index of the guided mode of the waveguide. The pressure can be detected and measured by monitoring the shift of the Bragg resonance wavelength, which results from the changes of effective index.[39] By integrating PDMS waveguide with organic light emitting diodes (OLEDs) and organic photodiode (OPD), stretchable and transparent optical pressure sensor has been fabricated. OLEDs and OPDs are used as light sources and photodetectors, respectively (Figure 2.16).[38] When pressure is applied, the PDMS waveguide layer will compress, light in the waveguide will simultaneously be out-coupled, and light detected by OPD at the out-coupling grating stage will decrease. The optical pressure sensor with PDMS waveguide shows a pressure sensitivity of 0.2 kPa^{-1} in pressure range of <1 kPa.

2.1.4 Piezoelectric Tactile Sensors

Pressure and tactile sensors based on piezoelectric materials are one of the most studied devices in the development of skin-like sensor arrays. Piezoelectric materials, mainly crystalline, develop an electrostatic potential when they are strained by external forces. A piezoelectric sensor measures pressure by transducing it to an electrical charge. Both inorganic materials and organic polymer can be used to generate piezo-potentials when applied with pressure (Figure 2.17).[40-42] In a typical sensor design, piezoelectric film is laminated by two layers of conductive films to collect the resultant charge, and the applied pressure can be reflected by its output voltage. Piezoelectric pressure sensors are active devices and ideal for dynamic measurement. Because piezoelectric materials generate charges when compressed or strained, the piezoelectric sensor does not require external power supply and can be attributed to self-powered sensors. They have been already utilized in many applications for tactile sensing, such as noise detection, flows detection and touch screens.

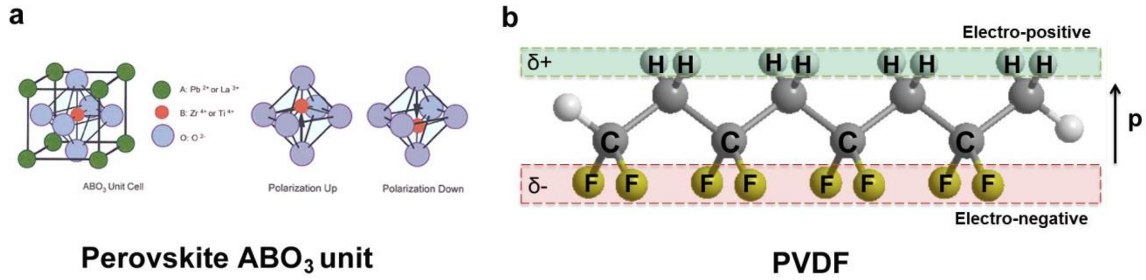

Figure 2.17. Crystal structures of inorganic piezoelectric materials (PZT) and piezoelectric polymers (PVDF). a) Applied pressure induces changes in polarization in the PZT structure (a) and PVDF (b). (Figure 2.17a, reprinted with permission from reference [42].)

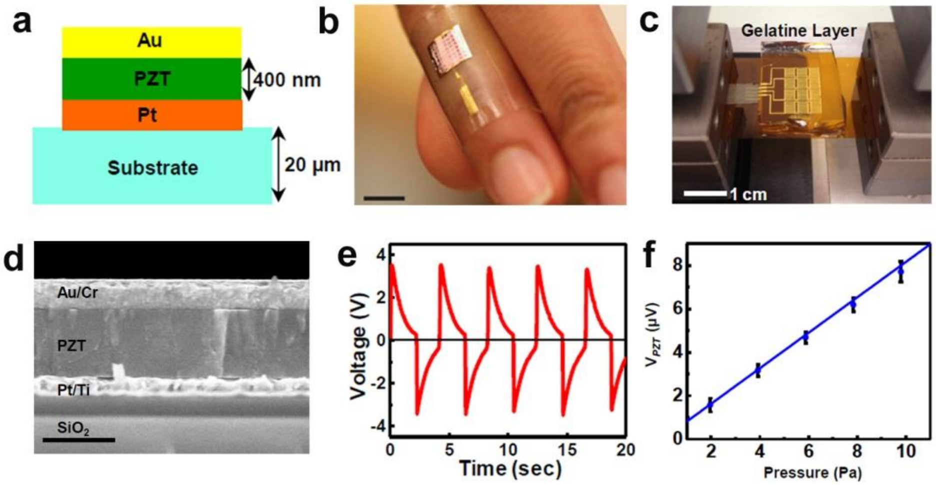

Figure 2.18 A flexible piezoelectric pressure sensor based on ultrathin PZT films. a) Schematic of the sensor configuration. b) A photo of the sensor array put on finger. c) A photo of sensor arrays for bending test. d) SEM image of the PZT film. Scale bar: 500 nm. e) Instant voltage-current curve of the sensor. f) Piezo-voltage generated by the PZT films with different applied pressures. (Reprinted with permission from reference [43,44].)

Polycrystalline lead zirconate titanate (PZT) and barium titanate ($BaTiO_3$) are piezomaterials that attract the most widely attention for practical applications because of their high piezo-coefficient.[42,45,46] However, the inorganic piezomaterials are rigid and brittle, limiting their application in flexible tactile sensors. To render piezoelectric sensor flexible and conformal, J. Roger's group applied ultrathin PZT films on PDMS substrates

(Figure 2.18). The soft PDMS substrate also benefits the sensor with enhanced pressure sensitivity. The thin film PZT based sensor demonstrated an ultra-fast response time of 0.1 ms, a low detection limit of only 0.005 Pa.[43,44]

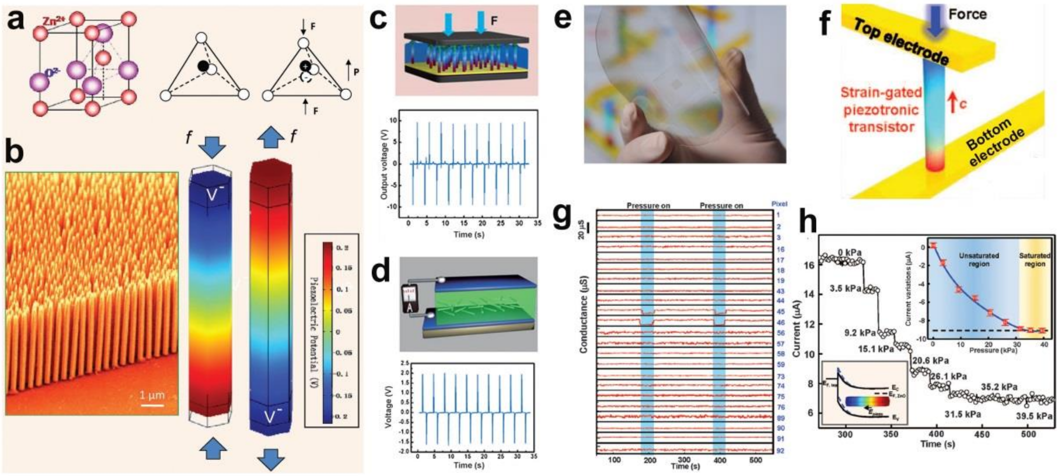

Figure 2.19 ZnO nanowires based piezoelectric pressure sensors. a) Hexagonal structure of wurtzite ZnO crystal cell. b) A SEM image of ZnO nanowires and simulated piezoelectric potential under strain. c-d) Schematic of a ZnO NWs based nanogenerators and piezo-voltage outputs. e) A photo of flexible pressure sensing arrays based on ZnO nanowires. f) Schematic of a ZnO NWs based 2-terminal piezotronic transistor. g) Pressure response of the sensor arrays. h) Instant current-time curve of the sensor under different pressures. (Reprinted with permission from reference [47-49].)

ZnO nanowires have emerged as excellent piezoelectric material for transducing mechanical stress to piezoelectric outputs (Figure 2.19).[47,48,50] Z. Wang's group has demonstrated a variety of ZnO NWs based devices to harvest mechanical energy in last decade. ZnO nanowire generate piezo-voltages under stain or pressure, thus it can be laminated with either vertically or horizontally for sensing pressure or stain. By virtue of the ease of fabrication, ZnO NWs can be grown on patterned substrates to obtain high density pixels for pressure sensing. By applying ZnO nanowires arrays in 2-terminal piezotronic transistors, tactile sensing matrix with a high resolution of 20 × 20 μm^2 was reported. The pixel density of the arrays (8464 cm^{-2}) is higher than the receptors density in human fingertips (~240 cm^{-2}). The sensor arrays also demonstrates a fast response time of 0.15 s and a good response to low-range pressure (<10 kPa).[49]

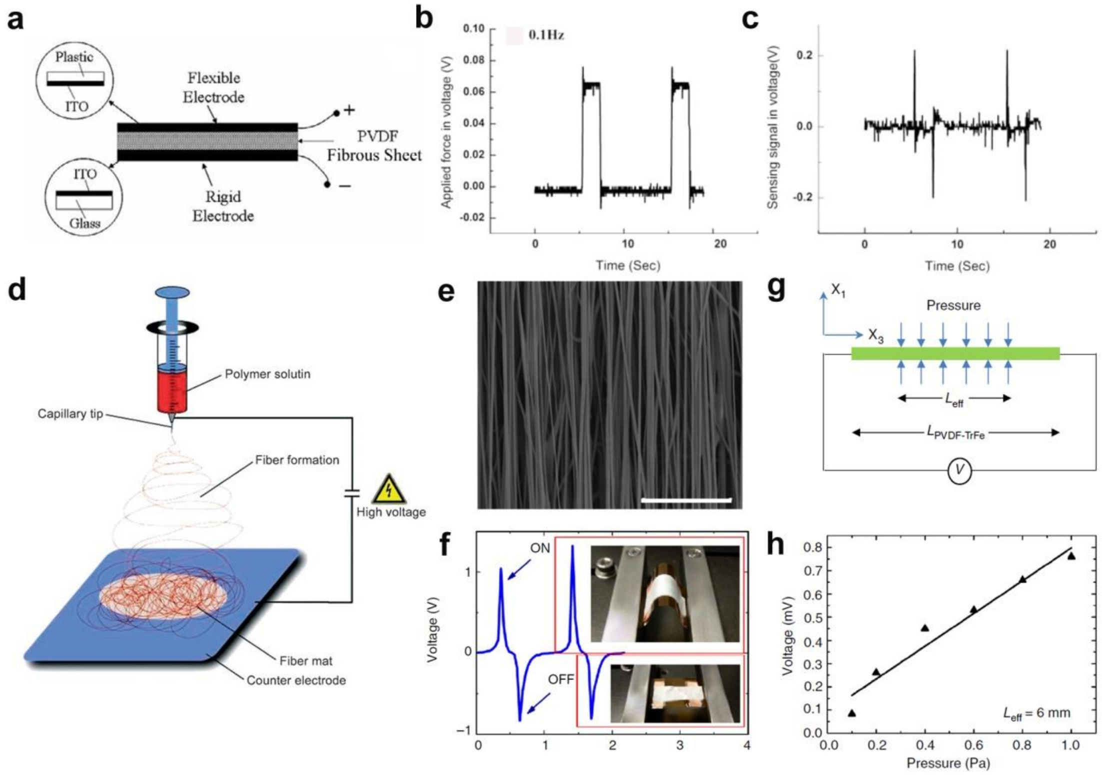

Figure 2.20. Piezoelectric polymers based tactile sensors. a) Schematic of a piezoelectric sensor based on PVDF. b) Real-time curve of applied force loading. c) Real-time curve of the piezo-voltage of the sensor. d) Schematic of electrospinning process. e) SEM image of aligned PVDF-TFE nanofibers. f) Piezoelectric performance of the PVDF-TFE based sensor under strain. g) Schematic of the PVDF-TFE film based sensor. Pressure induces piezopotentials. h) Pressure response of the sensor. (Reprinted with permission from reference [51-53].)

Polyvinylidene fluoride (PVDF) and its copolymers are widely used as piezoelectric materials for flexible electronics.[16] PVDF film is lightweight and low cost, and can be directly applied onto a curved surface without disturbing its mechanical motion. Due to its wide dynamic range and high sensitivity, it is suitable for sensing small pressure fluctuations. PVDF based sensors have been applied in erosive environment to detect pressure or strain, and for medical use such as monitoring heartbeat. A typical PVDF based pressure sensor design and corresponding pressure response are illustrated in Figure 2.20a-c.[51] With loading/unloading a pressure, the sensor produces two opposite peak signals. To improve the performance, PVDF polymer fibers are often fabricated by electrospinning process.[52] Pressure sensor based on aligned nanofibers of poly(vinylidenefluoride-co-trifluoroethylene) (PVDF-TFE) exhibits a high sensitivity with a detection limit of 0.1 Pa.[53]

2.1.5 Triboelectric Tactile Sensors

Triboelectric tactile sensors are self-powered sensors based on triboelectric nanogenerators developed by Z. Wang's group.[54] A triboelectric nanogenerator transduces mechanical energy into electrostatic charges by friction and separation between two separated polymer films with opposite triboelectric characteristics (Figure 2.21).[54,55] When a triboelectric nanogenerator is experiencing a pressure loading, separated films contact together and generate electrostatic charges, and electrons can flow through external loadings to produce an electric output.[56] Because high voltages can be generated by electrification phenomenon, triboelectric sensors are possible to provide high tactile sensitivity.

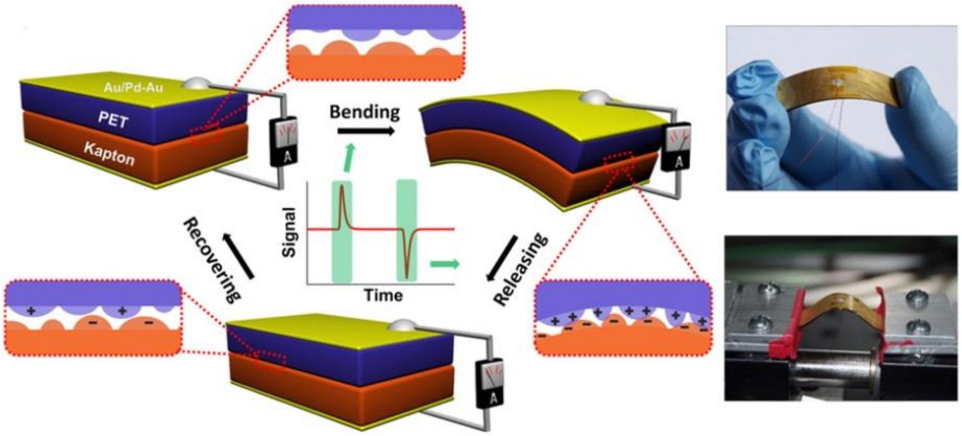

Figure 2.21 Schematic illustration of the working mechanism of a triboelectric generator. Electric outputs with opposite polarity are generated under bending and releasing operations. (Reprinted with permission from reference [54].)

By introducing microstructured PDMS films as a functional layer in a triboelectric nanogenerator, Z. Wang's group developed a transparent pressure sensor with a high sensitivity.[57] The sensor is fabricated by sandwiching two ITO coated PET films with a thin PDMS membrane. As PET and PDMS have distinctly different triboelectric characteristics, when the device deforms with applied pressure, opposite triboelectric charges are generated and can subsequently be detected. By replacing flat PDMS film with microstructured film, the performance can be significantly improved. The sensor showed high sensitivity and good stability, capable of detecting a weight of a feather. In a following work, a triboelectric sensor based on microstructured PDMS film and Al film deposited with Ag nanowires was reported with static sensing capability.[58] Both the microstructures of PDMS and nanostructures of Ag nanowires contribute a high triboelectric effect, thus benefit the performance of the sensor in pressure sensing. The sensor demonstrates a sensitivity of 0.31 kPa^{-1}, a fast response time of <5 ms, and a detection limit of 2.1 Pa.

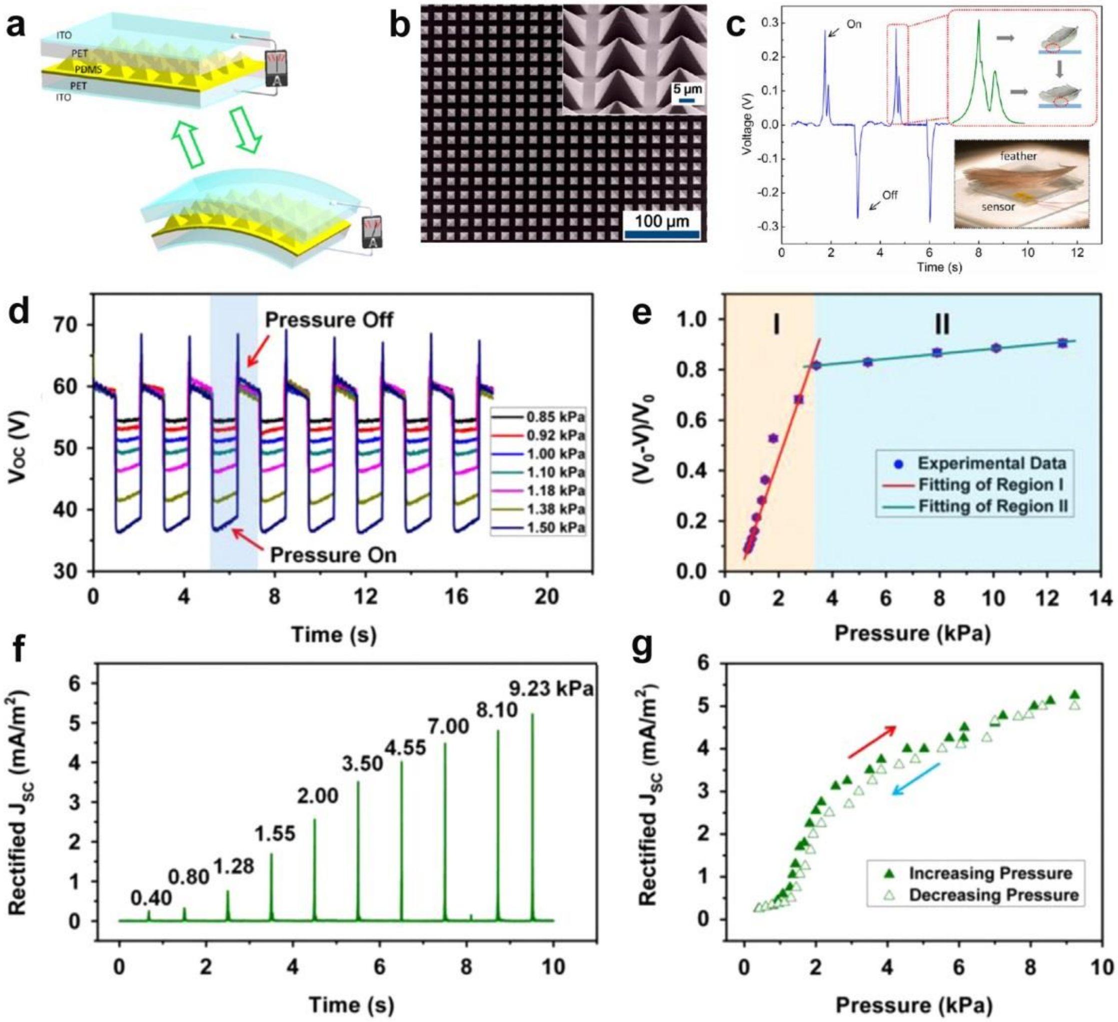

Figure 2.22 Flexible pressure sensor based on triboelectric nanogenerators. a) Schematic of the pressure sensor. b) SEM image of PDMS film with pyramidal microstructures. c) Instant voltage-time curve of the sensor in response to the weight of a feather. d) Open-circuit voltage change of the sensor response to different pressure loading cycles. e) The sensor exhibits a high sensitivity of 0.31 kPa^{-1} in pressure range of <4 kPa. f) Real-time short circuit current density change of the sensor with different applied pressures. g) Pressure response of the sensor in a test cycle. (Reprinted with permission from reference [57,58].)

2.2 Summary and Current Status

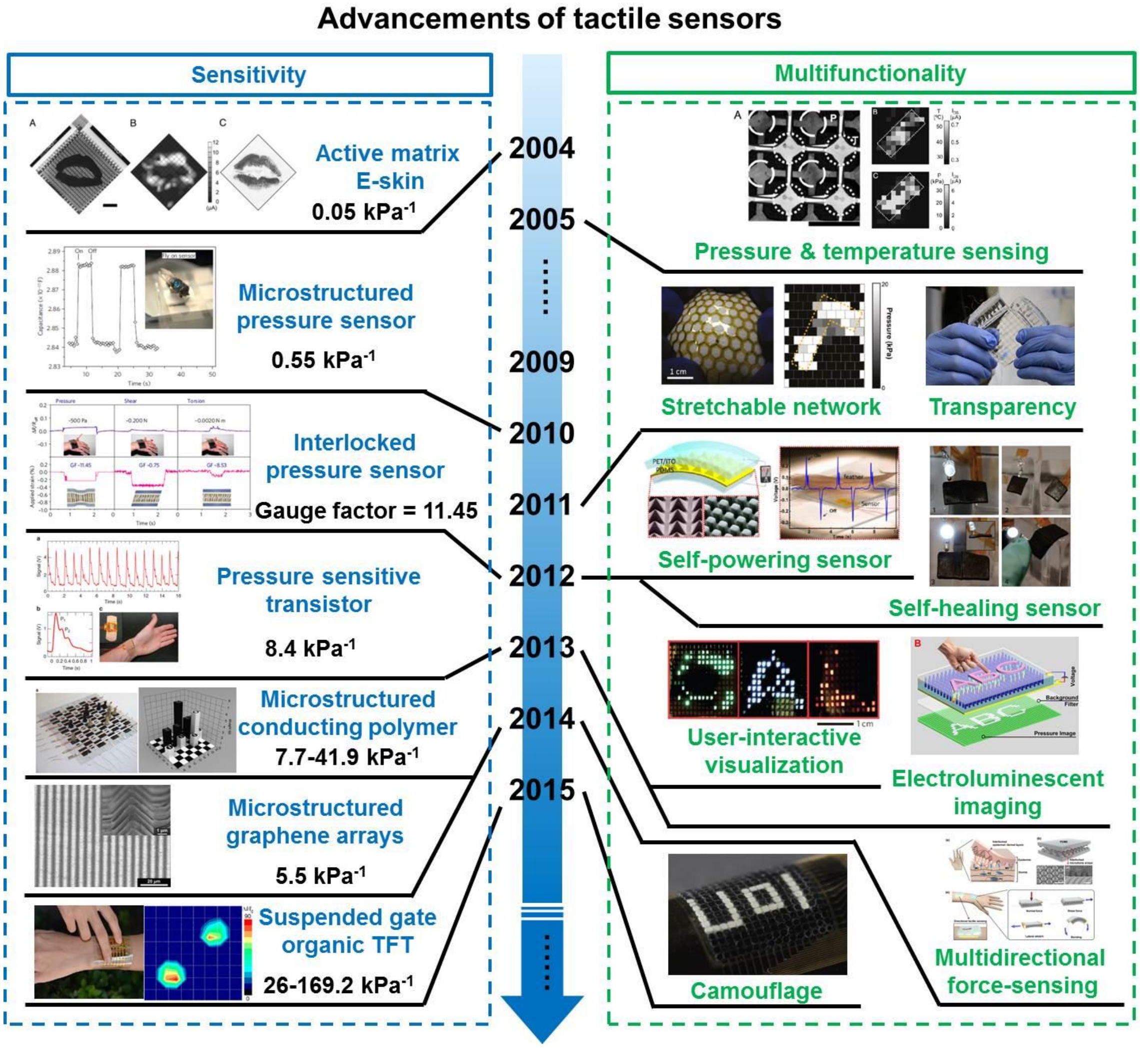

Figure 2.23 Advancements of tactile sensing devices in two aspects: sensitivity and multifunctionality. (Reprinted with permissions: "Active matrix E-skin".[19] "Microstructured pressure sensor".[32] "Interlocked pressure sensor".[18] "Pressure sensitive transistor".[34] "Microstructured conducting polymer".[28] "Microstructured graphene arrays".[59] "Suspended gate organic TFT".[35] "Pressure & temperature sensing".[20] "Stretchable network".[60] "Transparency".[33] "Self-powering sensor".[57] "Self-healing sensor".[61] "User-interactive visualization".[62] "Electroluminescent imaging".[63] "Camouflage".[64] "Multidirectional force-sensing".[65])

In order to emulate the exquisite tactile sensation of natural skin, the last decade has witnessed tremendous improvements in the design and integration of high performance tactile sensing devices for applications in electronic skins, humanoid robotics, and human-machine interfaces.[8] Various sensing techniques have demonstrated feasibilities in tactile sensing and a number of sensor prototypes have been devised. In terms of performance, we can attribute the advancements of tactile sensing devices in last decade to two aspects: 1) the improvement of pressure sensitivity, and 2) the implementation of multifunctionality (Figure 2.23). On one hand, numerous efforts have been delivered to improve sensitivities together with detection limits of pressure sensors. In the last several years, the sensitivity of pressure sensors has a tremendous increase from <1 kPa^{-1} to >100 kPa^{-1}, especially for sensing pressure value in low regime, by virtue of the introduction of micro-/nano-structures. At the same time, the minimum pressure value that E-skin devices can detect has been put forward to <0.5 Pa.[35] The pressure sensing performance of tactile sensors has surpassed the tactile sensation of natural skin. On the other hand, different kinds of sensing units, such as temperature and strain sensors, have been integrated with pressure sensors to achieve multifunctionality in an individual sensor device so as to maximally mimic the function of natural skin.[30] At the same time, many intriguing properties that are not possessed by natural skin, such as transparency,[33,38] high stretchability,[21,66-68] wireless detection,[69] self-powering,[70] user-interactive,[62] and ultra-lightweight,[24] have been implanted in tactile sensors to endow them with new opportunities for building next-generation smart and super electronic skin devices.

Still, though these pioneering endeavors have shed light on the further improvements of E-skin devices for emulating natural skin, sensory memory, a significant function of natural skin, has yet been addressed. Human skin perceives touch sensations and provide brains with valuable sensory information, such as temperature and pressure, to describe the surrounding environment. Skin can not only sense and distinguish different environmental stimulus, but remember the physical quantity with the help of sensory memory. Haptic memory is one of the five forms of sensory memory that endows human with ability to remember the pressure stimuli applied on the skin. Such challenge summons intense research efforts for the rise of highly sensitive tactile sensors that not only have high sensitivity, but can memorize the signals for the mimicry of human sensory memory.

3. Experimental Methodology

This chapter introduces the design and fabrication of conductive microstructured PDMS films which serve as sensitive layers in resistive tactile sensors. First we introduced the role of microstructures in human sense of touch. Then silicon masters with concaved pyramidal microstructure arrays are fabricated by conventional photolithography and wet etching methods. Then, by moulding PDMS to the silicon master, the pyramidal patterns can be replicated and transferred to the PDMS films. Two methods of producing conductive microstructured PDMS films are introduces. Finally, experimental setup for characterizing the performance of tactile sensors is illustrated.

3.1 Rationale for Selection

Different parts of human skin have varied tactile sensitivities. The high density of mechanoreceptors together with the papillary ridges make fingers the most sensitive parts of human body.[71] The presence of papillary ridges (fingerprints) on the skin surface, with parameter in micrometer range, contributes to the gripping ability and renders fingers capable of sensing and perceiving fine textures with spatial resolution of less than 200 micrometers.[1] The exquisite tactile sensation of fingers by virtue of fingertips inspires to introduce microstructure arrays into tactile sensors for the mimicry of human sense of touch.

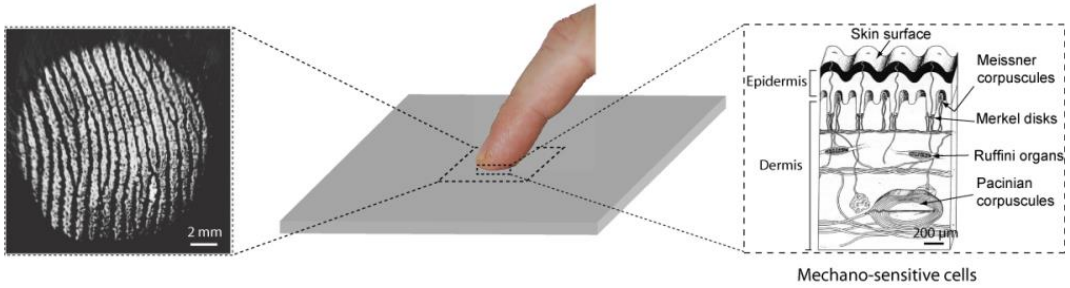

Figure 3.1. Illustration of a finger contacts with a surface. Fingertips have fingerprints in micrometer size which play an important role in tactile sensation and perception. (Reprinted with permission from reference [71]).

For resistive tactile sensors, the sensing of applied pressure relies on the deformation sensitive layers. Thus, the introduction of microstructures can improve the performance of tactile sensing devices in many aspects. First, the sensitive layer has numerous sensing units to deform when it is downsized to micrometer level. Compared with bulk films, microstructures can deform more easily and quickly, providing a higher sensitivity and faster response. Moreover, pyramidal structures can contribute to a superior sensitivity than cube or column structures because of the anisotropic effect. Furthermore, the parameters of microstructure arrays are precisely defined through conventional photolithography and etching processes, rendering the pressure response of tactile sensors stable and reliable.

PDMS is an important elastomeric polymer material for tactile sensing devices because of its excellent mechanical properties, transparency, ease of molding, as well as biocompatibility.[1,5] In chapter 2, we have introduced several reports applying microstructured PDMS films in pressure sensing devices. The sensitivity of a capacitive pressure sensor with microstructured dielectric layer is almost 30 times of that without microstructures. Also, the pyramidal microstructure arrays contribute a higher sensitivity to triboelectric pressure sensor than unstructured ones. However, PDMS is dielectric and cannot be directly as sensitive layers in resistive tactile sensor.

To apply microstructure arrays in resistive tactile sensors, sensitive layers should be conductive to transduce applied force into electrical signals. To address this, this chapter introduces two methods, layer-by-layer assembly and embedment of conductive materials, to realize the fabrication of conductive microstructure arrays for applications in resistive tactile sensors.

3.2 Preparation of Silicon Master with Microstructure Arrays

PDMS films can be molded with microstructure arrays by replicating the structures fabricated on silicon wafers. To prepare PDMS with convex pyramidal microstructures, silicon masters with concaved structures should be firstly fabricated. The preparation of the silicon master is based on the conventional photolithography process and anisotropic etching of silicon (Figure 3.2).[72,73] Photolithography patterning is used to shape the parameters of an individual pyramid structure. Then wet chemical etching is used to fabricate concaved pyramidal three-dimensional microstructures. Wet etching of silicon was developed two score years ago and went through several improvements. The etching mechanism is based on the fact that the bonding energy of Si atoms is different for each crystal plane, where the wet etching rate of (100) plane is much higher than that of the (111) plane, which makes silicon etching highly anisotropic. By patterning a SiO_2 mask with grid patterns, (100)-orientated Silicon wafers will form concaved pyramidal structures with (111) surfaces, with an angle of 54.74˚.

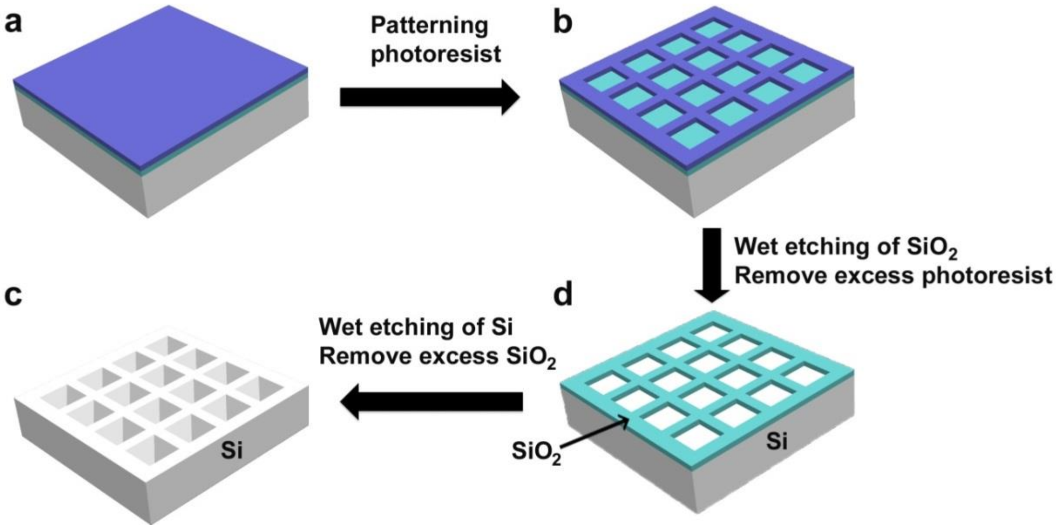

Figure 3.2. Schematic illustration of the fabrication of silicon masters with concaved pyramidal microstructures.

In a typical experiment process, cleaned silicon wafer a SiO_2 oxide layer of 280 nm is placed on a 110 °C hotplate for 5 minutes to remove moisture. Then positive photoresist AZ1518 (AZ Electronic Materials) is spin-coated onto the Si wafer at 3000 rpm for 45 s (Figure 3.2a). After pre-baking (90 °C, 3min), the wafer goes through a photolithography process through a mask aligner (SUSS MJB4 Mask Aligner, Garching, Germany) with a grid chrome mask and is then developed with AZ 300 MIF developer (Figure 3.2b). Then, the exposed SiO_2 patterns are etched by buffered hydrofluoric acid (NH_4F : HF = 7:1, volume ratio) for 3 minutes (Figure 3.2c). Subsequently, the remaining photoresist is washed away by acetone, and then Si master is anisotropically etched by a strong alkaline solution (35%wt KOH in H_2O: isopropanol = 4:1, volume ratio) at 80 °C with vigorous stirring to form concaved pyramid microstructures. And then excess SiO_2 grids are removed by buffered HF solution again (Figure 3.2d). After washing the master several times with ethanol, IPA and water alternately, it is cleaned with Piranha solution (H_2SO_4: H_2O_2 = 7:3, volume ratio) at 80 °C for 1 hour to make it hydrophilic. Finally, the master is modified with a saline layer of 1H,1H,2H,2H-perfluorodecyltrichlorosilane through a silanization process in gas phase. The silanization process is necessary as it prevents adhesion and makes the following peeling-off of PDMS easier. After fabrication, a silicon master can be used for hundreds of times without damage.

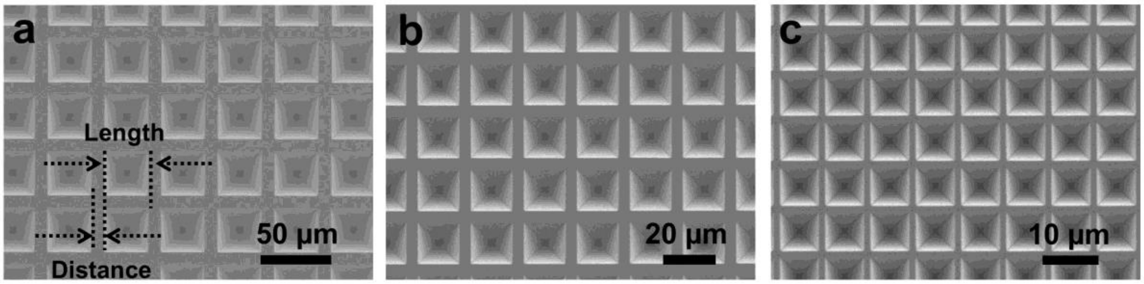

Figure 3.3. SEM images of silicon masters with different pattern sizes. a) Pyramidal structure with length of 30 μm and a distance of 10 μm. b) Pyramid structure with length of 15 and distance of 5 μm. c) Pyramidal structure with length of 6 and distance of 2 μm.

Due to the precise controlling of parameters in photolithography process, silicon masters was successfully fabricated with concaved pyramidal microstructures of different pattern sizes (period) but with same pattern length : distance ratio of 3:1 (Figure 3.3).

3.3 Methods to Prepare of Conductive Microstructured PDMS Films

To introduce pyramidal microstructures into elastomeric PDMS films to serve as the sensitive layer in a resistive tactile sensor, we developed the following two methods:

1) To deposit conductive films on microstructured PDMS film.
2) To embed metal nanowires to the PDMS film.

The difference of the two methods can be attributed to the different sequence of process. In the first method, PDMS films with microstructures are firstly fabricated. And then graphene layers are deposited on the surface of PDMS. In the second method, silver nanowires are firstly dropped on the silicon master, and then PDMS is used to replicate the pyramidal microstructures.

3.3.1 Deposition of Conductive Layers on Microstructured PDMS Films

The PDMS films with microstructure patterns are fabricated by spin-coating the mixture of PDMS elastomer and cross-linker on as-prepared silicon masters (Figure 3.4). After degassing in vacuum and curing at 90 °C for 1 h, the PDMS film is peeled off from the master, and its convex pyramidal microstructures replicate the patterns of the silicon master.

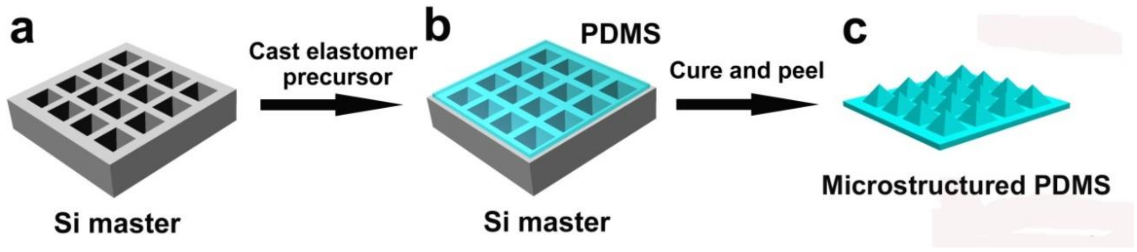

Figure 3.4. Schematic illustration of preparing PDMS films with pyramidal microstructures.

In a typical experiment, PDMS elastomer and cross-linker (Sylgard 184, Dow Corning) are mixed at a weight ratio of 10:1 and mechanically stirred for 5 minutes. Then the mixture is degassed in a desiccator under vacuum. It usually takes around 1 hour to remove all the bubbles in the pre-crosslinking mixture in the desiccator. The mixture can be stored at low temperature (-4 °C) to extend its solidification time. Freestanding PDMS film is prepared by spin-coating the uncured mixture onto a silicon master (45 s, 1000 rpm). The thickness of the PDMS film can be adjusted by applying different spin-coating rates. After the elastomer mixture is degassed in a desiccator under vacuum to remove any bubbles, it is cured at 90 °C for 1h and then peeled off with a scalpel from the silicon master. The microstructured PDMS films are capable of large-area fabrication and its area is defined by the silicon master applied. The smallest pyramidal pattern size can be less than 5 µm due to the accuracy of photolithography process. A digital photo and the transmittance spectrum of the PDMS film with the smallest pyramidal microstructures are illustrated in Figure 3.5, where each pyramid microstructure has a length of 4.5 µm and the distance between two nearby pyramids is 1.5 µm. The microstructured PDMS film has excellent uniformity which is indicated by the interference fringes.

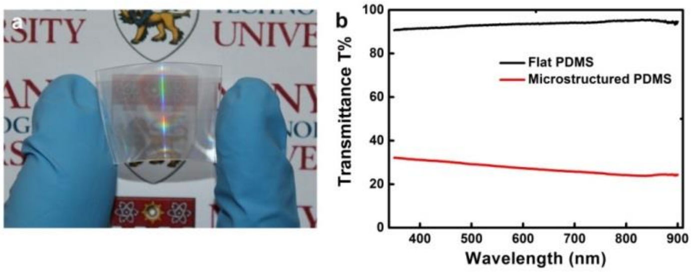

Figure 3.5. PDMS film with pyramidal microstructure arrays. a) Digital photo of the microstructured PDMS film. The interference fringes indicate the good uniformity of the microstructures. b) The transmittance of PDMS film towards visible range decreases with the introduction of microstructure arrays.

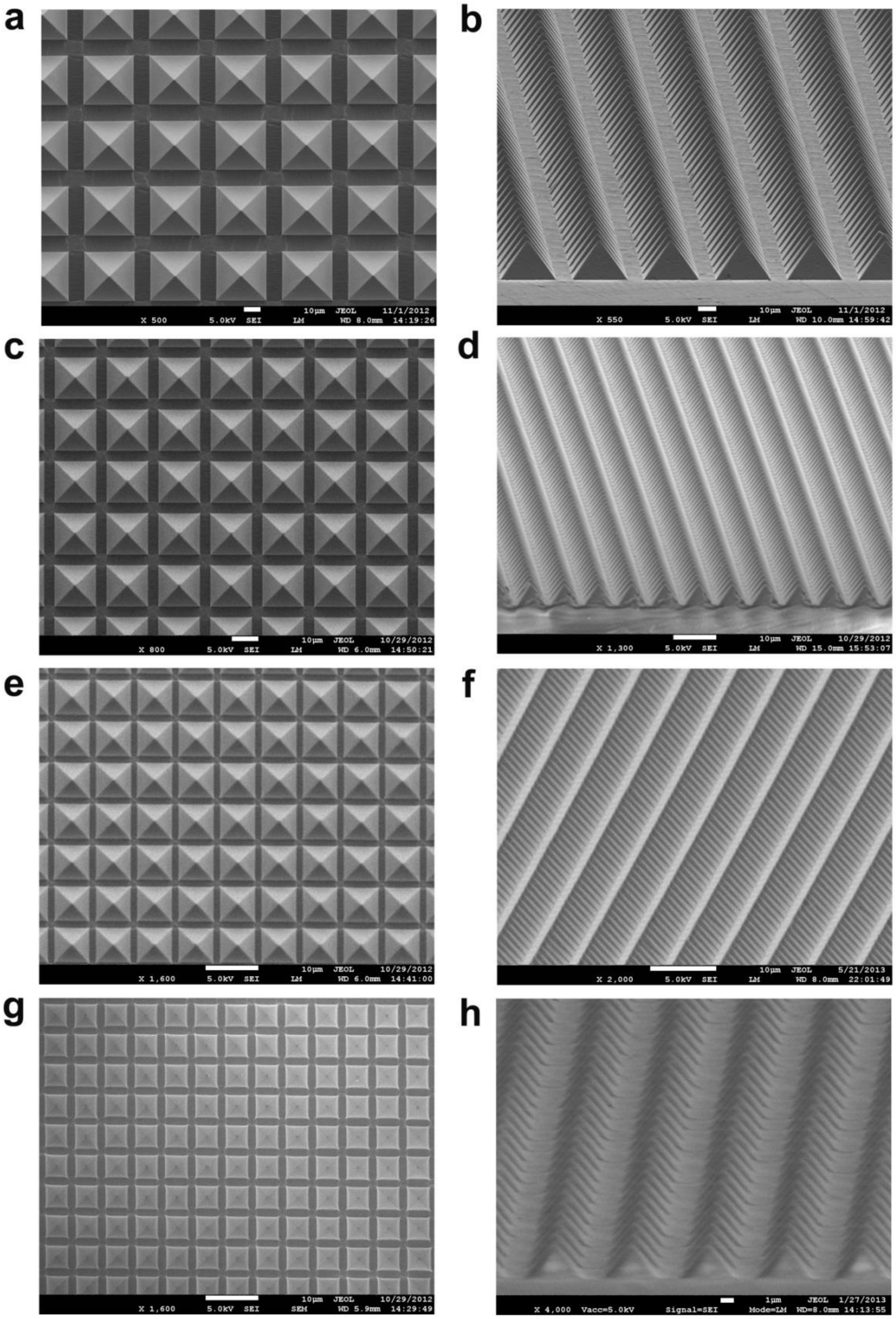

Figure 3.6. SEM images of microstructured PDMS films with different pattern sizes. a-b) Top-view and tilted SEM images of pyramid patterns with length and distance of: a-b) 30 µm and 10 µm; c-d) 15 µm and 5µm; e-f) 6 µm and 2 µm; and g-h) 4.5 µm and 1.5 µm.

To further investigate the morphology and uniformity of the microstructured PDMS films, both tilted and top-viewed SEM images of the PDMS films with different pyramidal pattern sizes, namely 30 µm, 15 µm, 6 µm and 4.5 µm, are characterized. As presented in Figure 3.6, all the patterns keep perfect pyramidal structure with high uniformity, providing a stable and reliable platform for tactile sensing. Many fabrication methods have been developed to deposit nanoscale films on flat substrates. However, it is difficult to deposit homogeneous conductive layers on curved or three-dimensional structures by commonly used methods such as spin-coating, dip-casting, drop-drying or transfer-printing. For 3-D pyramidal microstructures, films generated by these methods will have high thickness at the bottom while leaving the tips of pyramids thin or even exposed. For tactile sensing applications, it is important to ensure the uniformity of the sensitive layers. Here we use layer-by-layer (LBL) assembly process to deposit conductive graphene layers on the microstructured PDMS films.

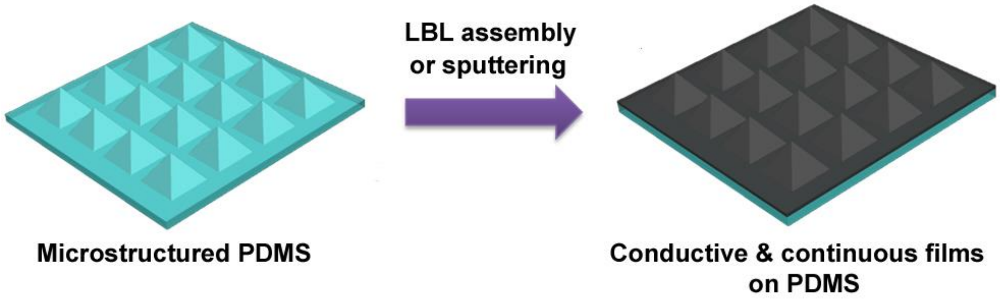

Figure 3.7. Schematic illustration of depositing conductive layers on PDMS films with microstructures.

LBL assembly, using polyelectrolytes with opposite charges, is a common technique to fabricate uniform films because of its simplicity and versatility. Another benefit is that, thanks to the conformal and self-limiting property of LBL assembly, the fabricated film can take on the shape of the curved substrate, which cannot be expected for other methods such as dip-casting or transfer-printing. Also, continuous films can be deposited onto the PDMS microstructures through thermal evaporation or RF sputtering methods. However, these methods generate high temperature to substrates during operation process, and the as-deposited films on PDMS suffer poor mechanical issues.

3.3.2 Embedment of Metal Nanowires into Microstructured PDMS films

Another effective way to fabricate conductive microstructured PDMS films is to embed metal nanowires. A schematic of an experimental process is illustrated in Figure 3.8. Firstly, AgNWs are dropped and dried on the silicon master. Then PDMS precursor and cross-linker mixture is casted on the master and degassed in vacuum to remove bubbles. After a curing process, the PDMS is peeled off, and the AgNWs will be embedded into the microstructured PDMS films because of the weak adhesive force between the AgNWs and the silicon master.

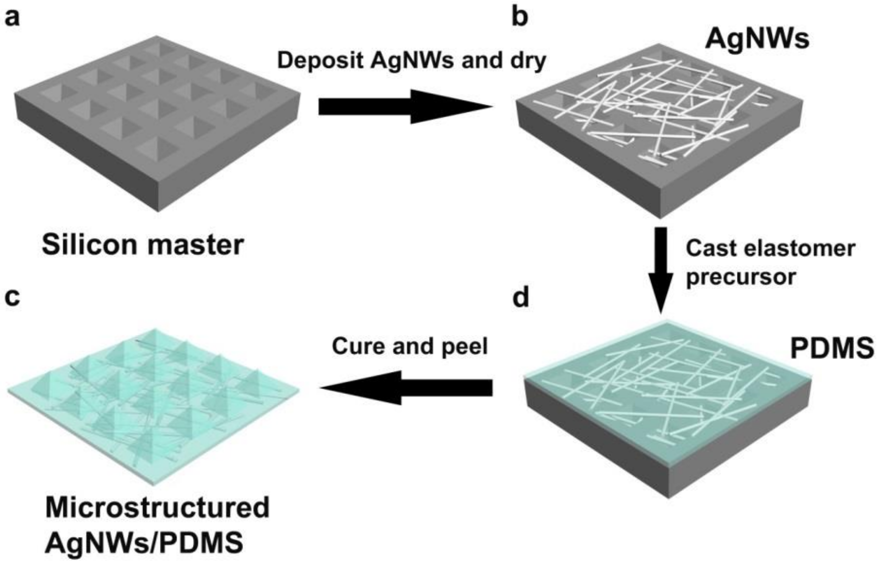

Figure 3.8. Schematic illustration of preparing microstructured AgNWs/PDMS films.

3.4 Experimental Setup for Measurement of Sensor Performance

Resistive tactile sensors transduce applied force/pressure stimuli into the resistance changes of sensitive layers. In this thesis, to quantify the tactile sensitivity of a sensor, a motorized vertical test stand (Mark-10 ESM301) combined with a digital force gauge (Mark-10 M5-2) are used to provide forces. By measuring the response area of a sensor, the value of applied pressure can be obtained. To characterize the electrical signals of a tactile sensor, a semiconductor parameter analyzer (Keithley 4200 semiconductor characterization system) is used to measure electrical performance, including current-voltage (I-V) and current-time (I-t) curves. An oscilloscope (Tektronix DPO5054B) is used to measure the voltage drop when a sensor response to applied pressure, signifying the response time.

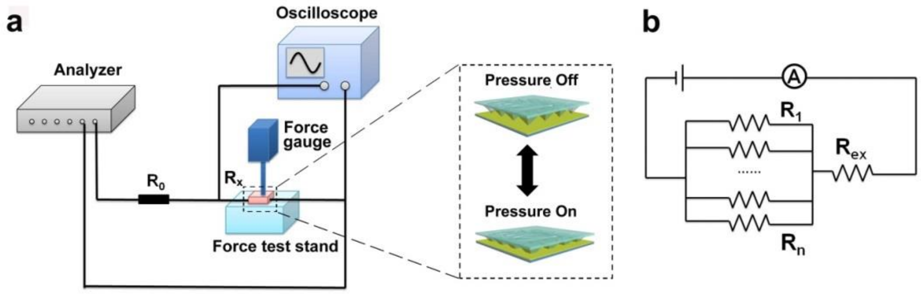

Figure 3.9. Schematic illustration of the experimental setup and circuit diagram. a) Equipment for measuring the pressure sensing performance of a tactile sensor. b) The equivalent circuit depicting the sensing mechanism of microstructures tactile sensors.

A schematic of the experimental setup is illustrated in Figure 3.9, where the analyzer provides a voltage bias to a tactile sensor (R_x) which is connected with a constant resistor (R_0) in series. A z-axis motorized test stand provides force to the sensor, where its value is measured by a force gauge. The dashed area in Figure 3.9a illustrates the working principle of the resistive tactile sensor, where the microstructured conductive film serves as the pressure sensitive layer, and a flat indium tin oxide coated flexible poly(ethyleneterephthalate) (ITO/PET) film acts as the bottom electrode. The loading or unloading of a pressure will induce the deformation or recovery of the microstructure arrays, leading to change of the contact resistance between the pyramid patterns and the substrate. The conductive pyramidal microstructures face the flat ITO film, forming numerous connections. An equivalent circuit diagram is shown in Figure 3.9b. Each connection between the pyramid and ITO can be attributed to a resistor (R_n) with variable resistance value which responds to the deformation of the microstructures. Typically, the resistance of a tactile sensor decreases when external pressure is applied, because the microstructure deforms and the contact area between pyramid pattern and the bottom electrode increases. On the other hand, when external pressure is removed, the pyramid patterns will recover to its initial state because of the elasticity of the PDMS film, leading to the reduction of contact area and the increase of resistance values. A photo of experiment setup is shown in Figure 3.10.

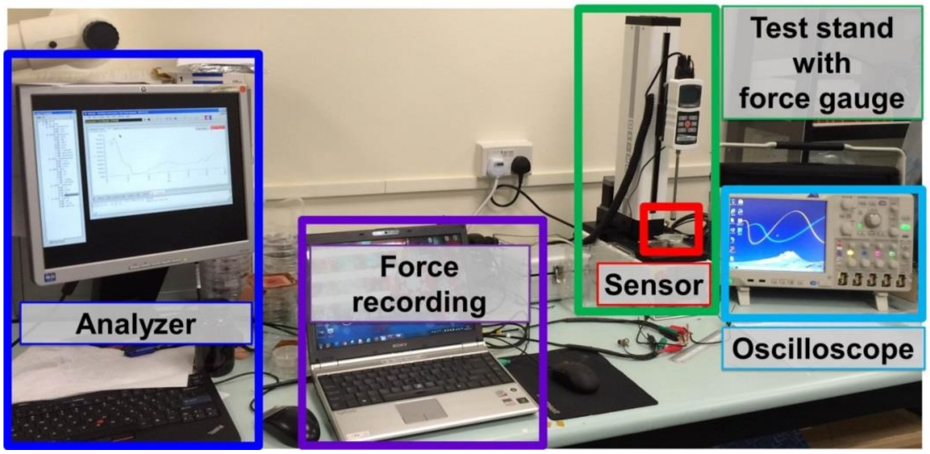

Figure 3.10. Experiment setup for characterizing the pressure sensing performance.

4. Highly Sensitive Tactile Sensor Based on Microstructured Graphene Arrays

Flexible tactile sensing devices with high sensitivity towards pressures in low range are highly demanded to emulate the exquisite tactile sensation of human skin. The introduction of anisotropic geometry and judicious selection of sensitive materials are two effective approaches to improve the sensitivity of a tactile sensor. In order to have the merits of both anisotropic effect and graphene material, we devise a tactile sensor applying graphene/PDMS films with pyramidal microstructures as pressure sensitive layers. The graphene microstructure arrays contribute to a sensitivity of 5.53 kPa^{-1} in low pressure range, an ultra-fast response time of <1 ms, and great stability and reliability. The sensor is capable of encoding tactile information in Morse code and measuring pulse signals, signifying great potential for the mimicry of human sense of touch.

4.1 Introduction

Natural skin demonstrates high tactile sensitivity so as to sense and perceive tiny mechanical stimuli in the environment, which enables humans to discern the properties of different objects and conduct precise manipulation works. To realize the mimicry of the exquisite tactile sensing capability of natural skin, judicious selection of sensing materials and configuration should be delivered to tactile sensing devices to render them highly sensitive towards pressure in low regime for detecting tiny forces or objects. The pressure value from several examples of external stimuli is presented in Figure 4.1. Tactile sensation in less than 1 kPa range is significant for sensing and distinguishing different stimuli. Thus, in this chapter, we are engaged in designing and fabricating tactile sensors with high sensitivity in low pressure range.

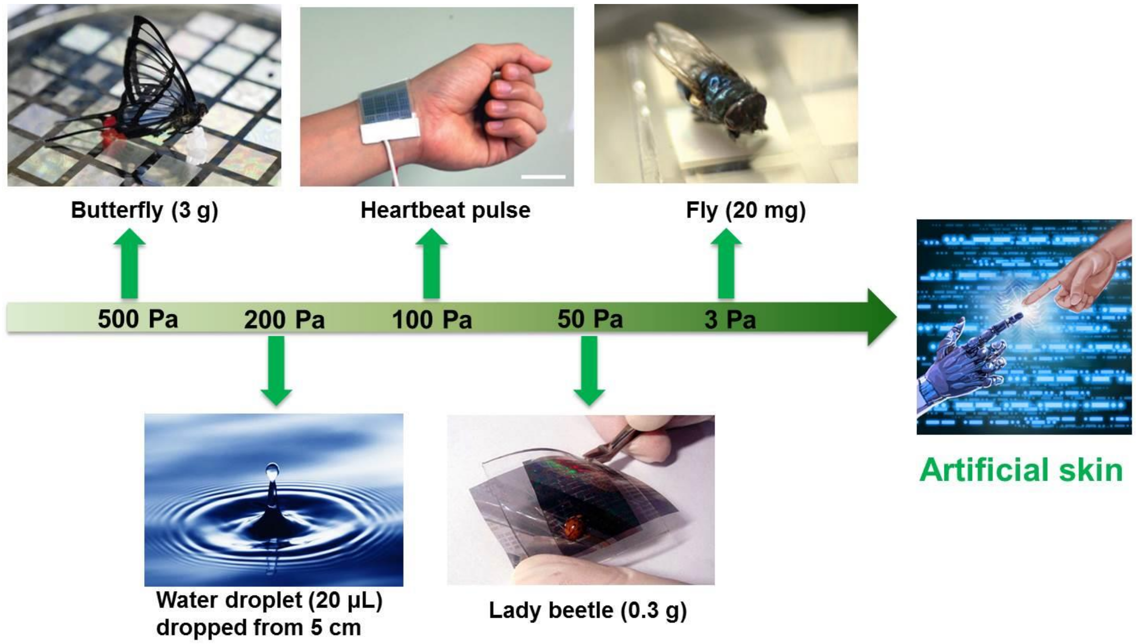

Figure 4.1. Significance of high sensitivity towards low pressure range. To make artificial skin emulate the sensation of natural skin, tactile sensors should be able to effectively detect pressures of <1 kPa. (Reprinted with permission from reference[18,32,59].)

As previously illustrated, many resistive sensor prototypes have been reported to emulate the high sensitivity of human skin. However, some intrinsic defects restrain their further utilization and demand vigorous improvements. For example, tactile using conductive rubber as sensitive layers can only respond to high pressures and suffers hysteresis. The sensitivity of strain gauges is limited by the flat cross-sections. Still, the development of high-performance flexible tactile sensors is rudimentary, and challenges remain in exploring tactile sensors with high sensitivity regarding to low-range pressure distribution (<1 kPa), short response time, and ease of fabrication as well as low power consumption.

One efficient way to improve the sensitivity is to introduce three-dimentional microstructures into tactile sensors. The sensors with pyramidal microstructures demonstrated superior sensitivity than their unstructured counterparts, because the sensitivity of the latter is limited by the constant sensitive area during deformation induced by applied pressure.[29,32,57] The anisotropic effect renders the microstructured tactile sensors highly sensitive in low pressure ranges together with a fast response time. Bao's group demonstrated that a capacitive sensor with microstructured sensitive layer showed 30 times higher sensitivity than its unstructured counterpart, and the sensor can detect a pressure value as low as 3 Pa.[32] By integrating microstructred PDMS with triboelectric nanogenerators, Wang's group reported a highly sensitive self-powered pressure sensor which can even sense a falling feather that corresponding to only 0.4 Pa.[57]

On the other hand, the selection of conductive materials is also important for transducing external force into electrical signals. To date, though metallic films and conducting polymers have been well utilized in flexible pressure sensors and have shown good performance, graphene, a two-dimensional carbon based material, has attracted increasing attention due to its unique mechanical and electrical properties.[74-78] Graphene is a promising material with fascinating properties which has been vigorously developed for various applications in nanoelectronics, energy conversion and storage, catalysis as well as sensors.[79-81] In particular, graphene's unique physical properties render itself capable of being utilized in next-generation electronics, especially flexible devices.[79] In the last several years, a wide range of high performance flexible devices based on graphene have been reported, such as thin film transistors, sensors, solar cells, lithium-ion batteries and supercapacitors.[82-84] Hardly can be achieved by metallic films or conductive polymers, graphene's unique properties endow it with promising potential to be applied as pressure sensitive materials to transduce external mechanical stimuli or contacts to electrical signals for utilization in high-performance flexible tactile sensors for emulating the sensation of tactility in natural skin.

Graphene oxide, a precursor material of graphene, is highly negatively charged in aqueous suspensions, which is suitable to generate graphene films on 3D microstructures through LBL assembly process. After chemical reduction, the conductivity of graphene films can be recovered. LBL assembly process relies on the electrostatic attraction of polyelectrolytes with opposite charges. It has been broadly applied to prepare nanoscale films in the last decade because of its efficiency. Graphene films fabricated by LBL assembly have been applied as water and gas barriers membranes because of the good mechanical strength.[85,86]

In this chapter, to significantly improve the sensitivity of sensors in low pressure range, we combine the advantages of both graphene and microstructure configuration, and devise a highly sensitive microstructured graphene arrays-based flexible tactile sensor through LBL assembly method. The pressure response of the sensor results from the change in resistance resulting from the deformation of microstructures under pressure. A sensor prototype shows a maximum sensitivity of 5.5 kPa^{-1} in the pressure range of <100 Pa. Moreover, sensors using microstructures of different pattern sizes demonstrated different sensitivities, paving the way for designing and fabricating multilevel tactile sensing systems for mimicking the different sensation characterizes of different body parts. For example, highly sensitive sensors can play the role of fingertips, while sensors with low sensitivity can mimic the sensation of less sensitive body parts such as elbows. Also, an ultrafast response time of 0.2 ms together with a detection limit of only 1.5 Pa are achieved.[59]

4.2 Materials and Methods

3D graphene arrays were fabricated onto the PDMS film with pyramidal microstructures through a LBL assembly method using graphene oxide as precursor. After a reduction process, reduced graphene oxide (rGO) microstructured film was achieved and served as the sensitive layer in a resistive tactile sensor. The performance of the sensor is characterized by the experiment setup described in Chapter 3.

4.2.1 Synthesis of Graphene Oxide

Graphene oxide was synthesized by a modified Hummers method. In a typical process, 0.75 g of $NaNO_3$ was firstly dissolved in concentrated H_2SO_4 of 34 mL. Then, 1 g graphite powder (Sigma, <45 μm) was added at 0 ° C cooling by water/ice mixture.

$KMnO_4$ of 5 g was used to oxidize the graphite powder with vigorous stirring. After keeping the mixture at 35 °C for 2 h, distilled water of 50 mL was slowly dropped into it at 0 °C and stirred for another 2 h. Then, H_2O_2 of 4 mL was dripped into the solution with vigorous stirring until no bubble was generated. The color of the mixture changed from brown to yellow when H_2O_2 was added. The solid mixture was filtered and then dispersed and washed by HCl (500 mL, 1:10) followed by distilled water (500 mL). To remove ions in solution, the mixture was dispersed in water and centrifuged for many times until the pH value of the solution reaches five. To obtain thin layer graphite oxide sheets, the resultant graphite oxide was sonicated in water for 5 h, and then centrifuged at 4000 rpm. Then the GO suspensions were collected from supernatants.

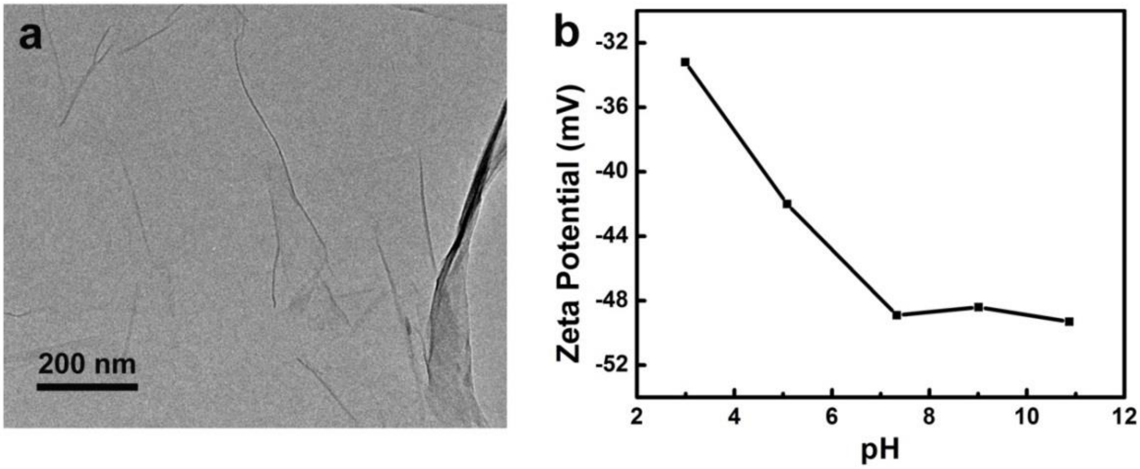

Figure 4.2. Characterization of as-prepared graphene oxide sheets. a) A TEM image of GO sheet. b) The negative zeta potential of GO suspensions decreases with increased pH values, showing that GO sheets have abundant negative charges.

A TEM image and zeta potential of the as-prepared GO suspensions are shown in Figure 4.2. The high negative value of the zeta potential indicates that the GO sheets possess a large amount of negatively charged groups.

4.2.2 Preparation of Microstructured Graphene Arrays

As illustrated in Figure 4.3, graphene oxide sheets contains many negatively charged groups, such as hydroxyl, epoxide, as well as carboxyl groups, rendering GO highly negatively charged which is suitable for fabricating nano-scale films by LBL assembly method. Polyethyleneimine (PEI), a positive polyelectrolyte, is used to provide electrostatic attraction force with GO sheets (Figure 4.3b).

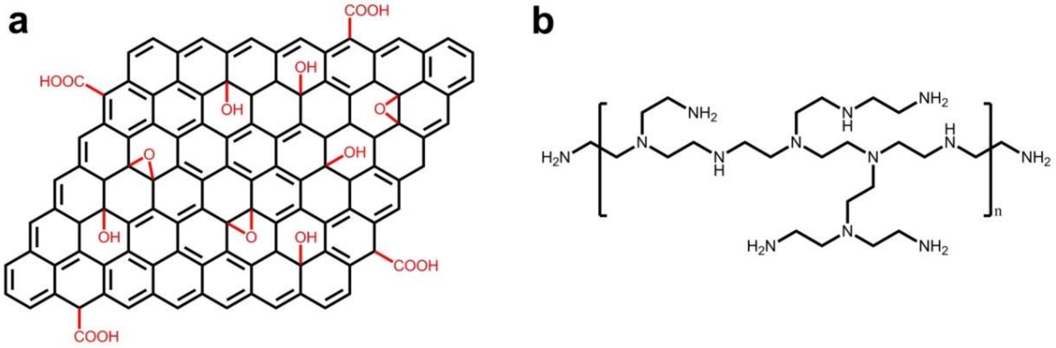

Figure 4.3. Chemical structures of GO and PEI. a) Many negatively charged groups exist in the GO sheet. b) The amine groups make PEI highly positively charged.

A schematic of the LBL process is illustrated in Figure 4.4a. In a typical experimental process, PDMS film was treated to be hydrophilic by introducing hydroxyl groups onto its surface by O_2 (200 mTorr) plasma with 200 W power for 1 minute. Before conducting LBL process, the pH value of both GO suspensions and PEI solutions was adjusted to 9.0; the former is neutralized with ammonia and the latter with hydrochloric acid. The film was then placed in PEI (Mw ~ 750,000, Sigma) aqueous solution (2.5 g/L) for 10 minutes. Then the film was washed with distilled water and dried with N_2 gas. The PEI-modified PDMS film was then dropped in GO suspensions (0.5 g/L) for 10 minutes, and washed and dried with water and N_2 gas too. The PDMS film was alternately immersed and modified with PEI and GO sheets for 10 cycles to form $(PEI/GO)_{10}$ multilayer films.

Finally, the graphene oxide multilayers were reduced to graphene films through a vapour reduction process by hydrazine at 90 °C. Digital photos of microstructured pure PDMS film, film with GO multilayers, and film with rGO layers are shown in Figure 4.4b, 4.4c and 4.4d, respectively. After reduction, the film's colour changed from brown to black.

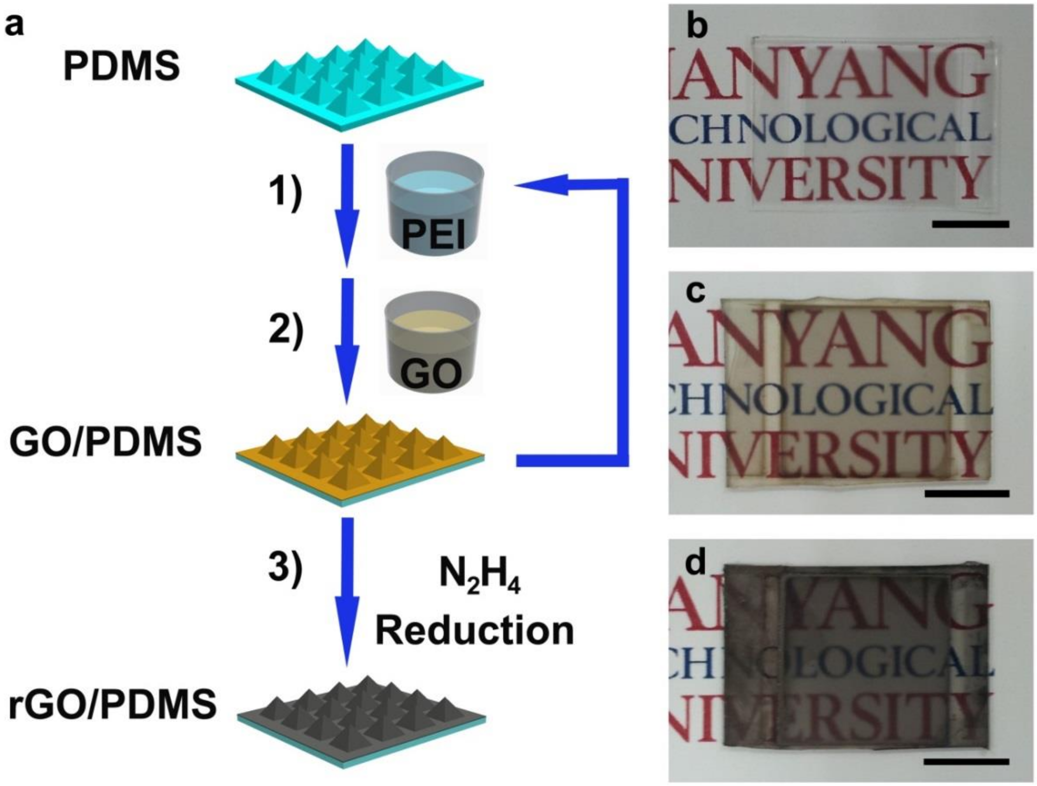

Figure 4.4. LBL assembly procedure of fabricating reduced graphene films on microstructured PDMS films. a) Schematic illustration of the fabrication procedure. b) A free-standing PDMS film with microstructure patterns. c) PDMS film deposited with GO multilayers after LBL process. d) PDMS film with rGO layers. Scale bars: 1 cm.

4.2.3 Preparation of Tactile Sensor Device

To prepare a tactile sensor prototype, the graphene/PDMS film is laminated onto an ITO counter electrode, forming numerous connections between the graphene arrays and the substrate. Silver paint (Structure probe, Inc.) was used to connect graphene films or ITO/PET film with copper wires for electrical characterization.

4.2.4 Microstructured Graphene/PDMS Based Tactile Sensor

The morphologies of the microstructured graphene films were characterized by Field Emission Scanning Electron Microscopy (FESEM) (JSM-7600F) and Transmission Electron Microscope (TEM) (JEOL 2010). Raman spectra were characterized by confocal Raman microscope (WITec, 488 nm). Contact angel was measured by FTA32. Resistance was meausured by Keithley 4200 semiconductor parameter analyzing system. Response time of the sensor was recorded by an oscilloscope (Tektronix MDO4104-6). The sensitive area of a tactile sensor is 2 cm^2.

4.3 Results and Discussion

4.3.1 Property of Microstructured Graphene Arrays

The property together with the morphology of the microstructures of the as-prepared graphene films are characterized to demonstrate the feasibility of applying LBL method to prepare continuous conductive graphene arrays with high regularity. A digital photo of as-prepared microstructured graphene/PDMS film is shown in Figure 4.5a, where the interference fringes clearly indicate that the film possesses patterns with high uniformity. The pyramidal microstructures can be clearly observed in an optical image of the graphene/PDMS film (Figure 4.5b). In the Raman spectrum (Figure 4.5c), the peaks at about 1340 cm^{-1} and 1590 cm^{-1} are inaccordance with the D band and G band of both GO and RGO, respectively. After reduction, the G band has a small down-shift to the G band of graphite (1580 cm^{-1}), indicating a recovery of honeycomb networks of carbon atoms. The D/G intensity ratio shows an increase which suggests a decrease in the average sizes of sp^2 domains. This is becasue that rGO has more numerous numbers of sp^2 domains than GO, but the new domains have smaller sizes.[87]

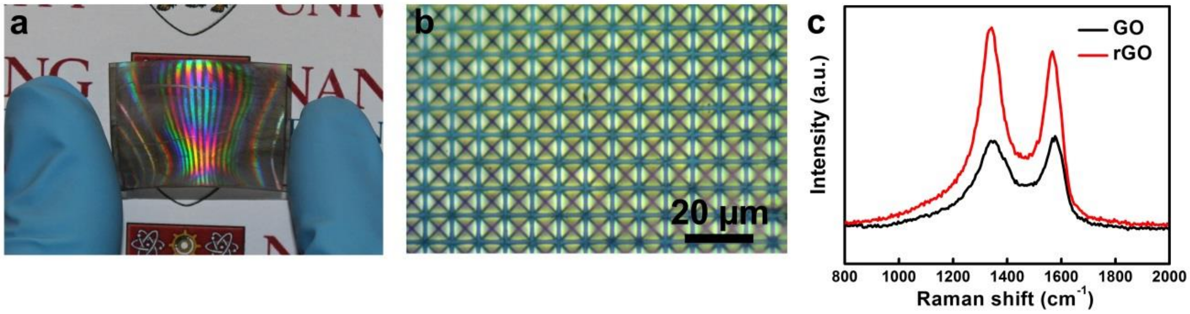

Figure 4.5. Photo and Raman spectrum of as-prepared graphene/PDMS films with pyramidal microstructures. a) Digital photo of free-standing graphene/PDMS film. b) Optical image of the graphene/PDMS film. c) Raman spectra of the film before (GO) and after reduction (rGO).

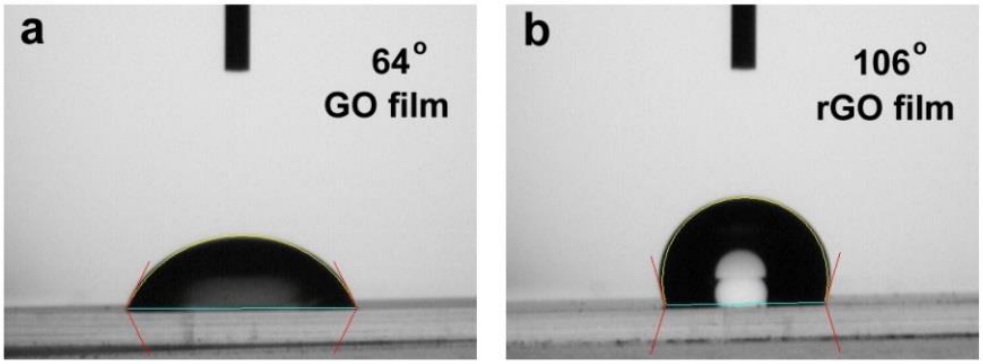

Figure 4.6. Contact angles of GO film and rGO film.

The contact angle of rGO film (106°) is higher than that of GO films (64°) on flat PDMS films (Figure 17). This confirms that the hydrophilic groups of graphene oxide reduced and honeycomb carbon networks recovered after reduction by hydrazine.

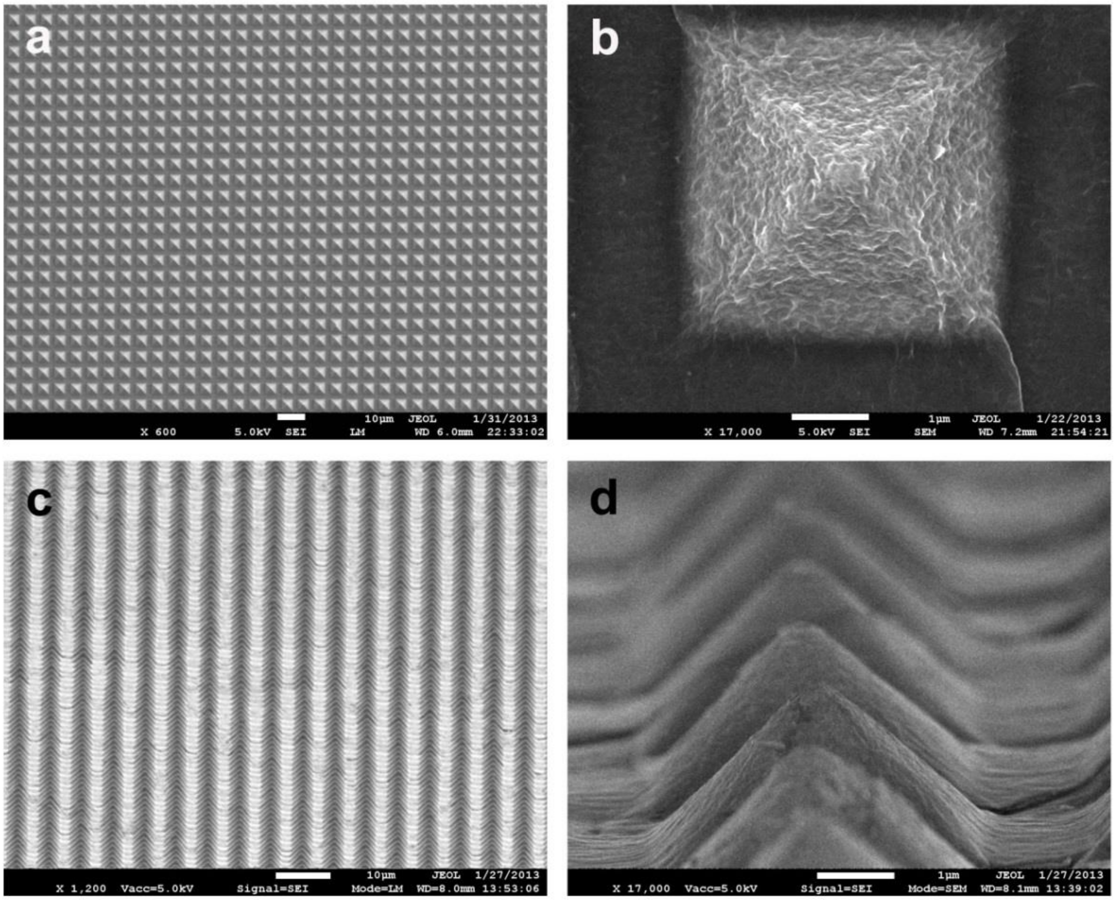

Figure 4.7. SEM images of as-prepared microstructured graphene films on PDMS. a,b) Top-view and tilted-view of the graphene film with pyramidal microstructures. b,d) Enlarged SEM images of the pyramidal patterns. Wrinkles of the graphene film can be viewed. The images were captured without sputtering thin metal layers.

The scanning electron microscopy (SEM) images of graphene/PDMS films with pyramidal microstructure arrays are shown in Figure 4.7. The as-prepared graphene films possess the pyramid configuration of the PDMS substrate with a pattern length of 4.5 µm. The size of an individual graphene pyramid is determined by the pattern sizes of the photomask used in photolithography process. From SEM images (Figure 4.7b, 4.7d) of high magnification, graphene wrinkles can be directly viewed.

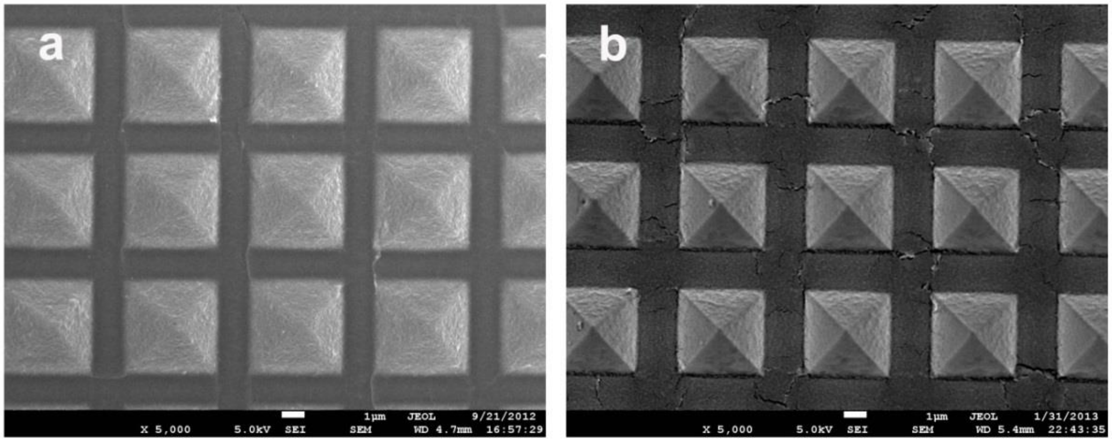

Figure 4.8. SEM images of microstructured graphene film through LBL assembly and Pt film by sputtering.

Compared with metal films deposited on PDMS by sputtering process, the as-prepared graphene films through LBL method exhibit superior continuity, which can be verified by the SEM images in Figure 4.8. The graphene films are intact and continuous thanks to the strong electrostatic attraction force and π–π stacking interactions between GO sheets and PEI in the LBL process (Figure 4.8a), while the Pt film (Figure 4.8b) suffers from inevitable cracks.

Another merit contributed by LBL assembly method is that graphene microstructures with different pattern sizes (pyramid length = 30, 15, and 6 µm) could be fabricated without scarifying the high uniformity. Also, the ratio between pyramid pattern length and distance can be readily controlled during photolithography process. SEM images of these microstructured graphene films are presented in Figure 4.9. Each sample retains the pyramidal geometry with high regularity regardless of the feature size of pattern.

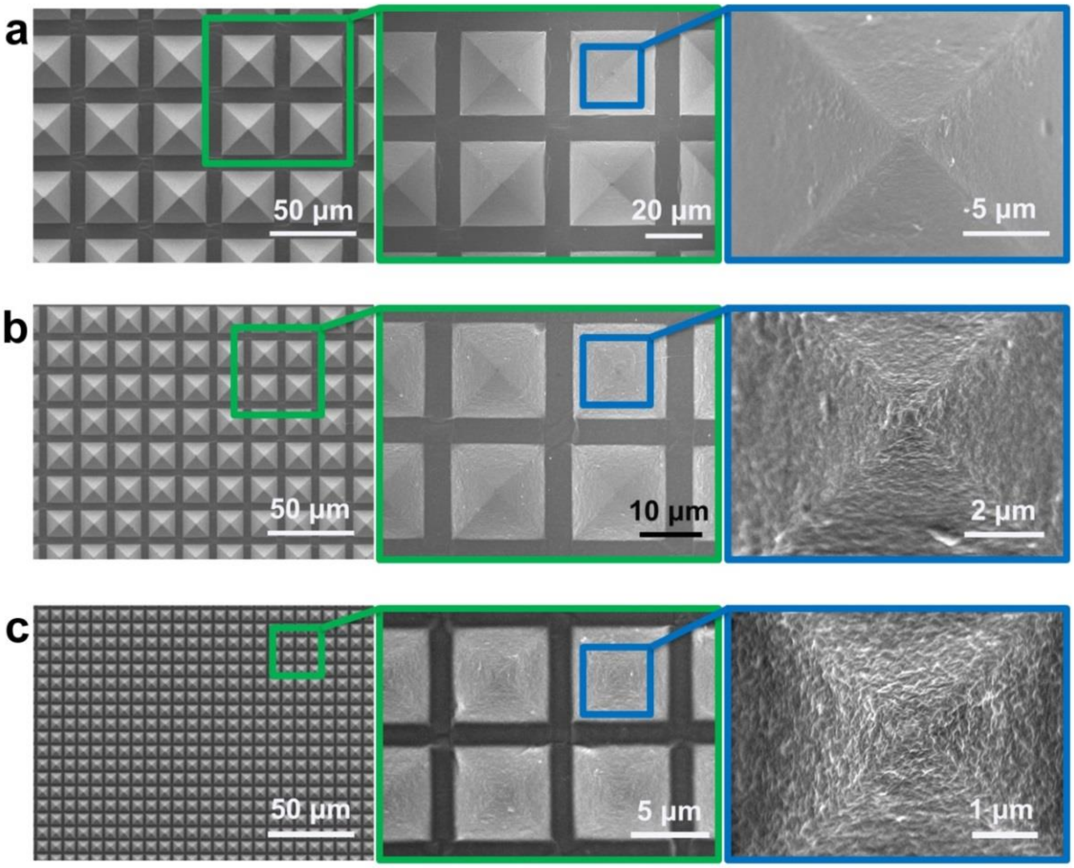

Figure 4.9. SEM images of graphene/PDMS films with different pattern sizes. a) Pattern length: 30 μm; distance: 10 μm. b) Pattern length: 15 μm; distance: 5 μm. c) Pattern length: 6 μm; distance: 2 μm.

4.3.2 Pressure Sensing Performance of graphene/PDMS Based Sensor

The working principle is schematically illustrated in Figure 4.10. A bias of 1 V is supplied with the device. The microstructured graphene/PDMS films contact with the ITO surface to form numerous conductive connections. Applied external pressure will induce the deformation of pyramid structures and increases the contact area between the pyramids and substrate, causing resistance decrease of the device. When the pressure is removed, the pyramid patterns will reach to their original place because of the elastic property of PDMS. To optimize sensitivity, the film with pattern length of 4.5 μm was selected.

Because applied pressure cannot influence the resistivity of graphene or ITO films, thus, the pressure sensing response can be mostly attributed to the deformation of the pyramidal microstructures.

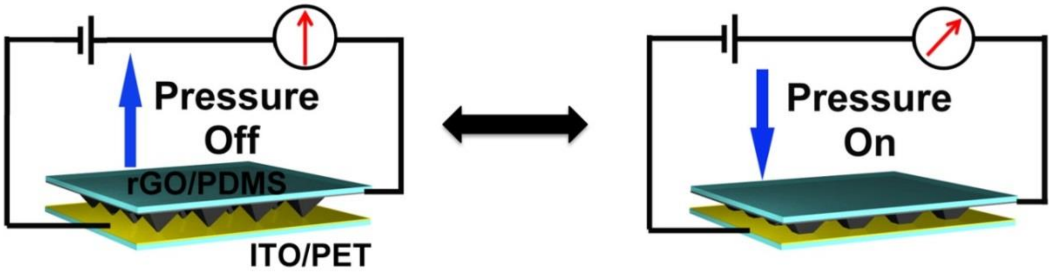

Figure 4.10. Schematic illustration of the sensing mechanism of the microstructured graphene films based tactile sensor.

The current-voltage curves of the sensor responding to applied pressure are illustrated in Figure 4.11a. Without the application of pressure, the I-V curve shows a straight character, indicating the graphene microstructures have Ohm contact with the ITO electrode. Thus pressure response of the device originates from the deformation of pyramidal microstructures, rather than from the increase or decrease of conductive paths. The current through the sensor increases with the addition of applied pressure. The pressure sensitivity is defined by the slope of the relative resistance change toward applied pressure:

$$S = \frac{\delta \Delta R / R_0}{\delta P}$$

Where R_0 is initial resistance value, ΔR is resistance change towards the application of a pressure of P. Graphene/PDMS film without microstructures prepared with the same LBL assembly process method was applied as comparison. As illustrated in Figure 4.11b, sensors that with unstructured graphene films as sensitive materials illustrates a low sensitivity of 0.1 kPa^{-1} (Figure 4.11). Absence from the contribution of pyramid microstructures, pressure response of the unstructured device mainly originates from the compression of graphene films other than the deformation of microstructures. When pressure is applied, the graphene sheets are compressed, resulting in a decrease in the resistance. On the other hand, pressure response of the microstructured sensor mostly derives from the deformation of pyramid structures. The pressure sensitivity of microstructured sensor shows a distinct difference from that of the unstructured one. It showed a high sensitivity of 5.53 kPa^{-1} in pressure ranges of <100Pa, which is 50 times of the sensitivity of the sensor without microstructures. The sensitivity becomes saturated above 100 Pa, which can be attributed to the increased elastic resistance of the compressed pyramid PDMS.

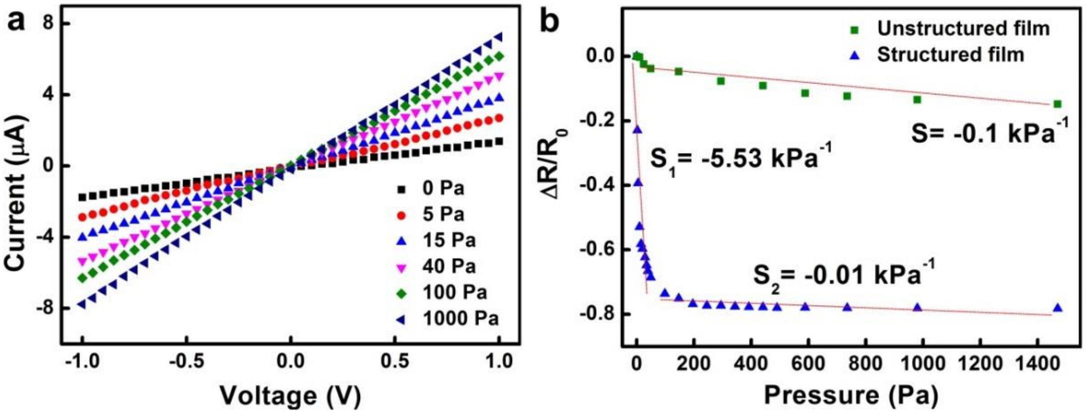

Figure 4.11. Pressure sensing performance of a microstructured graphene/PDMS based sensor. a) Typical current-voltage curves of a sensor responding to applied pressure. b) Sensitivities of the sensors with and without microstructure arrays.

The difference in performance between the unstructured and microstructured films results from the different sensing mechanisms: resistance change of the former relies only on the compression of graphene sheets which promise a small sensitivity, while that of the later one mainly comes from deformation of pyramid structure which affords higher sensitivity and stability.

To study the influence of different feature sizes on the sensitivities, we also compared the pressure response of microstructured films with pyramid pattern length of 6 μm, 15 μm and 30 μm, whose sensitivities are lower than that of the 4.5-μm-sized one, yet higher than that of the unstructured one (Figure 4.12). The diverse performance among pyramid microstructured films with different pattern sizes lies in the difference of total numbers of pyramid patterns and distinct deformation extents. With a certain area, the number of pyramid patterns with a small feature size is more abundant than that with a large feature size, thus more pyramid microstructures will deform in the former, resulting in a superior pressure response than the latter. Moreover, with a certain pressure, smaller pyramidal microstructures deform more, so the pressure sensitivity is much better than the one with larger feature size.

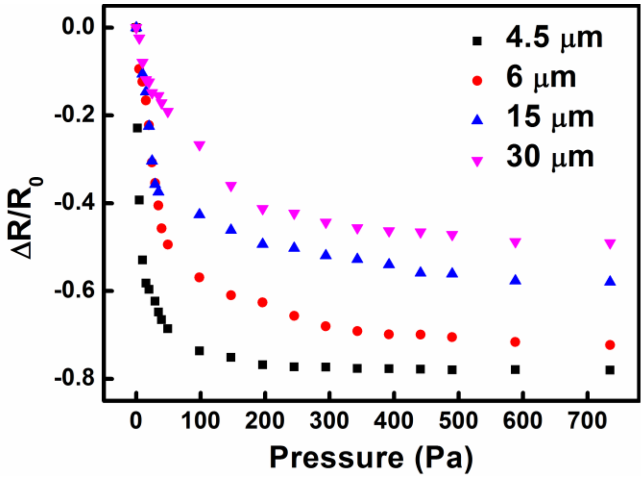

Figure 4.12. Sensitivities of tactile sensors with pyramidal microstructures of different sizes.

In addition to high sensitivity, reliability and fast response are important criteria for tactile sensors. To study the reliability of the sensor for sensing pressures in low range, we repeatedly apply and release a series of pressure with value of 1) 25 Pa, 2) 50 Pa, 3) 100 Pa and 4) 250 Pa, respectively (Figure 4.13a). The current change without hysteresis almost remains at an identical level to a certain pressure applied, revealing the excellent stability of the sensor in sensing pressure in low ranges. An instant I-t curve of the sensor when applied with a constant loading of 250 Pa for 10 cycles is showed in Figure 4.13b, indicating that it not only has a stable response to small pressures with no hysteresis.

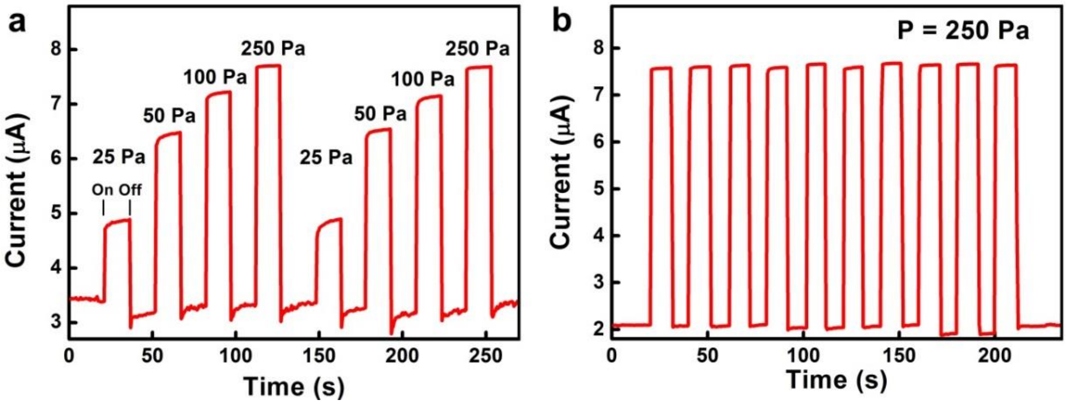

Figure 4.13. Instant I-t curves of the sensor towards applied pressure. a) The instant I-t curve of the sensor with regard to different external pressures. b) I-t curve of the sensor in responding to the loading/unloading a pressure of 250 Pa for 10 cycles.

Furthermore, the sensor is reliable to detect the loading/unloading of a staple (30 mg), corresponding to 1.5 Pa (Figure 4.14).

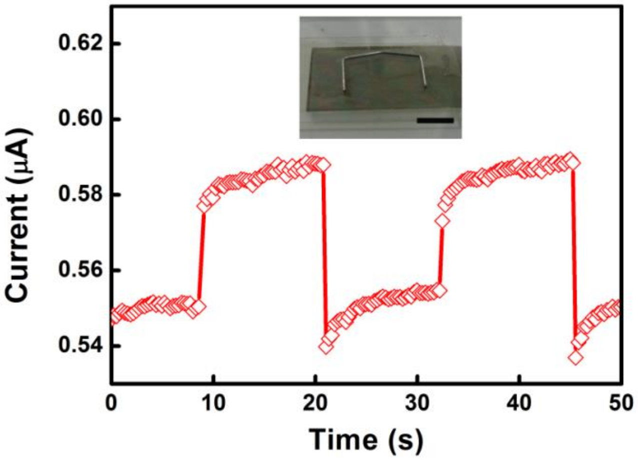

Figure 4.14. Instant I-t curve of a sensor when a staple of 30 mg are applied and removed for two cycles. The sensitive area is 2 cm^2. Scale bar: 5 mm.

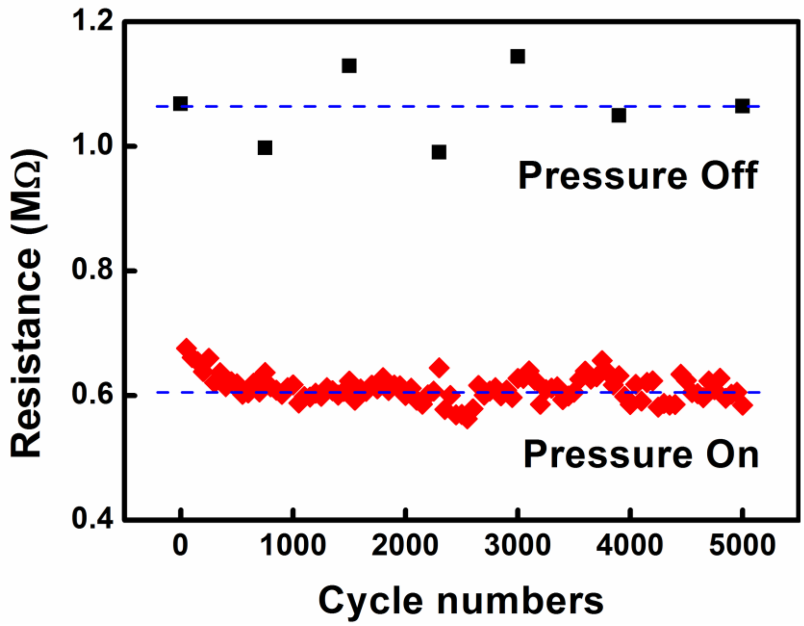

Figure 4.15. Resistance change of the sensor when loading and unloading a 100 Pa pressure for 5000 cycles.

Moreover, to further demonstrate the stability, we alternately load and unload a pressure of 100 Pa on the sensor for 5, 000 cycles (Figure 4.15). Despite a baseline fluctuation, in accordance with no pressure load, the sensor shows stable response to the loading of pressures, indicating a great stability of the microstructured graphene/PDMS films together with a promising potential for real application.

Also, the graphene microstructures endow the sensor with ultrafast response time to applied pressure, which can be confirmed by the rapid voltage drop of a constant resistor (500 kΩ) recorded by an oscilloscope when the sensor is applied with a pressure of 100 Pa (Figure 4.16). The resistor is connected with the sensor in series at a 1 V bias. From the insert of Figure 4.16, we can clearly notice an rapid voltage drop with a response time less than 1 milliseconds (0.2 ms), showing the ultra-fast response of the sensor and exhibiting a great potential of the microstructured graphene films for application in next-generation skin-like tactile sensing system.

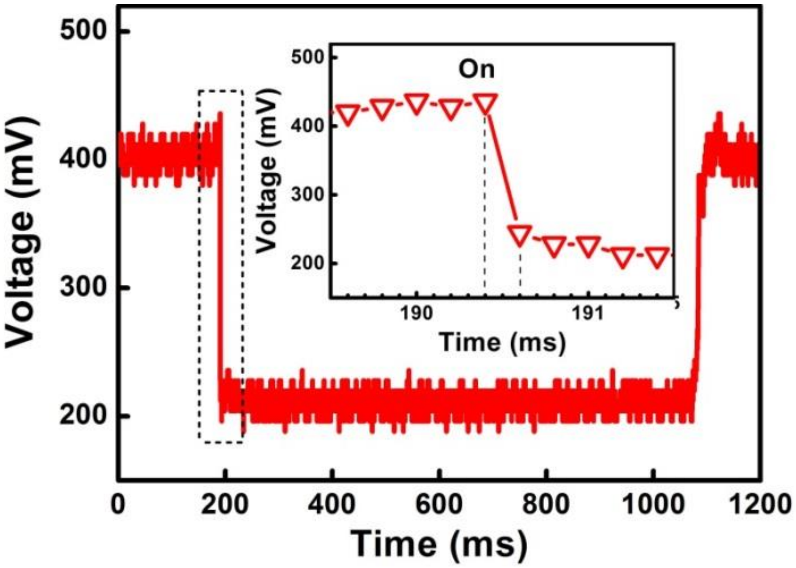

Figure 4.16. Voltage-time curve of the constant resistor connected with the sensor in series. Inset is an enlarged view of the dashed area, corresponding to loading a pressure of 100 Pa onto the sensor.

4.3.3 Applications of Microstructured Graphene/PDMS Based Tactile Sensor

To demonstrate the possibility of the sensor in the application of tactile sensing for the mimicry of natural skin, we used sensor prototype for conveying tactile information by encoding the signals into the Morse codes by virtue of its fast response time.

Figure 4.17a shows photos of the tactile sensor (top-right) and a sensor put on a model hand (down-left). Both static and temporal and tactile sensation information can be encoded by the short and long sequences in Morse code, respectively, where the “dots” corresponds to short-term signals, and the “dashes” are in accorded with long-term signals. By touching the sensor with different time scales, standardized sequences can be conveyed from fingers to the sensor. As for a demonstration, we applied certain sequences of touch, corresponding to the words of “AM” and “NTU”, onto the sensor, and the information can be readily transmitted (Figure 4.17b). Also, the information of “SOS”, consisting of a sequence of three dots, three dashes and three dots, can be transmitted from a finger to a sensor placed on the surface of a human hand (Figure 4.17c, d). (Figure 4d). For application in real environment, the time of encoding and conveying signals is capable of being reduced because of the ultra-fast response of the sensor.

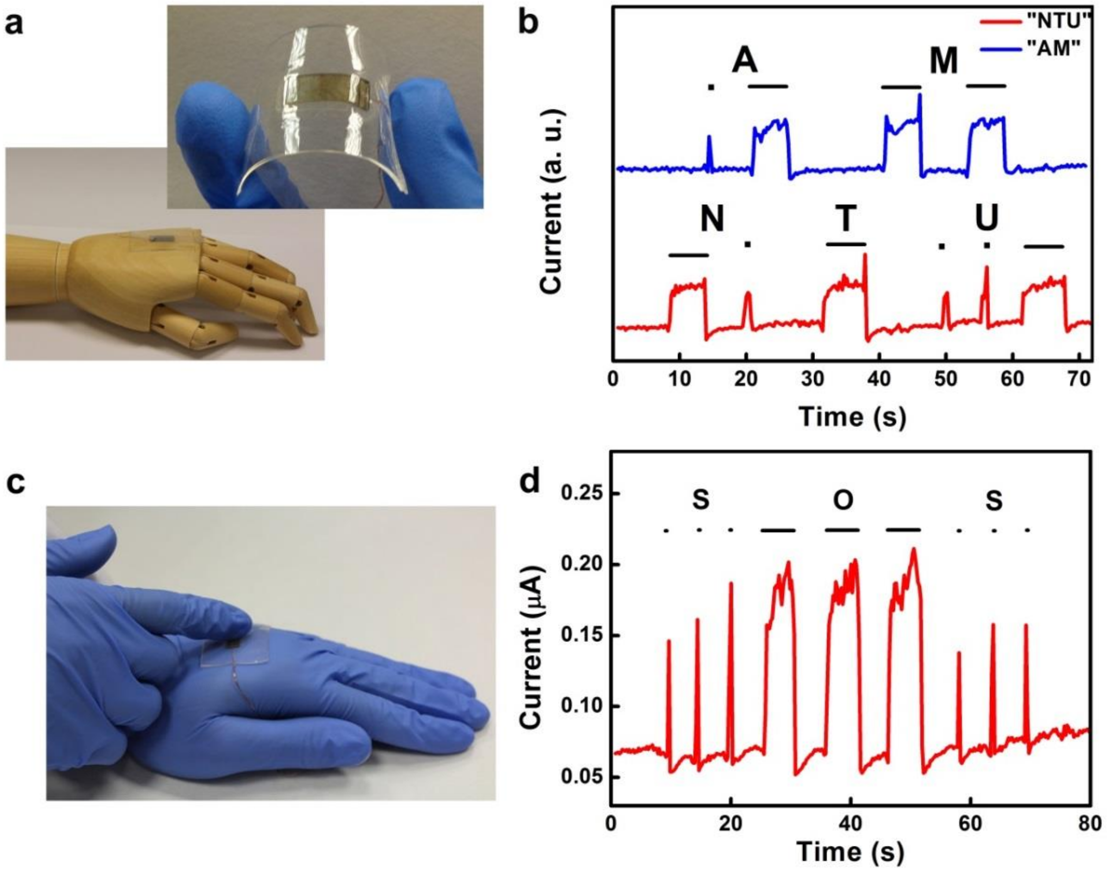

Figure 4.17. Demonstration of a sensor for information transmission. a) Photos of a tactile sensor (top-right) for conveying tactile information (down-left). b) Signal sequences indicating the words of “AM” and “NTU” in Morse code. c, d) To convey the information of “SOS” from one hand to another through touching the sensor.

Moreover, due to its high sensitivity in low pressure range, it is possible to use the sensor to measure human pulse wave signals. Figure 4.18a shows a sensor device attached to the human wrist. The sensor shows clear response to the pulse waves, demonstrating potential for diagnostics.

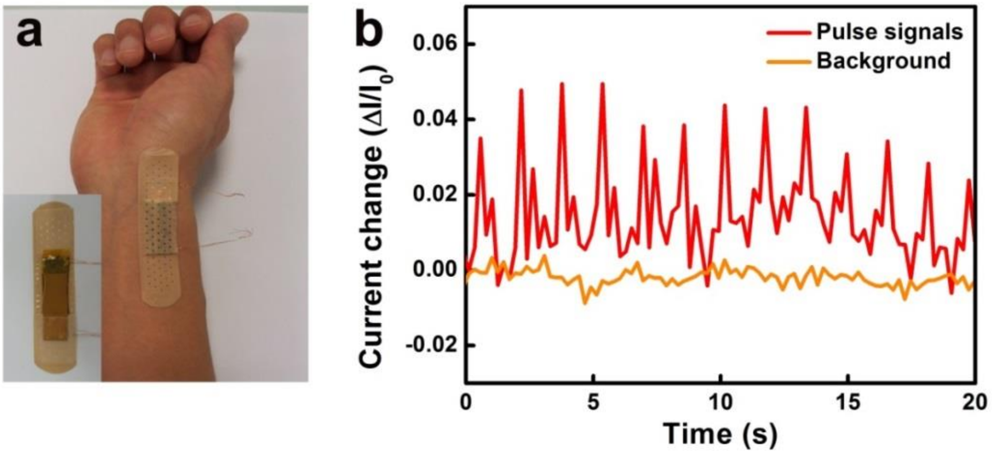

Figure 4.18. Application of a tactile sensor for measuring pulse wave signals. a) The tactile sensor is placed on the wrist of an adult man. b) Real time current change of the sensor with pulse signals.

4.4 Conclusion

In summary, a new type of highly sensitive flexible tactile sensor based on graphene/PDMS films with pyramidal microstructure arrays has been demonstrated in this chapter. The microstructured graphene films were fabricated on the PDMS film by a simple LBL assembly method and served as the sensitive layer of the resistive tactile sensor. The graphene microstructure arrays not only rendered the sensor a high sensitive of 5.5 kPa^{-1} in low pressure range, but also contributed to an ultra-fast response time of <1 ms together with a great stability. Furthermore, pressure sensitivity can be modified by adjusting the pattern sizes, providing a facile but effective way for being applied in different sensing environments. Also, the sensor illustrated great capability of encoding tactile sensations for information transmission and measuring pulse wave. The flexibility, ease and capability of large-area fabrication, and high sensitivity together with fast response time endow the microstructured graphene/PDMS based tactile sensor with promising potential for future applications in electronic skin and robotics for the mimicry of human sense of touch.

5. Skin-inspired Sensory Memory Arrays

Human skin responds to external stimuli and transmits sensory information to the brain through afferent nerves to form sensory memory, allowing humans to perceive the sensations so as to recognize the surrounding environment and conduct daily activities.[1,7] The exquisite sensations and tactile afferents of the skin have inspired the emergence of sensory memory devices that not only emulate the tactile sensation of natural skin, but retain the sensory information after external stimuli vanishes. In this chapter, the challenge of integrating highly sensitive pressure sensing devices with resistive switching memory devices, where a memory cell can be electrically programmed from high resistance state to low resistance state by the application in of pressure, is addressed. The integrated device arrays demonstrate high sensitivity in the low pressures regime in accordance with tactile sensing, but can retain the pressure information after the removal of external pressure for more than a week by virtue of the nonvolatile nature of the memory devices. The rational integration of pressure sensors and memory devices will allow for the mimicry of human sensory memory, opening new avenues for designing next-generation sensing systems for applications in electronic skins, humanoid robots and human-machine interfaces.

5.1 Introduction

5.1.1 Applications of Microstructured Graphene/PDMS Based Tactile Sensor

Sensory memory is the process by which the human body retains the sensations of interaction with human body after the external stimuli is removed, thus helpings humans describe the physical quantities in their environment and manipulate objects in daily activities.[7,88] Skin, the largest sensory organ in the human body, comprises a variety of sensory receptors and provides significant sensation information such as force, pain, shape and texture.[5,89] Skin perceives external stimuli and conveys the sensory information to the brain through afferent neurons to form haptic memory, allowing humans to remember the impressions of the stimuli applied on the skin (Figure 5.1).[2-4]

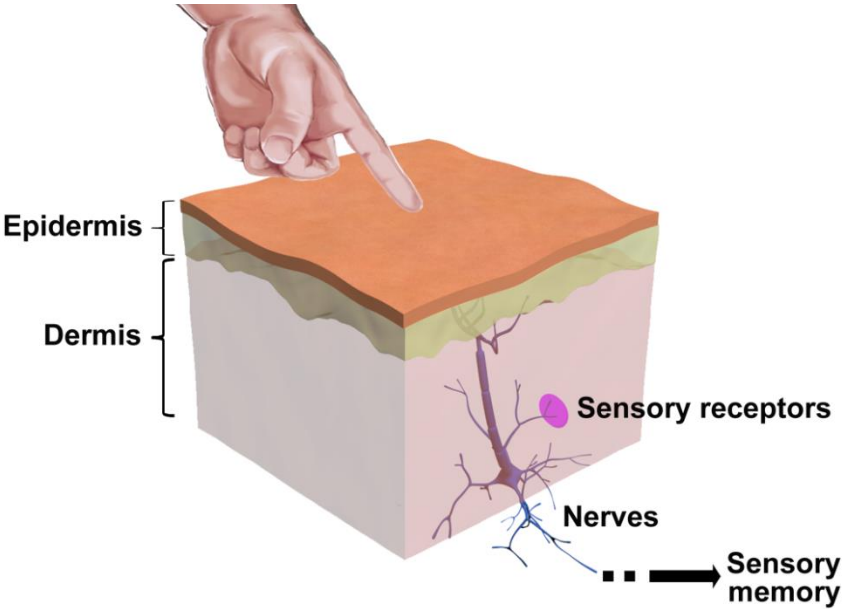

Figure 5.1. Schematic of human skin responding to applied pressure. When a finger touches skin, the sensory receptors perceive the force and convey the sensation information into brain through afferent nerves.

The recent decade has witnessed significant advancements in the design and integration of electronic skin (E-skin) devices in order to emulate the exquisite haptic sensation of natural skin.[8,90] One example is the improved sensitivity of pressure sensors towards the low-pressure regime. With the introduction of micro- and nano-structures, a tremendous increase in sensitivity for haptic sensing has been achieved. In addition a variety of intriguing properties together with various sensing units have been integrated with flexible pressure sensors to achieve multi-functionality so as to mimic the multiple sensing capabilities of natural skin. However, though current pressure sensing devices demonstrated capabilities in haptic sensing, they cannot retain the sensation information after the external stimuli were removed. This gap between the state-of-the-art E-skin devices and skin inspired the rational integration of memory devices into haptic sensors for the mimicry of haptic memory in natural skin presented here.

5.1.2 Resistive Switching Memory

Resistive switching memory has emerged as an excellent candidate for the integration with pressure sensors to achieve haptic memory because it could be utilized to emulate the memory functionality of the brain by constructing artificial neuromorphic networks as it behaves similarly to synapses among neurons in storing analogue value.[91-95] Resistive switching memory devices have emerged as promising candidates for future high-performance nonvolatile data memory to replace flash memory and dynamic random access memory (DRAM) due to their high density, large scalability, low power consumption, and high endurance and retention performance.[96-100]

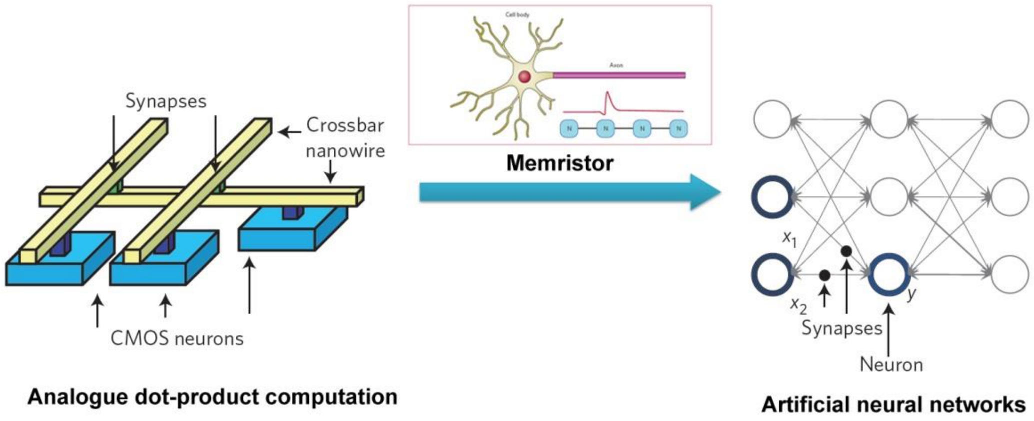

Figure 5.2. Prospective applications of resistive switching memory devices for building artificial neural networks. Synaptic circuits based on memristors process analogue computation, promising for building artificial neural networks. Each node can be attributed to a neuron, and the active potential can be mimicked by an electrical pulse. (Reprinted with permission from reference [95,100].)

Typically, a resistive switching memory cell comprises a capacitor-like two-terminal metal-insulator-metal (MIM) configuration, in which the insulating resistive switching material is sandwiched between two conductive electrodes. Information is stored and operated in resistive switching memory devices because a memory cell can be electrically configured between a high resistance state (HRS) and a low resistance state (LRS), corresponding to an OFF (0) and an ON (1) state, respectively (Figure 5.3a). In a similar way, a resistive pressure sensor reflects the loading or unloading of an external force by the changes in resistance. Typically, the resistance of a pressure sensor decreases when a pressure is applied, and vice versa (Figure 5.3b). Thus, the similarity lying in the resistive pressure sensor and resistive switching memory inspires us to integrate these two kinds of electric units together to realize the nonvolatile memory of applied pressure by programming memory cells with the resistance change in pressure sensors.

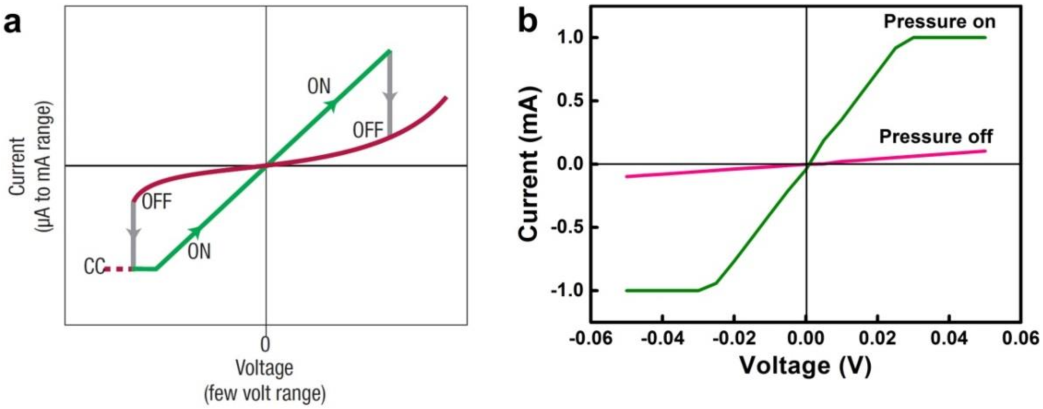

Figure 5.3. Typical current-voltage curves of a resistive switching memory device and a resistive pressure sensor. a) A certain voltage or current is required to program a memory cell from HRS to LRS. And the erase operation needs a voltage or current with opposite polarity. b) The resistance of a pressure sensor decreases with the application of pressure. (Figure 5.3a, reprinted with permission from reference [99].)

5.2 Materials and Methods

In this chapter, we successfully achieved the integration of resistive switching memory with resistive pressure sensor for the mimicry of the haptic memory of humans, where the resistance states in a memory cell can be electrically reconfigured by applied pressure on a pressure sensor. Moreover, the applied pressure distribution could be recorded by introducing memory cell arrays, where each integrated device could be attributed to combination of a pressure sensor and memory device that connect in series (Figure 5.4a). The integration of resistive pressure sensor and resistive switching memory devices is realized by replacing the bottom electrode of a pressure sensor with the electrode of a memory device (Figure 5.4b). In this way, the resistance changes in a pressure sensor induced by external pressures will result in the voltage changes on the electrode of a resistive switching memory cell, leading to its resistance state change, and the pressure information will be retained by the memory device.

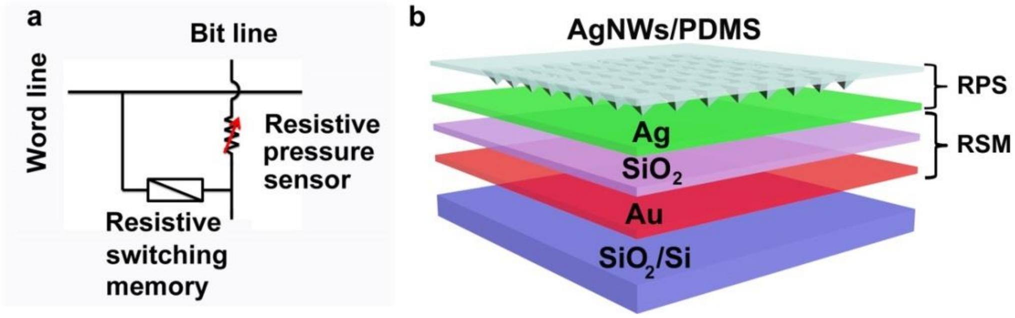

Figure 5.4. Design and integration of sensory memory devices to mimic the sensory memory of human. a) The proposed circuit diagram for the integrated device arrays. Each integrated device can be attributed to a combination of a resistive pressure sensor and a resistive switching memory device connected in series. b) Schematic illustration of the integrated device which comprises of pressure sensing and resistive switching memory devices.

The pressure sensor takes microstructured polydimethylsiloxane (PDMS) film embedded with silver nanowires (AgNWs) as sensitive layer. The introduction of microstructure arrays provides the pressure sensor with high sensitivity in low pressure regime (<1 kPa, in accordance to haptic sensing). The memory device takes advantages of typical MIM architecture with SiO_2 serving as switching layer, providing fast switching time, high endurance as well as nonvolatile memory by virtue of good resistance switching behaviors in SiO_2.[101,102]

5.2.1 Fabrication of Microstructured AgNWs/PDMS Films

The microstructured AgNWs/PDMS films were fabricated by curing PDMS precursor on microstructured silicon master cased with AgNWs (elucidated in chapter 3). Typically, 2 mL 0.5 mg/mL of AgNWs (SLV-NW-35, Blue Nano Inc., 35 nm diameter × 10 µm length) suspension was deposited and dried on the silicon master, which contained recessed pyramidal microstructure arrays. Then a mixture of PDMS elastomer and cross-linker was spin-coated on the master. After a degassing step, the elastomer precursor was cured and peeled off from the master. The convex pyramidal microstructures on PDMS replicated the patterns on silicon master. After peeling off the AgNWs were embedded on the surface of microstructured PDMS. The as-prepared AgNWs/PDMS are semi-transparent and flexible, with large-area fabrication capability together with good conductivity (Figure 5.5).

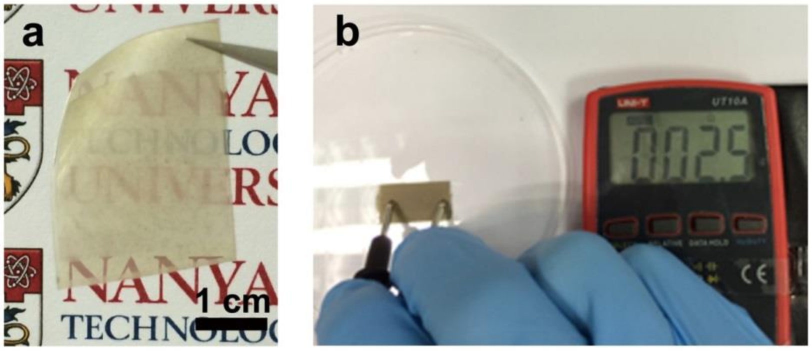

Figure 5.5. Conductive AgNWs/PDMS film with pyramidal microstructures a) A digital photo of as-prepared AgNWs/PDMS film. b) The as-prepared AgNWs/PDMS film shows a good conductivity (2.5 Ω).

Figure 5.6 shows scanning electron microscopy (SEM) images of the microstructured AgNWs/PDMS films, revealing that the film retains the regular pyramidal patterns after the placement of the AgNWs. The length of an individual pyramid pattern is 30 μm, controlled through photolithography process. The morphology of AgNWs can be clearly observed in the high magnification SEM image (Figure 5.6b). From the enlarged tilted SEM image (Figure 5.6d), sharp tips of the pyramids can be clearly observed, where the AgNWs were shaped with the same pyramidal microstructures. It is noteworthy that the SEM images were collected without sputtering a thin metal film, illustrating good conductivity of the film.

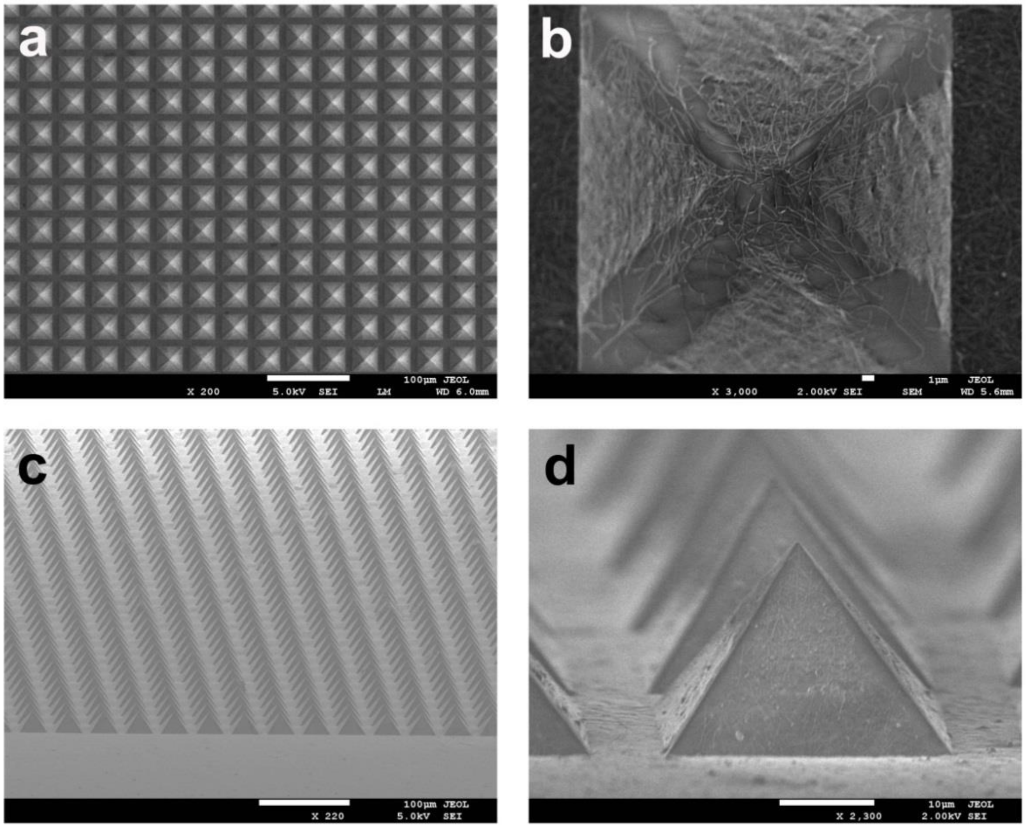

Figure 5.6. SEM images of as-prepared AgNWs/PDMS films with pyramidal microstructure arrays. The microstructures are perfectly retained after the embedment of silver nanowires. The length of an individual pyramid pattern is 30 µm. The morphology of AgNWs can be clearly observed in the enlarged images (b, d).

5.2.2 Fabrication of SiO_2 Based Resistive Switching Memory Device

In this study, the resistive switching memory cell employs MIM architecture of Ag/SiO_2/Au (Figure 5.7a). In a typical experiment, a 50 nm Au film with 5 nm Cr adhesion layer was deposited and patterned on SiO_2/Si substrate through thermal evaporation and photolithography methods to serve as the bottom electrodes. Then the SiO_2 insulating layer of 100 nm was deposited onto Au electrode patterns by RF sputtering. Finally, the Ag electrodes, with an area of 400 × 400 μm^2, were aligned and patterned on the top of SiO_2 film via a second photolithography process.

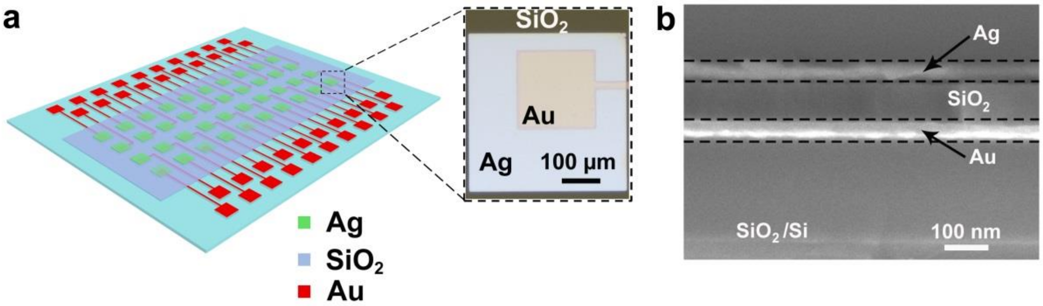

Figure 5.7. Resistive switching memory devices with layered structure of Au/SiO$_2$/Ag. a) Schematic illustration of the aligned MIM structure. Dashed area shows an individual memory cell (Au: bottom electrode; SiO$_2$: resistive switching layer; Ag: top electrode). b) Cross-section SEM image of the memory device with a layer-by-layer configuration on silicon wafer.

Figure 5.7a shows an optical image of an individual memory cell, where Au top electrode is aligned beneath the Ag top electrode to form a layered MIM architecture. The cross-section of a memory cell is illustrated in Figure 5.7b, where the layered structure can be clearly observed.

5.2.3 Integration of Memory Devices with Pressure Sensors

The memory device is then integrated with pressure sensor by placing the microstructured AgNWs/PDMS film face-to-face to the Ag electrodes of the memory cell arrays, where the Ag electrodes serve as both the bottom electrode of the resistive pressure sensor and the top electrode of resistive switching memory devices.

5.3 Results and Discussion

5.3.1 Pressure Sensing of Microstructured AgNWs/PDMS Films

The introduction of pyramidal microstructure patterns could contribute superior sensitivity to pressure sensors regardless of sensing techniques due to their anisotropic configuration, which has been introduced in previous chapters. Here, the microstructured AgNWs/PDMS film serves as the sensitive layer in the resistive pressure sensor. By applying the AgNWs/PDMS film onto a flat indium tin oxide (ITO)-coated flexible poly(ethyleneterephthalate) (PET) film, the pyramidal microstructure patterns face the conductive ITO film, forming infinite connections between pyramid tips and ITO substrate. Figure 5.8 illustrates the working principle of the resistive pressure sensor, where the AgNWs/PDMS film serves as both the top electrode and pressure sensitive layer, and ITO film acts as the bottom electrode. The loading or unloading of a pressure will induce deformation in the PDMS microstructures so as to change the contact resistance between the pyramids and substrate.

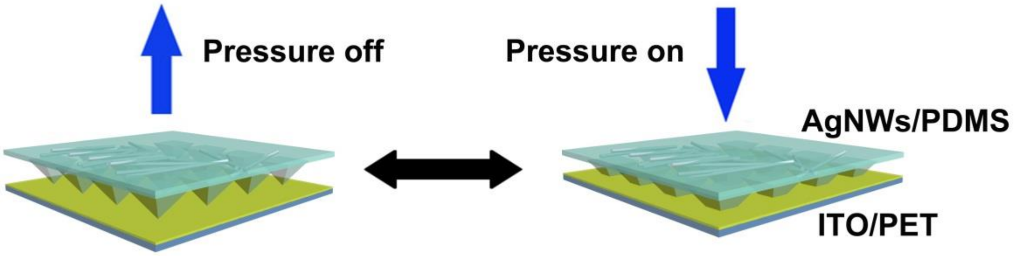

Figure 5.8. Schematic illustration of the sensing mechanism of the microstructured AgNWs/PDMS based pressure sensor. Applied forces induce the deformation of pyramidal microstructures, leading to resistance changes.

Figure 5.9 shows typical current-voltage (I-V) curves of a sensor responding to different applied pressures: its resistance drops obviously with the addition of external pressure in very low regime (0~1 kPa). The sensitivity of the sensor, S, is defined as S = dR/dP, where R is the resistance and P is applied pressure. The sensor shows little hysteresis in gradually increasing and decreasing cycles of applied pressure. Moreover, it has high sensitivity of 1.3-24.8 kPa^{-1} in the range of <1 kPa (Figure 5.9b).

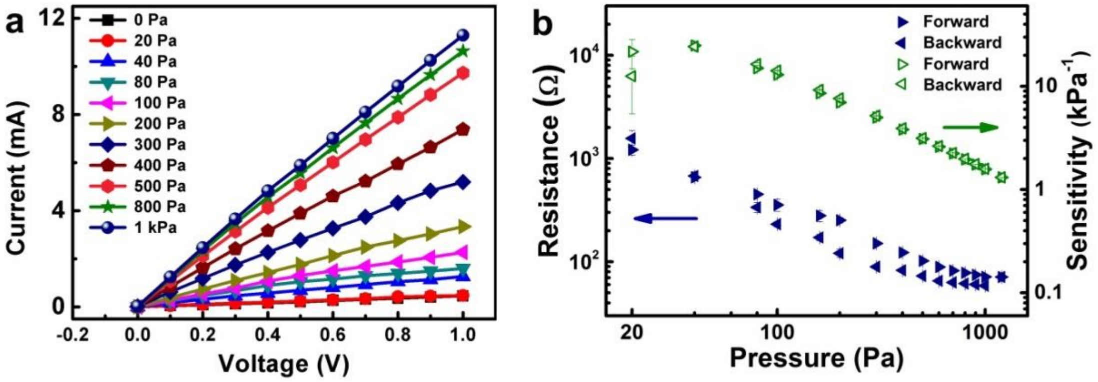

Figure 5.9. Pressure response and sensitivity of the microstructured AgNWs/PDMS based resistive pressure sensor. a) Typical current-voltage curves of a microstructured AgNWs/PDMS based sensor responding to different applied pressure. b) The resistance change towards applied pressure and sensitivity of the pressure sensor. The error bars stand for standard deviations from 5 test cycles.

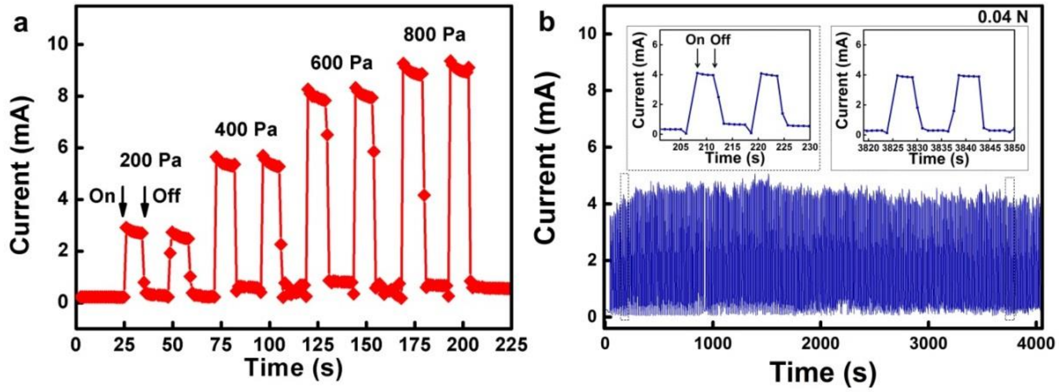

Figure 5.10. Real time current-time curves of the microstructured AgNWs/PDMS based sensor. a) Instant current change of the pressure sensor with different applied pressure value. b) Current-time curve of a microstructured AgNWs/PDMS based pressure sensor in response to loading and unloading of a force of 0.04 N for 400 cycles. Dashed areas show the details of current changes when pressure was applied and removed, demonstrating great stability of the sensor. The sensing area was 1 cm^2.

To demonstrate the reliability in detecting tiny pressure values, the sensor was applied with a series of pressures 1) 200 Pa, 2) 400 Pa, 3) 600 Pa, and 4) 800 Pa. The real-time current changes of the sensor are retained at the same level upon the applications of identical pressure values, and change when responding to pressure of different levels, exhibiting exquisite capability of sensing and discerning pressure in low regime (Figure 5.10a). The stability of the sensor was illustrated in Figure 5.10b, where the current changes of the sensor were recorded when a force of 0.04 N was alternately loaded and unloaded for 400 cycles (10 s for each cycle).

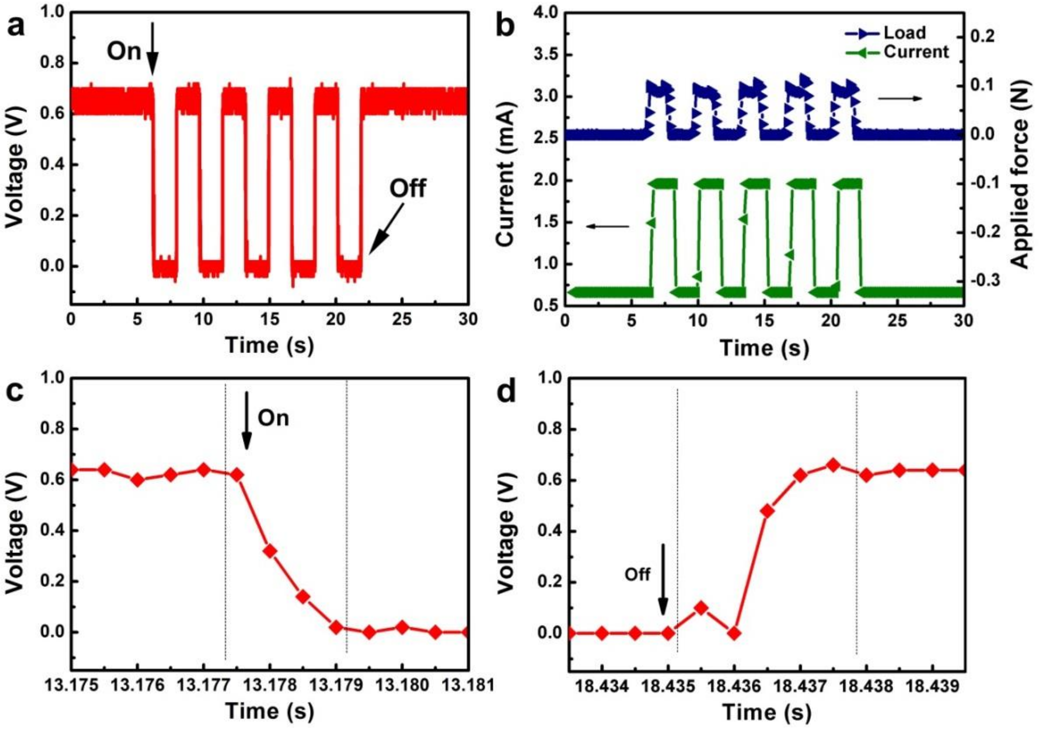

Figure 5.11. Characterization of response time of the sensor. a) Voltage changes of the pressure sensor towards the application of the same pressure value (1 kPa) for five times. The inset figure shows the. Current-time curve of the resistive pressure sensor responding to applied force. b) The applied force of the test stand and current change of the resistive sensor corresponding to (a). c-d) Voltage changes in accordance with an individual loading and an unloading process in (a). The response time in each operation is less than 4 ms.

Furthermore, the microstructured sensor shows ultrafast response time, which are shown in the voltage changes monitored by an oscilloscope. Figure 5.11a depicts the instant voltage changes of a sensor responding to 5 cycles of loading and unloading a force of 0.1 N (corresponding to 1 kPa), when connected in series with a 500 kΩ resistor and a voltage bias of 1 V is applied through both. In accordance to the voltage changes, the corresponding applied force, and current changes of the sensor are shown in Figure 5.11b, recorded simultaneously by the force gauge and analyzer, respectively. As shown in the inset of Figure 5.11c and d, the sensor illustrates ultrafast response time of less than 4 ms to both loading and unloading operations, comparable to the response time of the most sensitive parts (fingertips) of human body.

5.3.2 Resistive Switching Performance of SiO_2 Based Memory Device

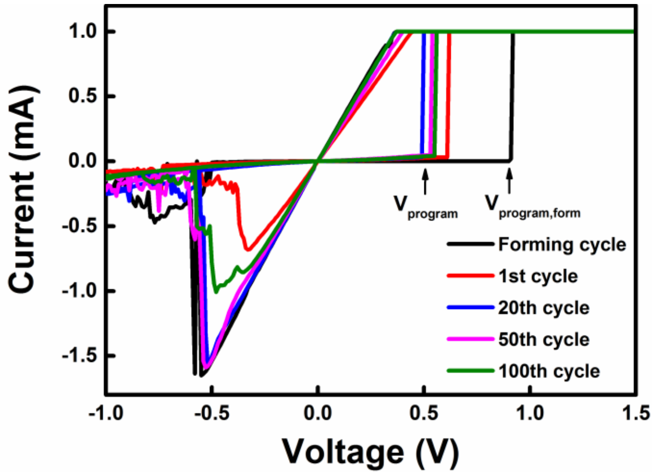

Figure 5.12. Current-voltage switching cycles of a memory cell with $Ag/SiO_2/Au$ structure. The initial programming voltage $V_{program,form}$ is significantly higher than the programming voltages of subsequent switching cycles.

As elucidated previously, the memory devices take MIM architecture with SiO_2 as switching layer, and the switching behaviors rely on the forming and dissolution of the Ag filaments. As shown in Figure 5.12, the initial voltage $V_{program,form}$ to start the programming process is obviously higher than the programming voltages for the following switching cycles, illustrating that a memory cell requires an electroforming step to incorporate ions in the insulating SiO_2 film.

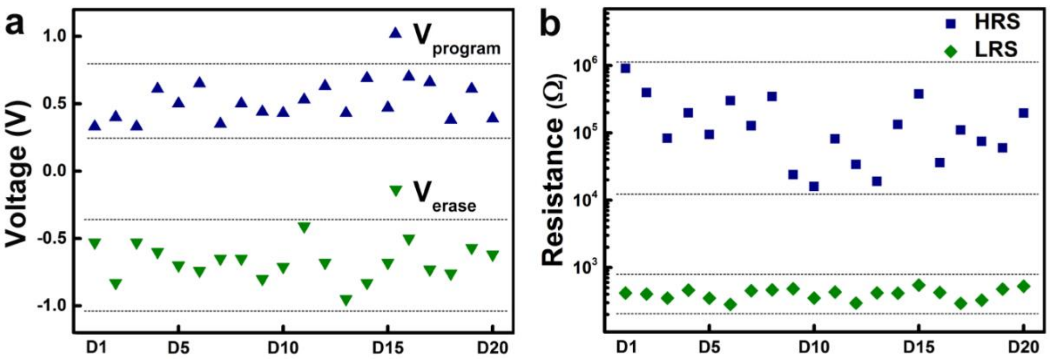

Figure 5.13. Device-to-device distributions of the SiO_2 based resistive switching memory devices. a) Device to device distributions of the programming voltage $V_{program}$ and erasing voltage V_{erase} from switching cycles of 20 devices. b) Device to device distributions of HRS resistance and LRS resistance from switching cycles of 20 devices, and LRS was obtained under a compliance current of 1 mA. Both HRS and LRS results were obtained under a 50 mV reading voltage.

Device-to-device distributions of the programming voltage, erasing voltages, HRS and LRS resistance values of the memory cells are illustrated in Figure 5.13. The programing and erasing voltages, $V_{program}$ and V_{erase}, of the memory devices locate in the range of 0.33 V ~ 0.70 V and -0.95 V ~ -0.5V. The resistance value at HRS and LRS locate in the range of 15893 Ω ~ 904066 Ω and 283 Ω ~ 547 Ω, respectively.

5.3.3 Sensory Memory Performance of Integrated Devices

The integration of the memory devices and pressure sensors was achieved by employing the Ag top electrode of a memory cell as the bottom electrode of a pressure sensor. As schematically illustrated in Figure 5.4, the whole device can be modeled as a circuit with each pixel constructed by connecting a resistive memory cell and a pressure sensor in series. After placing the microstructured AgNWs/PDMS film onto the top electrodes of memory devices, a switching cycle was conducted by applying a voltage to the microstructured AgNWs/PDMS film under a direct current sweeping mode, and the Au bottom electrode in a memory cell was grounded.

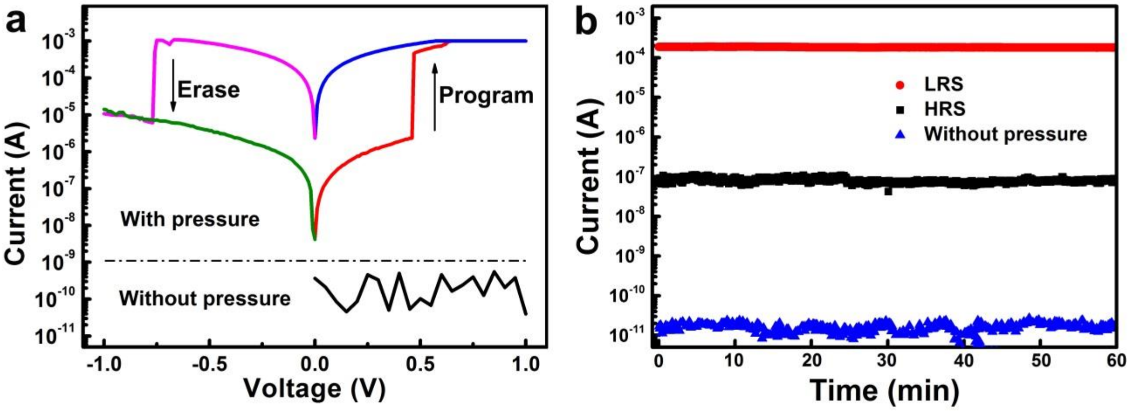

Figure 5.14. Typical current-voltage sweeping cycle and retention performance of the integrated device. a) Typical current-voltage curve of the integrated device without pressure and with pressure. Only when pressure is applied, the device can be programmed and erased. b) Retention performance of the integrated device for 60 minutes.

Figure 5.14a demonstrates typical I-V curves of the integrated device with and without external pressure. When no pressure was applied on the pressure sensor, the device has a very high resistance because both the sensor and the memory cell stay in the high resistance states, thus current through the device remains very low (<1 nA) with applied voltage bias increasing from 0 to 1 V. When a pressure of 500 Pa is applied, the memory device can be switched from high resistance state (HRS) to low resistance state (LRS) by a voltage sweep from 0 to a positive program voltage ($V_{program}$), with a compliance current of 1 mA. In the subsequent voltage sweep from 0 to 1 V, the device retains LRS. Still, the device could be switched back to HRS upon a voltage sweep from 0 to a negative erase voltage (V_{erase}) at the presence of applied pressure. In this way, the memory cell can conduct "write" and "erase" operations in the presence of pressures. As illustrated in Figure 5.14b, the retention performance was characterized at a read voltage of 50 mV, and resistances at both states have no changes for more than 60 minutes. The long retention time can be attributed to the excellent resistive switching memory performance of SiO_2.

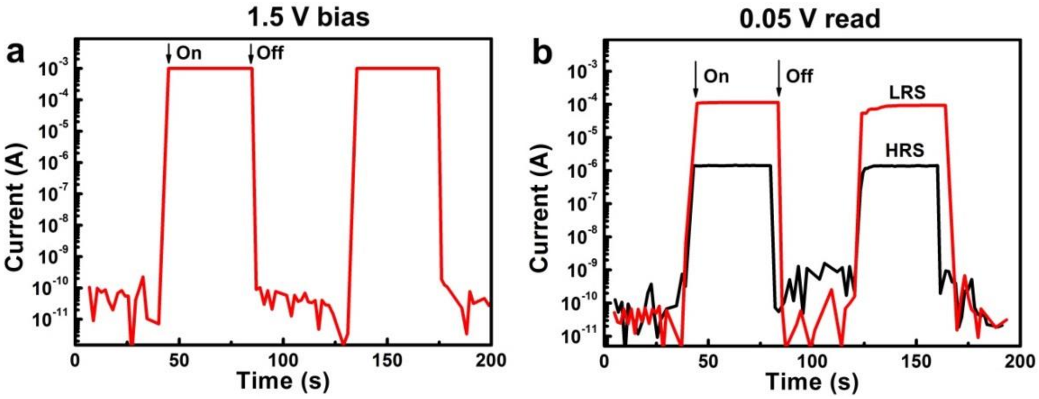

Figure 5.15. Instant current-time curves of the integrated device responding to an applied pressure of 500 Pa at different voltage bias. a) Instant current-time curve of the integrated device towards pressure on a bias of 1.5 V. The memory device was programmed to LRS when pressure was applied. b) Instant current-time curves of the devices at different resistance states responding to applied pressure with a reading voltage of 50 mV.

More noteworthy, under a positive voltage (1.5 V) higher than $V_{program}$, the device can be programmed from HRS to LRS by external pressure, demonstrating capability of dynamic pressure sensing and memory (Figure 5.15a). Also, both LRS and HRS of the memory cell can be recorded after the removal of applied pressure and be dynamically read under the application of pressure. As shown in Figure 5.15b, at a reading voltage of 50 mV, the current of an unprogrammed cell will raise to HRS when external pressure was applied, however a programmed cell will reach LRS rapidly in responds to the applied pressure.

The endurance performance of the device was characterized by programming and erasing the device for 50 cycles in existence of pressure. Read with a voltage of 50 mV, the LRS and HRS show little vibration (Figure 5.16a). Corresponding on/off ratios of different states of the devices are presented in Figure 5.16b. The memory cells demonstrates good resistive switching behaviors under pressure, thus providing a feasible way to record the application of the pressure in the form of resistance states.

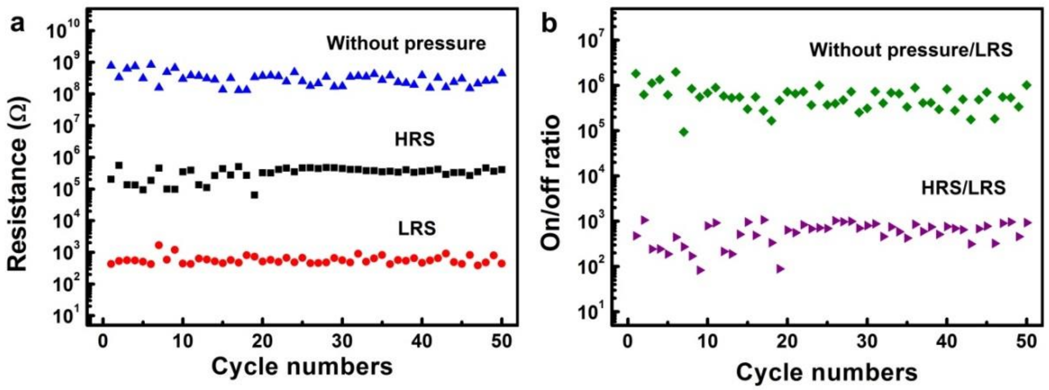

Figure 5.16. Endurance performance of the integrated device. a) Endurance of the device at different states for 50 switching cycles. b) On/off ratios between the HRS/LRS and the resistance without pressure/ LRS.

5.3.4 Sensory Memory Arrays for Recording Pressure Distribution

To illustrate the capability of mapping and memorizing external pressure distribution after the pressure and voltage were removed, devices composed of an array of 4 × 10 pixels were utilized to record the pressure applied through letter molds. Figure 5.17a schematically illustrates the operation process: letter molds made of SU-8 on PET film were put on the top of the device. Figure 5.17b shows a digital photo of a letter mold “T” on the top of device arrays. A weight of 5 g was applied on the top of PET film. The device arrays record the external pressure applied onto different letter molds of “N”, “T”, and “U”. As illustrated in Figure 5.17c, only devices beneath the letter molds can be programmed to LRS by a positive voltage sweep from 0 to $V_{program}$, providing discernable current mapping of the devices subjected to external pressure. In this way, applied pressure distribution was not only detected, but recorded in the memory arrays.

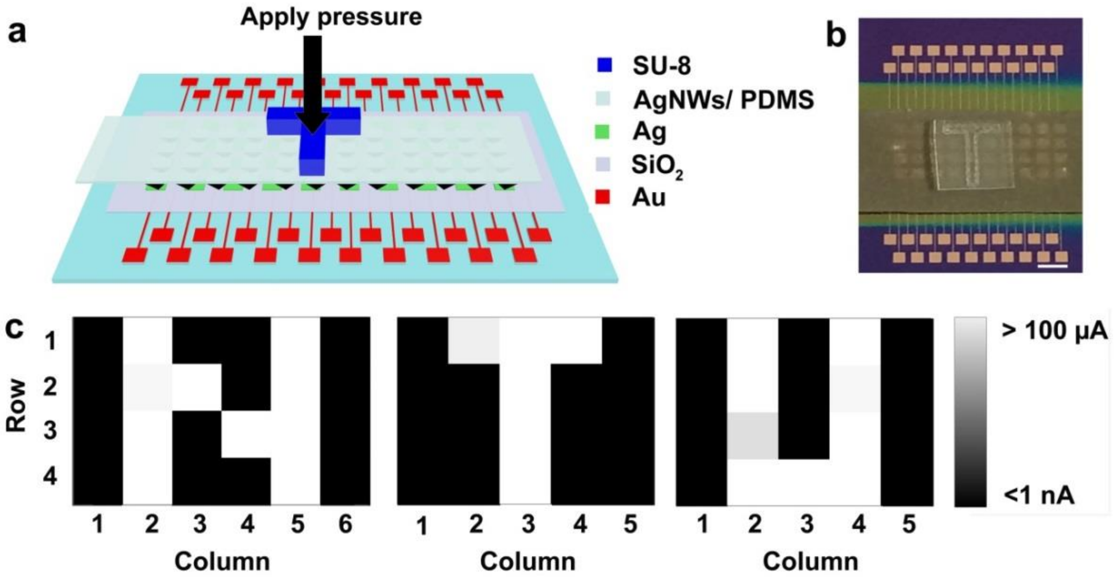

Figure 5.17. Demonstration of applying integrated devices for retaining applied pressure distribution after external stimuli removed. a) Schematic illustration of recording pressure distribution on word molds. b) A digital photo of the mold (letter "T") put on integrated device arrays. c) Mapping of the letters "N", "T" and "U". Only device cells beneath the letters can be programmed to LRS.

As illustrated in Figure 5.18, the arrays can retain the current mapping of "T", corresponding to applied pressure distribution, for a week with little decay. Moreover, pressure information stored in the device arrays can be easily erased to allow multi-cycle usage.

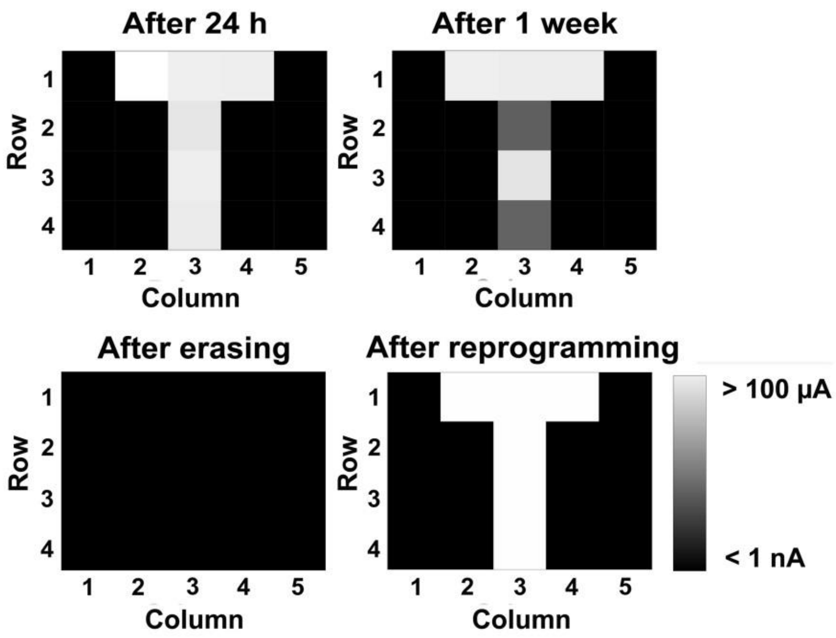

Figure 5.18. Demonstration of the sensing arrays for memorizing the applied pressure distribution for a long time and capability of reprogramming for multi-cycle usage.

5.3.5 Performance of Devices on Flexible Substrates

Flexible sensing and memory devices are required for practical applications in E-skin and human-machine interface. Though the pressure sensors composed by AgNWs/PDMS films is soft, the rigid silicon substrate limits the flexibility of the integrated devices. To solve this, we fabricated the Ag/SiO_2/Au memory arrays on flexible polyimide (PI) films (Kapton film 0.075 mm, DuPont) instead of a silicon wafer. The inset picture in Figure 5.19a shows a 4 × 10 memory arrays fabricated on PI film. Also, as shown in Figure 5.19a, the current of the device remains quite low (<1 nA) without pressure. And only when pressure (500 Pa) is applied on the device, the memory cells can be programmed to LRS by a positive voltage sweep. Still, the memory devices on PI films show good retention performance and no changes occur in either the HRS or LRS for 10^3 s.

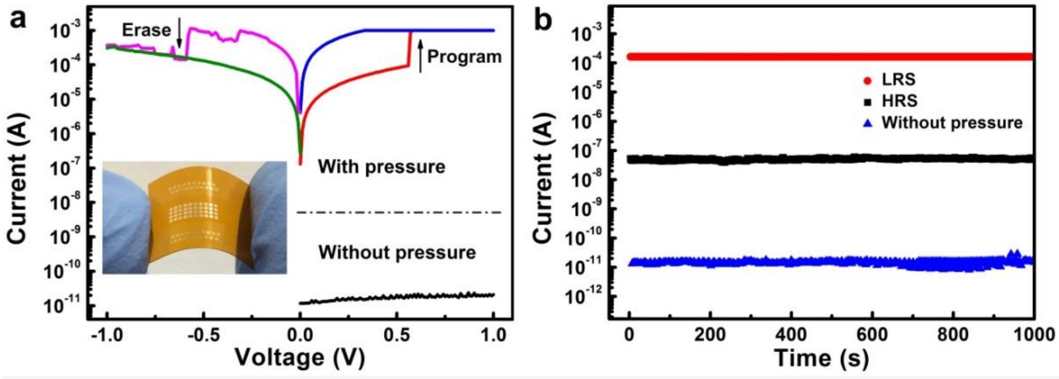

Figure 5.19. Electrically configuring the devices fabricated on flexible substrate at the presence of pressure. a) Typical current-voltage curves of the device fabricated on polyimide film with and without applied pressure. The memory cell could only be programmed to LRS at the presence of applied pressure. The inset shows a 4 × 10 memory device array on PI film. b) Retention performance of the device on PI film.

Finally, we used a LED connected in series with a memory cell to demonstrate the programming of a memory device by touching a pressure sensor. A cross-bar memory array with the same MIM structure was fabricated on PI film, and then a AgNWs/PDMS film was placed on the surface of the memory array. A voltage bias (V_1) of 2 V was supplied to the LED and a memory cell, and the LED didn’t light because the memory stayed in HRS (Figure 5.20a). Then another voltage bias (V_2) of 2 V was supplied to the integrated device sensor and memory device, with one end connected with AgNWs/PDMS film and the other connected with the bottom Au electrode of the memory cell. Pressure was then applied to program the memory cell from HRS to LRS by pressing a finger on the device (Figure 5.20b). After the removal of the finger, V_1 was powered again and the LED lighted up because the memory cell in the circuit was in the LRS (Figure 5.20c). Lighting of the LED after pressing with a finger illustrates that a memory cell was programmed from HRS (“0”) to LRS (“1”), showing that the integrated devices are capable of retaining the haptic sensation information after external pressure ceased.

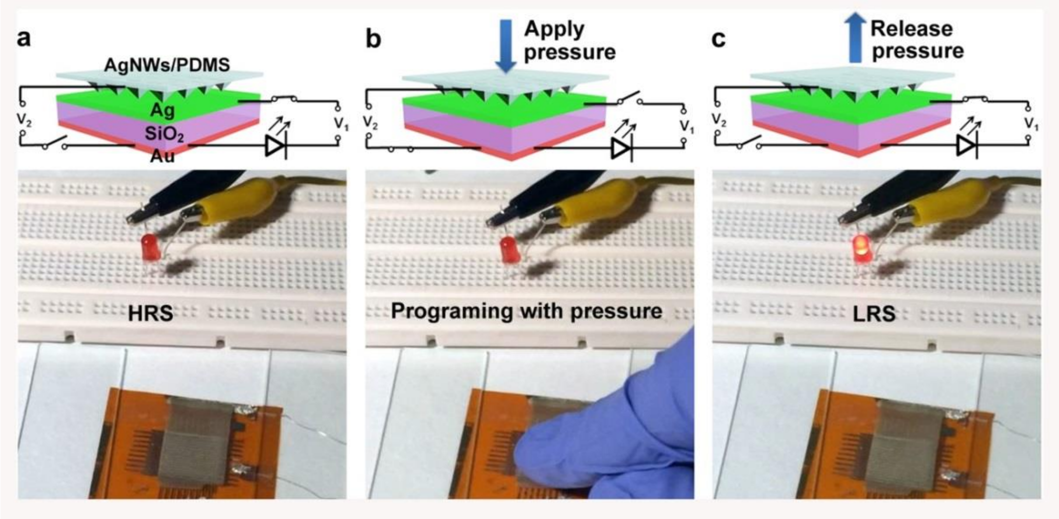

Figure 5.20. Demonstration of programming a memory cell from HRS to LRS with the touch of a finger. The lighting or not of the LED is accords with the LRS or HRS of the memory cell.

5.4 Conclusion

Sensory memory allows human to perceive the sensations after external stimuli has vanished. To mimic the haptic memory of human, electronic devices should comprise: 1) high performance tactile sensors for detection in the low pressure regime; and 2) integrated memory devices that can preserve the sensation information.

High sensitivity and fast response time are important criteria for designing tactile sensors in the applications of electronic skins and robotics. In this chapter, we addressed the high sensitivity through the introduction of pyramidal microstructures in resistive pressure sensors. The microstructured AgNWs/PDMS films, serving as pressure sensitive layer, contribute both a high sensitivity (1.3-24.8 kPa^{-1}) and a fast response time (<4 ms) due to anisotropic effect. Pressure sensors based on the AgNWs/PDMS film were capable of detecting and discerning different applied pressure values lower than 1 kPa, illustrating great possibility in the application of haptic sensing.

More significantly, we achieved the retention of external pressure distribution in resistive switching memory devices integrated with pressure sensing devices in order to realize the mimicry of the haptic memory of human. Applied pressure distribution can be detected and transduced to the different resistance states of the electrically reconfigurable memory devices. The integration was realized by a facile design of replacing the bottom electrode of a pressure sensor with the top electrode arrays in memory devices. The memory devices could be electrically programmed by the resistance changes in pressure sensor regarding external pressure and thus to “write” the pressure information in memory devices. Pressure distribution could be detected and recorded by memory devices arrays, and spatial resolution can be further improved by increasing the densities of sensor pixels to emulate the sensation of highly sensitive body sites like fingertips. The applied pressure distribution can be retained in the memory devices for more than 1 week with little decay by virtue of the nonvolatile performance of resistive switching memories. Also, the memory devices can be electrically reconfigured for sequent recording of external applied pressure. The integrated device demonstrated capability of memorizing the press of a finger, showing great potential for applications in sensing and retaining the haptic sensations. The rational integration of resistive switching memory devices with pressure sensors delivers a new way to realize the mimicry the haptic memory of humans, and also provides a guide for designing and integrating future sensing and memory devices to mimic other sensory memory functions of humans such as iconic and echoic memory, opening new avenues for the advancement of next-generation high performance sensing systems for applications in electronic skins, humanoid robots as well as human-machine interfaces.

6. Interactive Sensory Memory Device with Visible Readout

Interactive tactile sensing devices that can transduce external pressure to human-readable signals are of high significance for applications in next-generation prosthetics, robotics and human-machine interfaces.[62,71] In this chapter, the state-of-the-art pressure sensing electronics with electroluminescence outputs are firstly introduced. Then, to overcome the issues of high operation voltage and low sensitivity suffered by them, eletrochromic device based on WO_3 films is fabricated and integrated with microstructured AgNWs/PDMS based highly sensitive tactile sensors. The integrated device is able to transduce pressure stimuli into visible color change, and, more significantly, retain the tactile sensation information without the need of a voltage bias after stimuli ceased. The integration of electrochromic materials with resistive tactile sensors opens new opportunities for devising sensory memory devices with user-interactive readouts.

6.1 Introduction

With the advancements in micro-/nano-fabrication and integration processes, and the development of new materials, the last decade has witnessed a significant improvement of "skin-like" sensing devices for the mimicry of natural skin. As previously elucidated in chapter 2, the state-of-the-art tactile sensing electronics have demonstrated great potential in the application of electronic skin, robotics, and human-machine interfaces, facilitating conformable health monitoring, biological diagnostic and smart touch panels.[8,103] The performance of tactile sensors has already emulated or even surpassed the sensation of natural skin in many fields. In term of the property of materials, the introduction of elastomeric polymers endows electronic devices with stretchability of several times higher than that of human skin. In respect of sensitivity and spatial resolution, the engineering ways to apply micro-/nano-materials render tactile sensor highly sensitive and contribute to better spatial resolution compared with a human finger, the most sensitive part of human with a fine resolution of 40 μm.[30,89] In respect to functionality, many sensing units have been integrated with tactile sensing devices, such as temperature sensors, strain sensors, and new techniques like near-field communication (NFC),[69] to achieve multi-functionality in an individual sensing device so as to maximally mimic the function of natural skin. Also, intriguing properties—transparency,[33] self-powering,[48,57] self-healing,[61,104] and ultra-light weight[24]—have been introduced, providing new opportunities for the development of next-generation tactile sensing devices superior than the touch of sense in human.[49,105-107] However, pioneering endeavors on tactile sensors require equipment to analyze and provide electrical output. Still, the development of interactive sensing devices with visible output is at a rudimentary stage.

Interactive devices are of high significance for building next-generation smart and active sensing systems by converting external stimuli to visible and human-readable output, which reduces the complicity of fabrication and characterization processes. More significantly, it is possible to re-establish the tactile sensation to people who lost the sense of touch by transducing the tactile information to optical signals that can be perceived by the sensory modality of vision. For example, people suffers deficient tactile sensation cannot precisely describe contact states or mechanical stimuli through touching objects, thus they would have difficulties with daily activities even for simple work such as grasping a pen from sliding. Nevertheless, interactive sensing devices with visible readouts could help compensate the loss of tactile sensation by emitting light or color changes that can be accessed by sight.

To address interactive tactile sensing, integrating light-emitting diodes (LED) into tactile sensing devices is an effective way to transduce external mechanical stimuli into electroluminescent images.[62] Moreover, applied pressure value can be quantified by measuring the electroluminescence intensity. To date, the tactile sensors with visible output can be divided into two categories according to the pressure response mechanism: one responds to applied pressure with resistance change, and the other relies on piezo-phototronic effect.

6.1.1 Resistive Electroluminescent Imaging of Pressure

Tactile sensor with visible output was firstly introduced by R. Saraf, et al, based on the electroluminescence of semiconductor (CdS) nanoparticles.[30,71] The sensitive layer of the device takes layered structures of Au NPs/ CdS NPs/ Au NPs, and the interfaces between

Au NPs and CdS NPs are separated by thin dielectric layers. Applied pressure will induce the electroluminescent lighting produced by CdS NPs through electron tunneling effect.

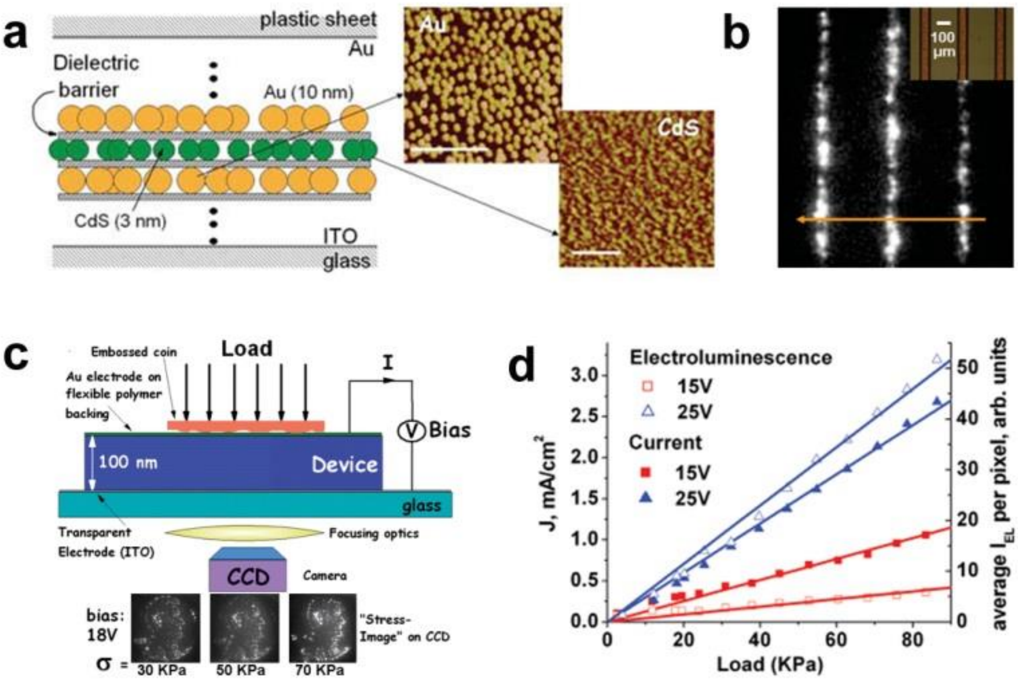

Figure 6.1. Electroluminescent imaging of pressure distribution by electron tunneling. a) Schematic illustration of the sensor structure and AFM images of Au NPs and CdS NPs. Scale bar: 50 nm. b) Pressure induced electroluminescent image with a grid pattern with a bias of 18 V at 40 kPa. Inset shows an optical image of the pattern. c) Schematic illustration of applying the sensor for imaging pressure distribution through a US 1 cent coin and corresponding images at different applied pressure. d) Both current density and electroluminescent intensity increase linearly with applied pressure. (Reprinted with permission from reference [71].)

A schematic of the device is shown in Figure 6.1. The dielectric layers is compressed upon the application of external pressure, leading the decreases of the ohmic resistance of the device and the spacing among the nanoparticles, which induce the CdS NPs to produce electroluminescent light with a wavelength of 580 nm. Both the current density of the device and the light density of electroluminescence increase linearly with the increase of pressure loadings, thus applied pressure value can be quantified by measuring the light density. The CdS NPs based sensor demonstrates a high spatial resolution of ~ 50 µm, which is comparable to the sensation of human fingertips (~ 40 µm). By virtue of electron tunneling effect among nanoparticles, the device can address imaging the pressure distribution without complicated fabrication of patterned sensing pixels.

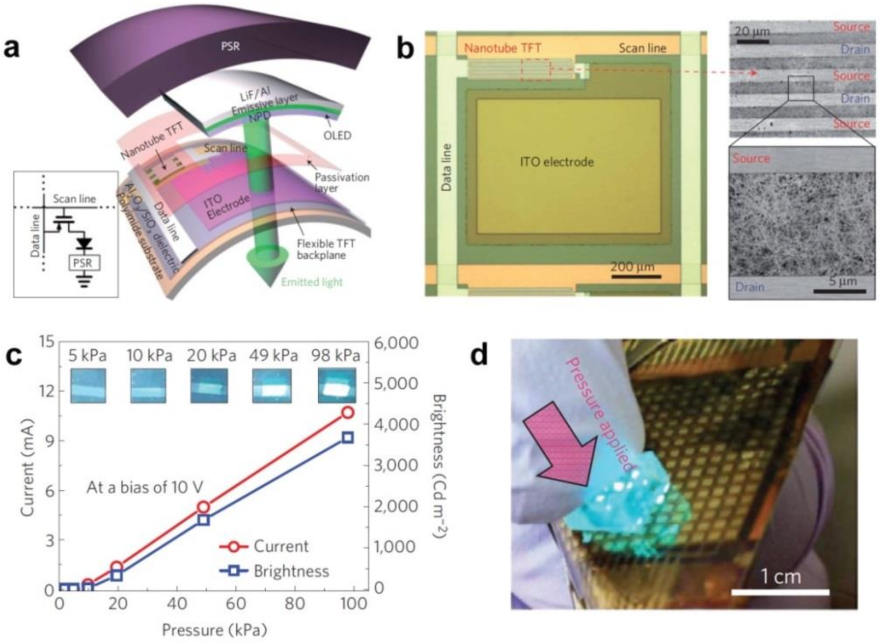

Figure 6.2. An interactive tactile sensor using conductive rubber as pressure-sensitive layer. a) Schematic of a sensor pixel that comprises a pressure sensor, an OLED and a TFT. b) Optical image of a carbon nanotubes based TFT connected with ITO electrode of OLED. c) The relationship between the current and brightness of an OLED and applied pressure. Inset shows the photos of an OLED. d) A digital photo of device array with 16 × 16 pixels. Pressure is applied through a PDMS mold, and only pixels beneath the mold can be ignited. (Reprinted with permission from reference [62].)

To achieve a broader pressure-response range, A. Javey's group integrated pressure-sensitive rubber (PSR) with OLEDs.[62] A PSR is connected with the cathodes of OLEDs and regulates the current flowing through both. With applied pressure, PSR deforms and its resistance decrease, leading to an increase of current density that can turn on the lighting of an OLED. To address the imaging of external pressure distribution, thin-film transistor (TFT) arrays based on semiconducting carbon nanotubes are also integrated with the OLEDs. Schematic illustration of the integrated device configuration and circuit is shown in Figure 6.2a. The three kinds of units, PSR, OLED and TFT, are integrated on flexible polyimide (PI) film substrate. In an individual pixel, the anode of OLED is connected with the drain of TFT (Figure 6.2b). The integrated device can provide visible light output when applied pressure is of >10 kPa. And the brightness increases linearly with applied pressure in the range of 10 ~ 100 kPa (Figure 6.2c). The device is capable of visualize pressure distribution by fabricating sensor arrays (Figure 6.3d).

6.1.2 Piezo-phototronic Electroluminescent Imaging of Pressure

Pressure sensors based on piezoelectric effect can also produce an electroluminescent output through piezo-phototronic effect (Figure 6.3).[63,108-110] Piezo-phototronic effect was introduced by Prof. Wang Zhonglin's group, which uses piezo-potential induced by mechanical stress of a piezoelectric material to configure the photon excitation processes in p-n junctions. Piezo-potential could increase the charge recombination rate so as to improve the efficiency of LEDs. The piezoelectric LEDs based on piezo-photonic effect apply n-type ZnO nanowires as piezoelectric materials to form p-n junctions with p-GaN films. Under compression, ZnO nanowires produce piezo-potential along the c-axis which enhances the charge recombination process in the ZnO/GaN interfaces, leading to higher density of electroluminescence light. The relative change of the light intensity, defined as enhancement factor (E), shows a linear relationship with strain and applied pressure, showing capability for measuring pressure value.

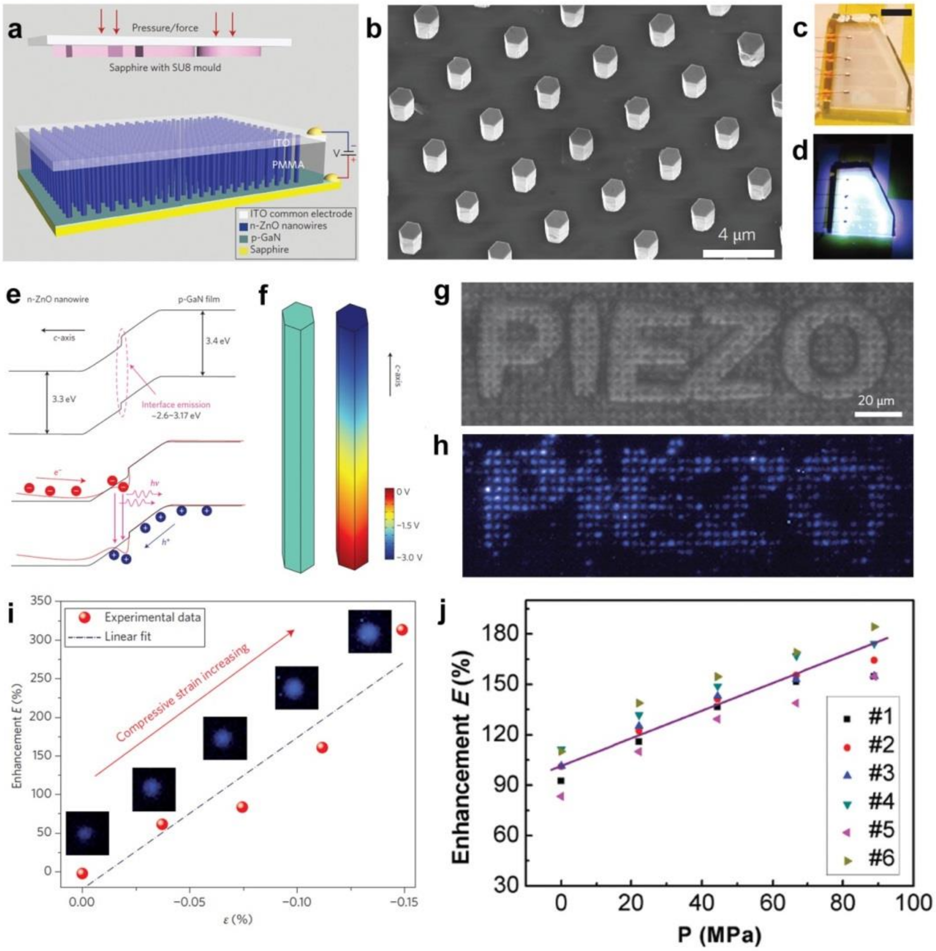

Figure 6.3. Pressure sensor with visible output based on piezoelectric LEDs. a) Schematic of the sensor structure. b) SEM image of the ZnO NW arrays. c, d) Photos of the LEDs at off and on states. e) Schematic band diagram showing the pressure imaging mechanism. Piezo-potential induced by the compression of ZnO NWs enhances the charge recombination process. f) Simulated piezo-potential distributions in ZnO NWs. g) An optical image of word mold "PIEZO" placed on the device. h) Electroluminescent light images of the device under mechanical stress. i, j) Linear relationship between enhancement of light intensity and mechanical stimuli. (Reprinted with permission from reference [63,109].)

6.1.3 Electrochromic Materials for Interactive Haptic Memory Devices

Even though the integrated devices of LEDs with pressure sensors (PSR or piezoelectric nanowires) show feasibility in transducing pressure distribution to visible light for applications in interactive sensing devices, the instinct properties of electroluminescence effect limit their further employment in highly sensitive tactile sensing devices. Firstly, such devices require a high voltage bias for light-emitting. Secondly, PSR or piezoelectric nanowires only responds to pressure in high ranges (>10 kPa). Thus, the pressure sensors with electroluminescence light outputs show very low sensitivity. Moreover, as illustrated in previous chapter, it is of high significance for tactile sensing devices to mimic the sensory memory of human by retaining the sensation information after external stimuli ceased. This challenge cannot be addressed by pressure sensor integrated with LEDs because the electroluminescence light will stop when mechanical stimuli is removed.

Electrochromic (EC) materials change their optical properties, such as transmittance, reflectance and absorbance, at different electric potentials, providing visible color changes.[111,112] Electrochromic devices (ECD) are widely studied for potential applications in smart windows and displays by virtue of low power consumption together with broad and adjustable color spectrum. An EC device often takes a four-layers structure of electrode/electrolyte/EC layer/electrode (Figure 6.4a).[111,113] WO_3 based electrochromic device has attracted extensive attention since first reported in 1969, because WO_3 films exhibit a high-contrast color change, good cycling stability, as well as fast switching time.[114-116] The color of WO_3 film can be reversibly switched between blue and colorless change by applying opposite voltage potentials, resulting from the redox reactions due to the electrochemical injection or extraction of positive ions (H^+, Li^+, Na^+, K^+) and electrons. The coloration and bleaching of WO_3 films can be operated at low potentials (Figure 6.4b).[116,117] More intriguingly, WO_3 film shows excellent color memory performance. The blue color induced by a negative potential can retain for a long period after applied potential ceased. Similar to a resistive switching memory device that can be electrically reconfigured between on and off states, the color states of WO_3 film can be readily modulated.

The low color switching potentials, together with the good color memory effect, inspire us to integrate WO_3 based electrochromic devices with tactile sensors to transduce external pressure into visible color change. Thanks to the low working potentials of WO_3, it is possible to achieve high sensitivity for detecting pressure in low range by integrating with microstructured resistive tactile sensor. On the other hand, applied pressure can be transduced and retained as the color state, providing an interactive way to mimic the sensory memory of human.

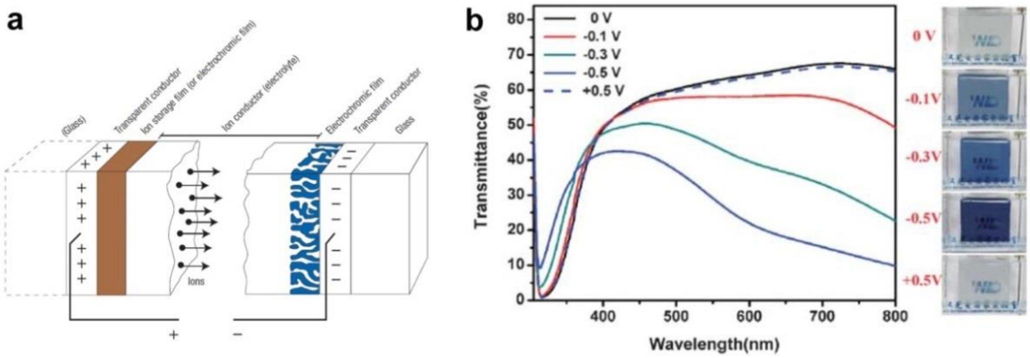

Figure 6.4. Typical configuration of an electrochromic device and the EC performance of WO_3 films. a) Schematic of an ECD. Electrochromic film deposited on transparent electrode changes color under opposite potential. b) Transmittance spectrum and photos of WO_3 film at different potentials. (Reprinted with permission from reference [111,116].)

6.2 Materials and Methods

6.2.1 Electrochemical Deposition of WO_3 films

In a typical experiment, tungsten powder (1.8 g, Alfa Aesar) is dissolved in 60 mL of hydrogen peroxide (30%, VWR) under stirring overnight to form a clear solution. A platinum wire is put into the solution to remove excess H_2O_2. It takes ~2 days to decompose all the H_2O_2 until no bubble exists. Then, the solution is diluted by mixed solution of H_2O and IPA (1:1, volume ratio) to 50 mM to be used for electrodeposition. Electrochmical deposition was conducted by a three-electrode system with Pt as counter electrode, Ag/AgCl as reference electrode, ITO/glass and ITO/PET films are used as working electrode. WO_3 films are deposited on ITO electrode at a voltage bias of -0.5 V for 500 s using a CHI 660D electrochemical station.

6.2.2 Materials Characterization

UV-Vis spectra of the films were measured by a UV-Vis spectrophotometer (Shimadzu UV-2550). Eletrochemical measurements were conducted by electrochemical station (CHI 660D).

6.3 Results and Discussion

6.3.1 Eletrochromic Performance of As-prepared WO_3 Films

Optical transmittance spectra of the electrodeposited WO_3 films at colored (-1 V) and bleached (0.5 V) states in 0.1 M $LiClO_4$/propylene carbonate (PC) solution are shown in Figure 6.5. The film demonstrates obvious changes in transmittance spectra and colors at colored state and bleached state. The film is colorless at positive potential and changes to blue when negative potential is applied.

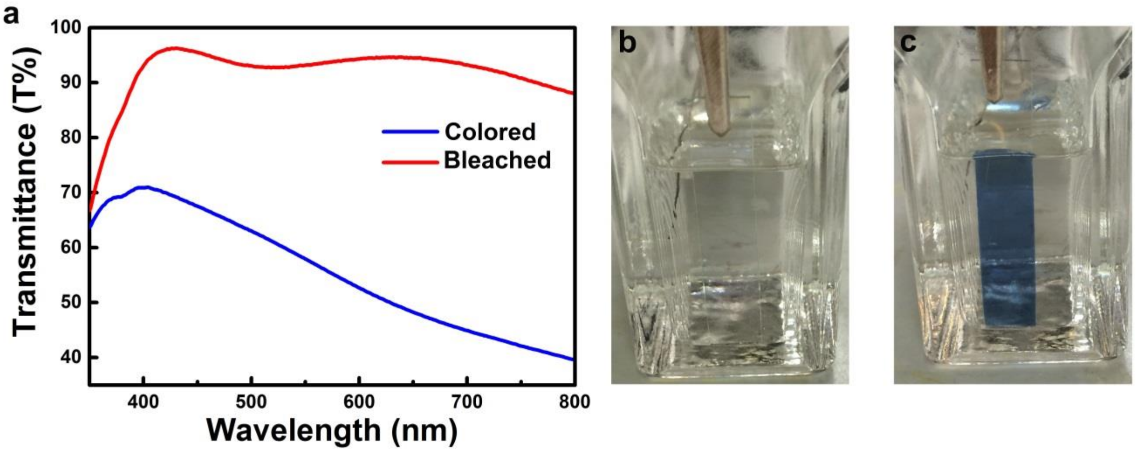

Figure 6.5. WO_3 film on ITO/glass substrate at colored and bleached states. a) UV-Vis transmittance spectrum of the WO_3 film at potentials of 0.5 V (bleached) and -1 V (colored). b-c) Digital photos of the WO_3 film at bleached state (b) and colored state (c).

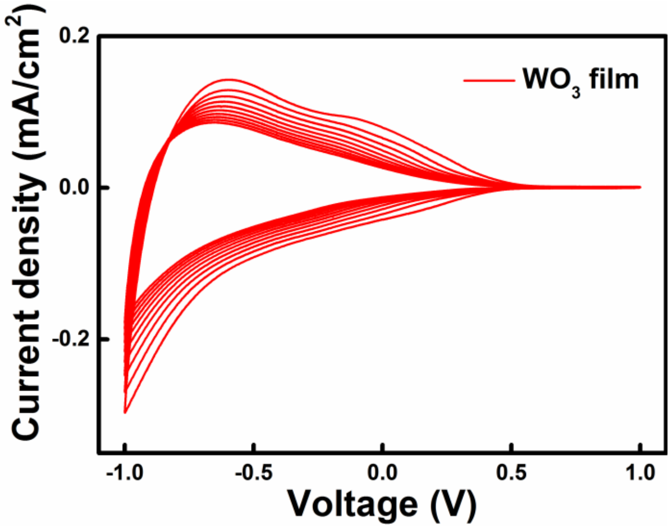

Figure 6.6. CV curves of the WO_3 film deposited on ITO/glass substrate in 1 M $LiClO_4$/PC with a scan rate of 50 mV s^{-1}.

Cyclic voltammetry (CV) curves of 10 cycles of the WO_3 film on the ITO/glass substrate is shown in Figure 6.6. After 10 cycles of CV test, the current density of WO_3 film becomes stable. To investigate the stability and reversibility of the WO_3 film, instant transmittance switching performance of the films is characterized at -1 V and 0.5 V for 100 cycles with a period of 20 s at 650 nm (Figure 6.7). A schematic of measurement setup is illustrated in Figure 6.7a.[118] Chronoamperometery (CA) curves and corresponding transmittance spectrum of the film are shown in Figure 6.7b and c. The film demonstrates fast coloration and bleaching speed, with 3.0 s and 1.5 s for 90% transmittance change, respectively.

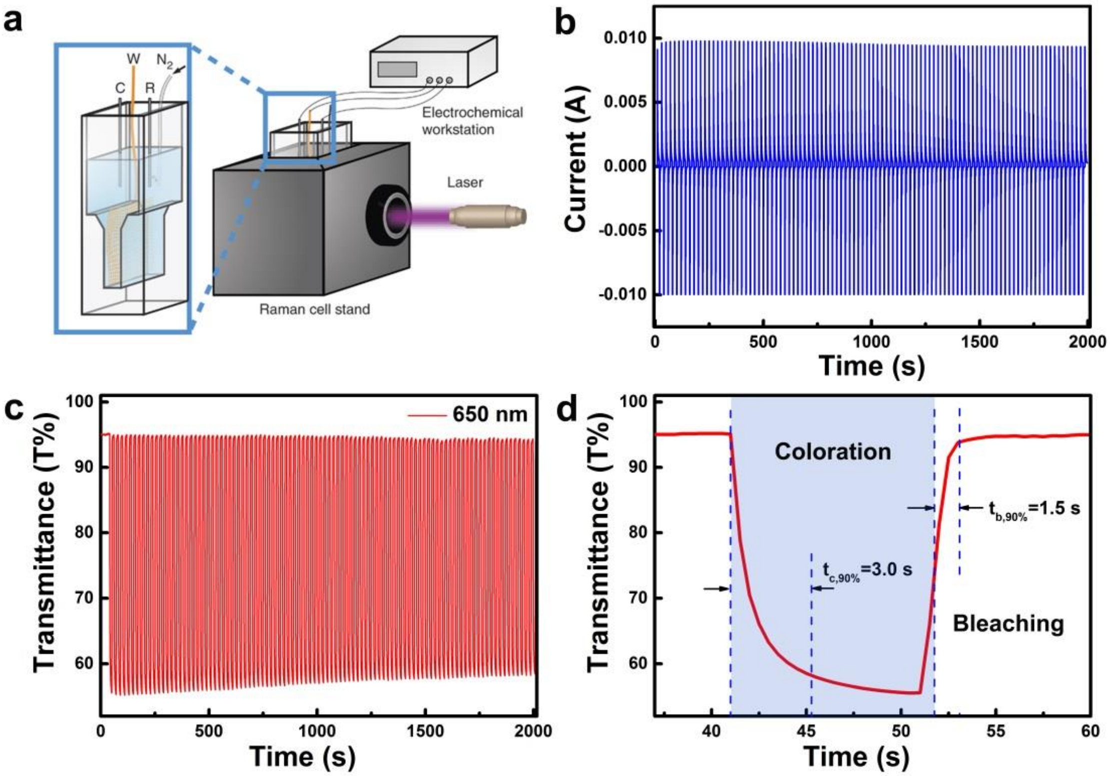

Figure 6.7. Instant transmittance spectrum of the WO_3 films at alternatively applied positive (0.5 V) and negative (-1 V) potentials. a) Schematic illustration of the setup. b) Chronoamperometry curves of the films under alternately applied potentials of 0.5 V and -1 V for 200 cycles. c) Transmittance switching of the film at 0.5 V and -1 V for 200 cycles at 650 nm wavelength. d) Response time of coloration and bleaching in one cycle. (Figure 6.7a is reprinted with permission from reference [118].)

6.3.2 Interactive Sensory Memory Device for Transducing and Retaining Tactile Sensation

The good electrochromic performance of the electrodeposited WO_3 film makes it a good candidate to integrate with tactile sensors for interactive sensory memory devices. A circuit diagram is shown in Figure 6.8a, where the working electrode of an electrochromic device is connected with one electrode of a tactile sensor. Here the microsturctured AgNWs/PDMS films, previously described in chapter 5, are used as the tactile sensing device to turn the voltage bias on the electrochromic device. Schematic of the integrated device structure is illustrated in Figure 6.8b. The microstructured AgNWs/PDMS based resistive tactile sensor can be attributed to a switch that tunes the voltages on the ITO electrode with WO_3 film.

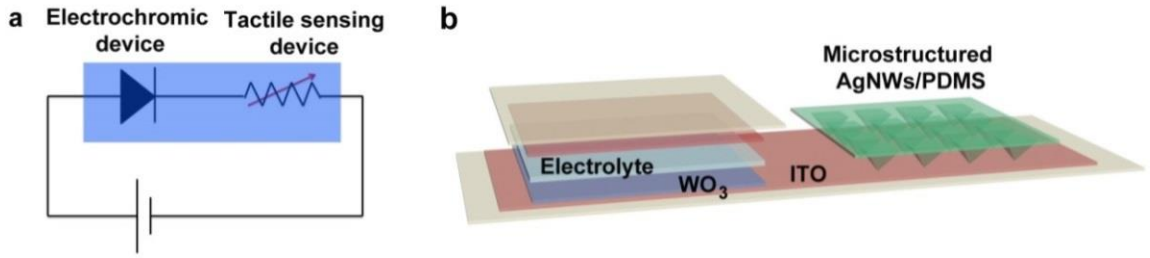

Figure 6.8. Schematic illustration of the configuration of the integrated device. a) Circuit diagram of the integrated device. The eletrochromic device is connected with a resistive tactile sensor in series.

The pressure sensing performance of the microstructured AgNWs/PDMS has been illustrated in previous chapter. Here, the microstructure has the same pattern parameters with a pyramid length of 30 µm. During a test procedure, a voltage bias is applied to the circuit. At initial state, the tactile sensor has high resistance and the ECM is at bleached state (colorless). At a voltage of -1 V, the applied pressure will reduce the resistance of the tactile sensor, which leads to an increased voltage on the electrochromic device, and thus switching the WO_3 film form bleached state to colored state (blue). In this way, the color change of the ECM is capable of describing the application of the external pressure. The bleached state and colored state can be attributed to "off" and "on" states, respectively. The ECM can also be switched from "on" to "off" by applied pressure at a positive voltage bias.

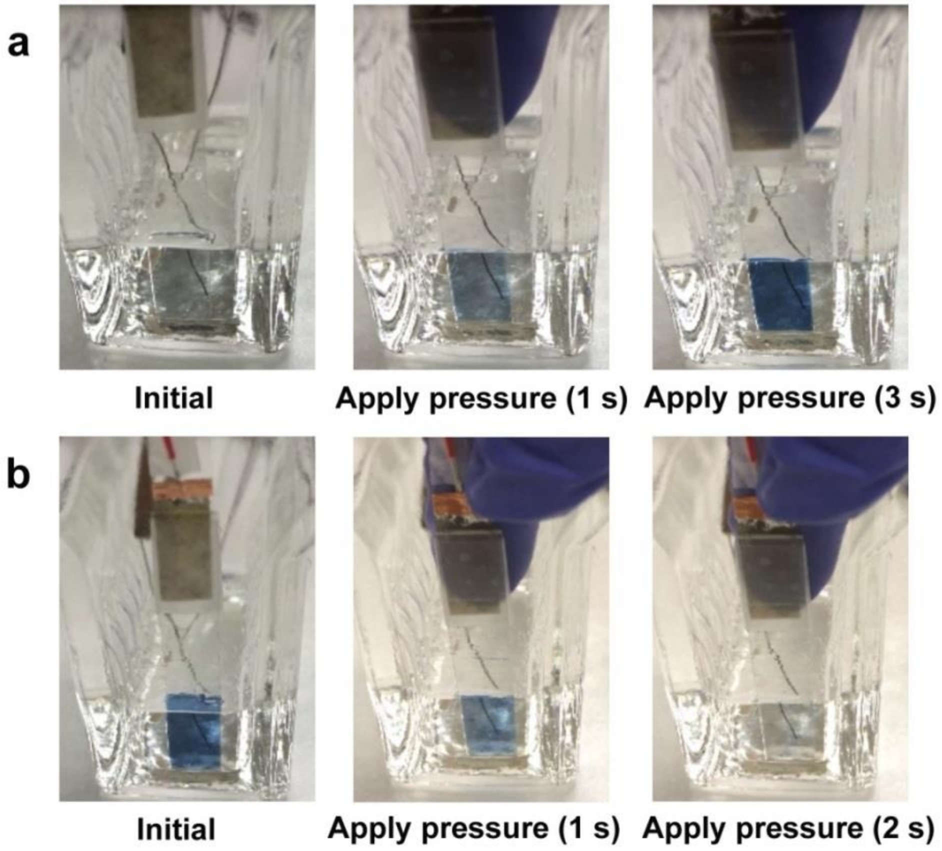

Figure 6.9. Demonstration of switching an electrochromic device by touching of a finger. a) Switching the WO_3 film from bleached state to colored state by touching a tactile sensor at a voltage bias of -1 V. b) Switching the WO_3 film from colored state to bleached state by pressure at a voltage bias of 1 V.

Figure 6.9 depicts the switching behaviors of WO_3 films induced by pressing a tactile sensor with a finger, showing obvious color changes. In figure 6.9a, the as-deposited WO_3 film is colorless at initial state when a voltage bias of -1 V is applied to the circuit, because the pressure sensor is at high resistance state and the current through the circuit is low. When the sensor is touched by a finger, its resistance decreases dramatically and the current increases, which induces the electrochromic reaction of the WO_3 film. Similarly, the bleaching reaction of the film also relies on the application of pressure.

The WO_3 film shows good color memory property that can retain the colored state in air without voltage bias for more than 2 hours (Figure 6.10). Because the colored “on” state of the WO_3 films was induced by pressing a finger, thus the retainment of the coloration state can be considered as the retention of the tactile sensation information.

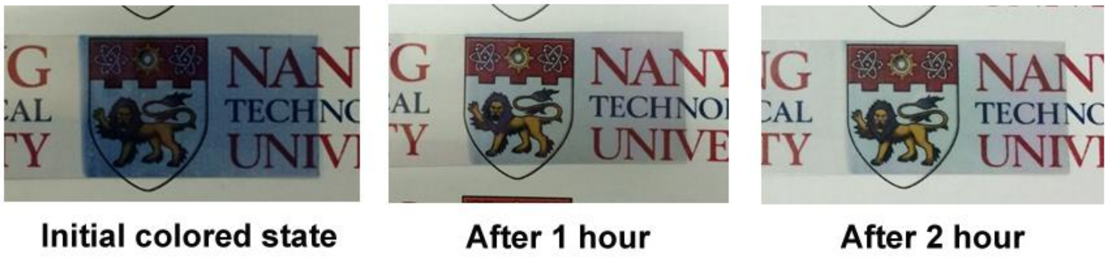

Figure 6.10. Demonstration of color memory effect of WO_3 film in air without voltage bias. The blue color is discernable for more than 2 hours.

6.4 Conclusion

In this chapter, eletrochromic device based on WO_3 films is fabricated by electrochemical deposition process. The as-deposited WO_3 film demonstrates good electrochromic performance such as low operation voltage, high reversibility, high color contrast as well as fast switching time. By integrating the WO_3 based electrochromic device with microstructured AgNWs/PDMS films, interactive tactile sensing device can be achieved to transduce applied pressure stimuli to visible color change. Moreover, by virtue of the color memory effect of WO_3 film, the tactile sensation information can be retained in the form of coloration states rather than resistance states of an electronic device, opening new opportunities for building sensory memory devices that keep the impressions of sensations in human-readable ways.

7. Conclusions and Future Recommendations

This chapter summarizes main conclusions of this thesis and proposes perspectives and recommendations for future works.

7.1 Conclusions

In this thesis, we discussed materials and engineering ways to design and integrate high performance tactile sensing devices for the mimicry of natural skin. Two important roles played by skin, exquisite tactile sensation and transmission to sensory memory, inspire the rise of sensory memory devices that not only possess tactile sensation, but also "memorize" the sensation information. To address these, tactile sensing devices are devised with high sensitivities in low pressure range to emulate the human sense of touch. Meanwhile, to mimic the perception of sensation information in skin, electrically configurable memory devices are introduced in tactile sensors to address the perception of sensations after stimuli stopped.

The utilization of three-dimensional microstructure arrays is an effective way to improve the pressure sensing performance of tactile sensor neglecting of sensing techniques. We developed highly sensitive resistive tactile sensors with microstructured graphene/PDMS films as pressure sensitive layers. The feasibility of LBL assembly method in producing continuous graphene film on 3D microstructuresd surface is demonstrated. High sensitivity, ultra-fast response, as well as great stability is achieved by the sensor by virtue of the graphene materials and anisotropic effect of microstructure arrays. Moreover, the sensitivity of sensors can be modified by adjusting the parameters of microstructure pattern, promising for being applied in diverse sensing environments. Also, the sensor illustrated remarkable capability of encoding tactile sensations for information transmission and measuring pulse wave, demonstrating great potential for applications in electronic skin devices and health monitoring.

Furthermore, in order to realize the mimicry of the haptic memory of human, we integrated resistive switching memory devices with microstructured tactile sensors to retain external pressure distribution. Applied pressure stimuli can be detected and transduced to the different resistance states of the electrically reconfigurable memory devices. Pressure distribution could be detected and recorded by memory devices arrays. The applied pressure distribution can be retained in the memory arrays for a long time by virtue of the nonvolatile performance of resistive switching memory devices. The integrated device demonstrated capability of memorizing the touch of a finger, showing great potential for applications in sensing and retaining the tactile sensations. The rational integration of resistive switching memory devices with pressure sensors provides a guide for designing and integrating future sensing and memory devices to mimic other sensory memory functions of humans such as iconic and echoic memory.

Lastly, WO_3 based electrochromic devices are integrated with resistive tactile sensors to response external tactile stimuli with human-readable signals. The low operation voltage for color switching of the electrochromic material renders it possible to provide an obvious color change with regard to a touch of finger. Thanks to the color memory effect of WO_3 films, the integrated device can retain the tactile sensation information without the need of a voltage bias after stimuli ceased. The integration of electrochromic materials with resistive tactile sensors opens new opportunities for devising sensory memory devices with user-interactive readouts.

In conclusion, high performance resistive tactile sensing devices were obtained by introducing anisotropic microstructure arrays into pressure sensitive layers. The tactile sensors demonstrated high sensitivity and fast response time, which are two primary criteria for the mimicry of human tactile sensation. The instinct character of the sensor that transduces pressure stimuli into resistance change renders it possible to integrate with resistive switching memory devices for the mimicry of human sensory memory. The possibility of devising interactive sensory memory devices with human-readable signals is also elucidated.

7.2 Recommendation for Future Work

7.2.1 Microstrucuture Arrays for Improving Performance of Devices

In addition to the microstructured graphene/PDMS films and AgNWs/PDMS films that are obtained from the silicon master with concaved pyramidal patterns, different kinds of functional material films can also be shaped with microstructure arrays by grown on the microstructured PDMS film or directly transferring from a silicon master. Several examples of as-prepared films with microstructures are presented in Figure 7.1. Flexible free-standing polymer films with microstructures such as silk fibroin and PEDOT:PSS films have been prepared by casting the polymer onto silicon master and peeling off after drying. Free-standing rGO films can also be obtained in the same way. Also, semiconductor nanowires can be grown on the microstructured films without scarifying the uniformity of pyramidal geometry.

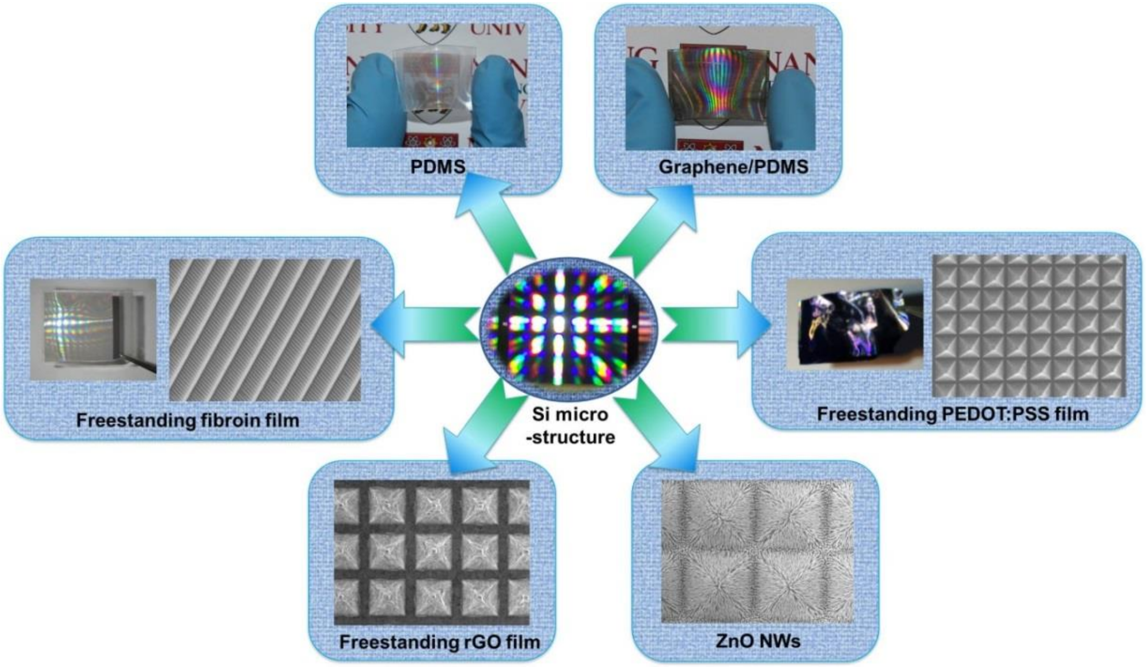

Figure 7.1. Several kinds of microstructured functional films obtained by replicating the patterns in silicon master.

The introduction of microstructures to various functional material films will benefit devices with enhanced performance for many applications. For example, microstructured ZnO NWs films may demonstrate superior photo-response compared with unstructured films because of increased surface area by the three-dimensional geometry. Microstructured PEDOT:PSS film could serve a sensitive layer of a multifunctional sensor responding multiple stimuli such as pressure, temperature and chemical gas. By virtue of light-trapping effect, the microstructured films could be used to build anti-reflective coatings for optoelectronics. Bio-resorbable silk fibroin films with microstructures may serve as a new platform for microfluids, on-site drug release as well as cell capture.

7.2.2 Sensory Memory Devices for Mimicking Human Perception

Human have five sensation modalities: touch, sight, hearing, taste and smell. Human perceive sensations when interact with the environment. Sensory memory of human helps remember the sensation information for subsequent processing and reactions. The state-of-the-art sensing devices have demonstrated great capability in responding to physical quantities, such as chemicals, gas, sound, light and pressure. However, a huge gap lies between sensing systems and biological systems. The five senses of human and sensory memory are not isolated. This inspires to integrate memory devices with multiple sensing units to build highly integrated systems for the mimicry of the sensory memory of human.

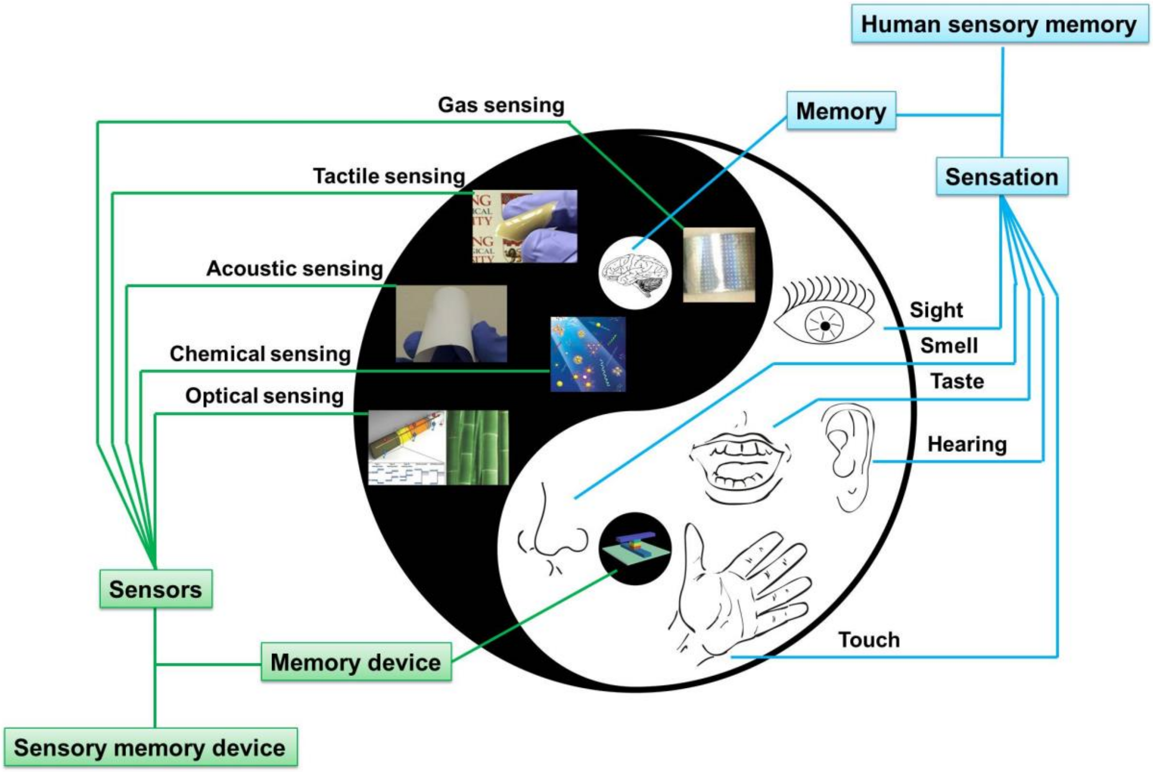

Figure 7.2. Schematic illustration of integrating different sensors with memory devices for the mimicry of human sensory memory. (Drawings of organs are taken from http://cliparts.co/)

List of Publications

Journal Articles

1. Skin-inspired Haptic Memory Arrays with Electrically Reconfigurable Architecture
   B. Zhu, H. Wang, Y. Liu, D. Qi, Z. Liu, H. Wang, J. Yu, X. Chen. *Advanced Materials* 2015, 27, doi:10.1002/adma.201504754.

2. Silk Fibroin for Flexible Electronic Devices
   B. Zhu, H. Wang, W. R. Leow, Y. Cai, X. J. Loh, M-Y. Han, X. Chen. *Advanced Materials* 2015, 27, doi:10.1002/adma.201504276.

3. Microstructured Graphene Arrays for Highly Sensitive Flexible Tactile Sensors
   B. Zhu, Z. Niu, H. Wang, W. Leow, H. Wang, Y. Li, L. Zheng, J. Wei, F. Huo, X. Chen, *Small*, 2014, *10*, 3625-3631. It was highlighted by inside cover of *Small*.
4. A Mechanically and Electrically Self-healing Supercapacitor
   H. Wang, **B. Zhu**, W. Jiang, Y. Yang, W. Leow, H. Wang, X. Chen, *Advanced Materials* 2014, *26*, 3638-3643. It was highlighted by Frontispiece of *Advanced Materials*, *Nanowerk Spotlight*, *AsianScientist*, and *ideaCONNECTION.*

5. Synergistic Capture Strategy for Enhanced Bacteria Detection and Elimination
   Y. Li, **B. Zhu**, Y. Li, W. Leow, R. Goh, B. Ma, E. Fong, M. Tang, X. Chen, *Angewandte Chemie International Edition*, 2014, *53*, 5947-5951. It was highlighted by inside cover of *Angewandte Chemie International Edition.*

6. Resistive Switching Memory Devices Based on Protein
   H. Wang, F. Meng, **B. Zhu**, W. Leow, Y. Liu, X. Chen, *Advanced Materials* 2015, *27*, doi: 10.1002/adma.201405728.

7. Highly Stretchable Integrated Supercapacitors Based on Single-Walled Carbon Nanotube Films with Continuous Reticulate Architecture

Z. Niu, H. Dong, **B. Zhu**, J. Li, H. Hng, W. Zhou, X. Chen, *Advanced Materials* 2013, *25*, 1058-1064.

8. Configurable Resistive Switching between Memory and Threshold Characteristics for Protein-based Devices

H. Wang, Y. Du, Y. Li, **B. Zhu**, W. Leow, Y. Li, J. Pan, T. Wu, X. Chen, *Advanced Functional Materials* 2015, *25*, 3825-3831.

9. Optoelectronics of Organic Nanofibers Formed by Co-assembly of Porphyrin and Perylenediimide

Y. Li, W. Wang, W. Leow, **B. Zhu**, F. Meng, L. Zheng, J. Zhu, X. Chen, *Small* 2014, *10*, 2776-2781.

10. Programmable Photoelectrochemical Hydrogen Evolution Based on Multi-segmented CdS-Au Nanorod Arrays

X. Wang, C. Liow, D. Qi, **B. Zhu**, W. Leow, H. Wang, C. Xue, X. Chen, S. Li, *Advanced Materials* 2014, *26*, 3506-3512.

11. All-Solid-State Flexible Ultrathin Micro-Supercapacitors Based on Graphene

Z. Niu, L. Zhang, L. Liu, **B. Zhu**, H. Dong, X. Chen, *Advanced Materials* 2013, *25*, 4035-4042.

Conference Presentation

1. Microstructured Graphene Arrays for Highly Sensitive Flexible Pressure Sensor

Bowen Zhu, Xiaodong Chen, Symposium U, EMRS 2014 Fall Meeting, Warsaw, Poland. (Keynote presentation)

References

1. Dahiya, R. S.; Metta, G.; Valle, M.; Sandini, G. Tactile sensing—from humans to humanoids. *Robotics, IEEE Transactions on* **26**, 1-20 (2010).

2. Squire, L. R. Chapter 24 - The somatosensory system In: *Fundamental neuroscience (4th ed).* Academic Press (2013).

3. Hendry, S. H.; Hsiao, S. S. Chapter 22 - Fundamentals of sensory systems. In: *Fundamental neuroscience (4th ed).* Academic Press (2013).

4. Dargahi, J.; Najarian, S. Human tactile perception as a standard for artificial tactile sensing—a review. *Int. J. Med. Robot.* **1**, 23-35 (2004).

5. Lucarotti, C.; Oddo, C. M.; Vitiello, N.; Carrozza, M. C. Synthetic and bio-artificial tactile sensing: A review. *Sensors* **13**, 1435-1466 (2013).

6. Yousef, H.; Boukallel, M.; Althoefer, K. Tactile sensing for dexterous in-hand manipulation in robotics—a review. *Sens. Actuators, A* **167**, 171-187 (2011).

7. Johansson, R. S.; Flanagan, J. R. Coding and use of tactile signals from the fingertips in object manipulation tasks. *Nat. Rev. Neurosci.* **10**, 345-359 (2009).

8. Hammock, M. L.; Chortos, A.; Tee, B. C. K.; Tok, J. B. H.; Bao, Z. A. 25th anniversary article: The evolution of electronic skin (e-skin): A brief history, design considerations, and recent progress. *Adv. Mater.* **25**, 5997-6037 (2013).

9. McEvoy, M. A.; Correll, N. Materials that couple sensing, actuation, computation, and communication. *Science* **347**, 1261689 (2015).

10. Zhao, N.; Wang, Z.; Cai, C.; Shen, H.; Liang, F.; Wang, D.; Wang, C.; Zhu, T.; Guo, J.; Wang, Y.; Liu, X.; Duan, C.; Wang, H.; Mao, Y.; Jia, X.; Dong, H.; Zhang, X.; Xu, J. Bioinspired materials: From low to high dimensional structure. *Adv. Mater.* **26**, 6994-7017 (2014).

11. Rogers, J. A. Electronics for the human body. *JAMA* **313**, 561-562 (2015).

12. Kim, D.-H.; Lu, N.; Ma, R.; Kim, Y.-S.; Kim, R.-H.; Wang, S.; Wu, J.; Won, S. M.; Tao, H.; Islam, A. Epidermal electronics. *Science* **333**, 838-843 (2011).

13. Xu, S.; Zhang, Y.; Jia, L.; Mathewson, K. E.; Jang, K.-I.; Kim, J.; Fu, H.; Huang, X.; Chava, P.; Wang, R.; Bhole, S.; Wang, L.; Na, Y. J.; Guan, Y.; Flavin, M.; Han, Z.; Huang, Y.; Rogers, J. A. Soft microfluidic assemblies of sensors, circuits, and radios for the skin. *Science* **344**, 70-74 (2014).

14. Rogers, J. A.; Someya, T.; Huang, Y. Materials and mechanics for stretchable electronics. *Science* **327**, 1603-1607 (2010).

15. Yeom, C.; Chen, K.; Kiriya, D.; Yu, Z.; Cho, G.; Javey, A. Large-area compliant tactile sensors using printed carbon nanotube active-matrix backplanes. *Adv. Mater.* **27**, 1561-1566 (2015).

16. Sun, Q.; Seung, W.; Kim, B. J.; Seo, S.; Kim, S.-W.; Cho, J. H. Active matrix electronic skin strain sensor based on piezopotential-powered graphene transistors. *Adv. Mater.* **27**, 3411-3417 (2015).

17. Bauer, S.; Bauer-Gogonea, S.; Graz, I.; Kaltenbrunner, M.; Keplinger, C.; Schwodiauer, R. 25th anniversary article: A soft future: From robots and sensor skin to energy harvesters. *Adv. Mater.* **26**, 149-161 (2014).

18. Pang, C.; Lee, G.-Y.; Kim, T.-i.; Kim, S. M.; Kim, H. N.; Ahn, S.-H.; Suh, K.-Y. A flexible and highly sensitive strain-gauge sensor using reversible interlocking of nanofibres. *Nature Mater.* **11**, 795-801 (2012).

19. Someya, T.; Sekitani, T.; Iba, S.; Kato, Y.; Kawaguchi, H.; Sakurai, T. A large-area, flexible pressure sensor matrix with organic field-effect transistors for artificial skin applications. *Proc. Natl. Acad. Sci.* **101**, 9966-9970 (2004).

20. Someya, T.; Kato, Y.; Sekitani, T.; Iba, S.; Noguchi, Y.; Murase, Y.; Kawaguchi, H.; Sakurai, T. Conformable, flexible, large-area networks of pressure and thermal sensors with organic transistor active matrixes. *Proc. Natl. Acad. Sci.* **102**, 12321-12325 (2005).

21. Sekitani, T.; Someya, T. Stretchable, large-area organic electronics. *Adv. Mater.* **22**, 2228-2246 (2010).

22. Sekitani, T.; Yokota, T.; Zschieschang, U.; Klauk, H.; Bauer, S.; Takeuchi, K.; Takamiya, M.; Sakurai, T.; Someya, T. Organic nonvolatile memory transistors for flexible sensor arrays. *Science* **326**, 1516-1519 (2009).

23. Takei, K.; Takahashi, T.; Ho, J. C.; Ko, H.; Gillies, A. G.; Leu, P. W.; Fearing, R. S.; Javey, A. Nanowire active-matrix circuitry for low-voltage macroscale artificial skin. *Nature Mater.* **9**, 821-826 (2010).

24. Kaltenbrunner, M.; Sekitani, T.; Reeder, J.; Yokota, T.; Kuribara, K.; Tokuhara, T.; Drack, M.; Schwodiauer, R.; Graz, I.; Bauer-Gogonea, S.; Bauer, S.; Someya, T. An ultra-lightweight design for imperceptible plastic electronics. *Nature* **499**, 458-463 (2013).

25. Gong, S.; Schwalb, W.; Wang, Y.; Chen, Y.; Tang, Y.; Si, J.; Shirinzadeh, B.; Cheng, W. A wearable and highly sensitive pressure sensor with ultrathin gold nanowires. *Nature Commun.* **5**, 3132 (2014).

26. Yao, H.-B.; Ge, J.; Wang, C.-F.; Wang, X.; Hu, W.; Zheng, Z.-J.; Ni, Y.; Yu, S.-H. A flexible and highly pressure-sensitive graphene-polyurethane sponge based on fractured microstructure design. *Adv. Mater.* **25**, 6692-6698 (2013).

27. Wang, X.; Gu, Y.; Xiong, Z.; Cui, Z.; Zhang, T. Silk-molded flexible, ultrasensitive, and highly stable electronic skin for monitoring human physiological signals. *Adv. Mater.* **26**, 1336-1342 (2014).

28. Pan, L.; Chortos, A.; Yu, G.; Wang, Y.; Isaacson, S.; Allen, R.; Shi, Y.; Dauskardt, R.; Bao, Z. An ultra-sensitive resistive pressure sensor based on hollow-sphere microstructure induced elasticity in conducting polymer film. *Nature Commun.* **5**, 3002 (2014).

29. Choong, C.-L.; Shim, M.-B.; Lee, B.-S.; Jeon, S.; Ko, D.-S.; Kang, T.-H.; Bae, J.; Lee, S. H.; Byun, K.-E.; Im, J.; Jeong, Y. J.; Park, C. E.; Park, J.-J.; Chung, U. I. Highly stretchable resistive pressure sensors using a conductive elastomeric composite on a micropyramid array. *Adv. Mater.* **26**, 3451-3458 (2014).

30. Maheshwari, V.; Saraf, R. Tactile devices to sense touch on a par with a human finger. *Angew. Chem. Int. Ed.* **47**, 7808-7826 (2008).

31. Sokolov, A. N.; Tee, B. C.; Bettinger, C. J.; Tok, J. B.-H.; Bao, Z. Chemical and engineering approaches to enable organic field-effect transistors for electronic skin applications. *Acc. Chem. Res.* **45**, 361-371 (2011).

32. Mannsfeld, S. C.; Tee, B. C.; Stoltenberg, R. M.; Chen, C. V. H.; Barman, S.; Muir, B. V.; Sokolov, A. N.; Reese, C.; Bao, Z. Highly sensitive flexible pressure sensors with microstructured rubber dielectric layers. *Nature Mater.* **9**, 859-864 (2010).

33. Lipomi, D. J.; Vosgueritchian, M.; Tee, B. C.; Hellstrom, S. L.; Lee, J. A.; Fox, C. H.; Bao, Z. Skin-like pressure and strain sensors based on transparent elastic films of carbon nanotubes. *Nature Nanotech.* **6**, 788-792 (2011).

34. Schwartz, G.; Tee, B. C. K.; Mei, J.; Appleton, A. L.; Kim, D. H.; Wang, H.; Bao, Z. Flexible polymer transistors with high pressure sensitivity for application in electronic skin and health monitoring. *Nature Commun.* **4**, 1859 (2013).

35. Zang, Y.; Zhang, F.; Huang, D.; Gao, X.; Di, C.-a.; Zhu, D. Flexible suspended gate organic thin-film transistors for ultra-sensitive pressure detection. *Nature Commun.* **6**, 6269 (2015).

36. Kulkarni, A.; Kim, H.; Choi, J.; Kim, T. A novel approach to use of elastomer for monitoring of pressure using plastic optical fiber. *Rev. Sci. Instrum.* **81**, 045108 (2010).

37. Rothmaier, M.; Luong, M. P.; Clemens, F. Textile pressure sensor made of flexible plastic optical fibers. *Sensors* **8**, 4318-4329 (2008).

38. Ramuz, M.; Tee, B. C. K.; Tok, J. B. H.; Bao, Z. Transparent, optical, pressure-sensitive artificial skin for large-area stretchable electronics. *Adv. Mater.* **24**, 3223-3227 (2012).

39. Dai, X.; Mihailov, S. J.; Blanchetière, C. Optical evanescent field waveguide bragg grating pressure sensor. *Opt. Eng.* **49**, 024401-024401-024405 (2010).

40. Chang, J.; Dommer, M.; Chang, C.; Lin, L. Piezoelectric nanofibers for energy scavenging applications. *Nano Energy* **1**, 356-371 (2012).

41. Eerenstein, W.; Mathur, N. D.; Scott, J. F. Multiferroic and magnetoelectric materials. *Nature* **442**, 759-765 (2006).

42. Haertling, G. H. Ferroelectric ceramics: History and technology. *J. Am. Ceram. Soc.* **82**, 797-818 (1999).

43. Dagdeviren, C.; Yang, B. D.; Su, Y.; Tran, P. L.; Joe, P.; Anderson, E.; Xia, J.; Doraiswamy, V.; Dehdashti, B.; Feng, X.; Lu, B.; Poston, R.; Khalpey, Z.; Ghaffari, R.; Huang, Y.; Slepian, M. J.; Rogers, J. A. Conformal piezoelectric energy harvesting and storage from motions of the heart, lung, and diaphragm. *Proc. Natl. Acad. Sci.* **111**, 1927-1932 (2014).

44. Dagdeviren, C.; Su, Y.; Joe, P.; Yona, R.; Liu, Y.; Kim, Y. S.; Huang, Y.; Damadoran, A. R.; Xia, J.; Martin, L. W.; Huang, Y.; Rogers, J. A. Conformable amplified lead zirconate titanate sensors with enhanced piezoelectric response for cutaneous pressure monitoring. *Nature Commun.* **5**, 4496 (2014).

45. Saito, Y.; Takao, H.; Tani, T.; Nonoyama, T.; Takatori, K.; Homma, T.; Nagaya, T.; Nakamura, M. Lead-free piezoceramics. *Nature* **432**, 84-87 (2004).

46. Park, K. I.; Lee, M.; Liu, Y.; Moon, S.; Hwang, G. T.; Zhu, G.; Kim, J. E.; Kim, S. O.; Kim do, K.; Wang, Z. L.; Lee, K. J. Flexible nanocomposite generator made of batio(3) nanoparticles and graphitic carbons. *Adv. Mater.* **24**, 2999-3004 (2012).

47. Wang, Z. L. Progress in piezotronics and piezo-phototronics. *Adv. Mater.* **24**, 4632-4646 (2012).

48. Xu, S.; Qin, Y.; Xu, C.; Wei, Y.; Yang, R.; Wang, Z. L. Self-powered nanowire devices. *Nature Nanotech.* **5**, 366-373 (2010).

49. Wu, W.; Wen, X.; Wang, Z. L. Taxel-addressable matrix of vertical-nanowire piezotronic transistors for active and adaptive tactile imaging. *Science* **340**, 952-957 (2013).

50. Wang, Z. L.; Wu, W. Nanotechnology-enabled energy harvesting for self-powered micro-/nanosystems. *Angew. Chem. Int. Ed.* **51**, 11700-11721 (2012).

51. Wang, Y. R.; Zheng, J. M.; Ren, G. Y.; Zhang, P. H.; Xu, C. A flexible piezoelectric force sensor based on pvdf fabrics. *Smart Mater. Struct.* **20**, 045009 (2011).

52. Greiner, A.; Wendorff, J. H. Electrospinning: A fascinating method for the preparation of ultrathin fibres. *Angew. Chem. Int. Edit.* **46**, 5670-5703 (2007).

53. Persano, L.; Dagdeviren, C.; Su, Y.; Zhang, Y.; Girardo, S.; Pisignano, D.; Huang, Y.; Rogers, J. A. High performance piezoelectric devices based on aligned arrays of nanofibers of poly(vinylidenefluoride-co-trifluoroethylene). *Nature Commun.* **4**, 1633 (2013).

54. Fan, F.-R.; Tian, Z.-Q.; Wang, Z. Flexible triboelectric generator. *Nano Energy* **1**, 328-334 (2012).

55. Wang, Z. L. Triboelectric nanogenerators as new energy technology for self-powered systems and as active mechanical and chemical sensors. *ACS Nano* **7**, 9533-9557 (2013).

56. Chen, J.; Zhu, G.; Yang, W.; Jing, Q.; Bai, P.; Yang, Y.; Hou, T.-C.; Wang, Z. L. Harmonic-resonator-based triboelectric nanogenerator as a sustainable power source and a self-powered active vibration sensor. *Adv. Mater.* **25**, 6094-6099 (2013).

57. Fan, F.-R.; Lin, L.; Zhu, G.; Wu, W.; Zhang, R.; Wang, Z. L. Transparent triboelectric nanogenerators and self-powered pressure sensors based on micropatterned plastic films. *Nano Lett.* **12**, 3109-3114 (2012).

58. Lin, L.; Xie, Y.; Wang, S.; Wu, W.; Niu, S.; Wen, X.; Wang, Z. L. Triboelectric active sensor array for self-powered static and dynamic pressure detection and tactile imaging. *ACS Nano* **7**, 8266-8274 (2013).

59. Zhu, B.; Niu, Z.; Wang, H.; Leow, W. R.; Wang, H.; Li, Y.; Zheng, L.; Wei, J.; Huo, F.; Chen, X. Microstructured graphene arrays for highly sensitive flexible tactile sensors. *Small* **10**, 3625-3631 (2014).

60. Takahashi, T.; Takei, K.; Gillies, A. G.; Fearing, R. S.; Javey, A. Carbon nanotube active-matrix backplanes for conformal electronics and sensors. *Nano Lett.* **11**, 5408-5413 (2011).

61. Tee, B. C. K.; Wang, C.; Allen, R.; Bao, Z. An electrically and mechanically self-healing composite with pressure- and flexion-sensitive properties for electronic skin applications. *Nature Nanotech.* **7**, 825-832 (2012).

62. Wang, C.; Hwang, D.; Yu, Z.; Takei, K.; Park, J.; Chen, T.; Ma, B.; Javey, A. User-interactive electronic skin for instantaneous pressure visualization. *Nature Mater.* **12**, 899-904 (2013).

63. Pan, C.; Dong, L.; Zhu, G.; Niu, S.; Yu, R.; Yang, Q.; Liu, Y.; Wang, Z. L. High-resolution electroluminescent imaging of pressure distribution using a piezoelectric nanowire led array. *Nature Photon.* **7**, 752-758 (2013).

64. Yu, C.; Li, Y.; Zhang, X.; Huang, X.; Malyarchuk, V.; Wang, S.; Shi, Y.; Gao, L.; Su, Y.; Zhang, Y.; Xu, H.; Hanlon, R. T.; Huang, Y.; Rogers, J. A. Adaptive optoelectronic camouflage systems with designs inspired by cephalopod skins. *Proc. Natl. Acad. Sci.* **111**, 12998-13003 (2014).

65. Park, J.; Lee, Y.; Hong, J.; Lee, Y.; Ha, M.; Jung, Y.; Lim, H.; Kim, S. Y.; Ko, H. Tactile-direction-sensitive and stretchable electronic skins based on human-skin-inspired interlocked microstructures. *ACS Nano* **8**, 12020-12029 (2014).

66. Sekitani, T.; Noguchi, Y.; Hata, K.; Fukushima, T.; Aida, T.; Someya, T. A rubberlike stretchable active matrix using elastic conductors. *Science* **321**, 1468-1472 (2008).

67. Yamada, T.; Hayamizu, Y.; Yamamoto, Y.; Yomogida, Y.; Izadi-Najafabadi, A.; Futaba, D. N.; Hata, K. A stretchable carbon nanotube strain sensor for human-motion detection. *Nature Nanotech.* **6**, 296-301 (2011).

68. Qi, D.; Liu, Z.; Yu, M.; Liu, Y.; Tang, Y.; Lv, J.; Li, Y.; Wei, J.; Liedberg, B.; Yu, Z.; Chen, X. Highly stretchable gold nanobelts with sinusoidal structures for recording electrocorticograms. *Adv. Mater.* **27**, 3145-3151 (2015).

69. Kim, J.; Banks, A.; Cheng, H.; Xie, Z.; Xu, S.; Jang, K.-I.; Lee, J. W.; Liu, Z.; Gutruf, P.; Huang, X.; Wei, P.; Liu, F.; Li, K.; Dalal, M.; Ghaffari, R.; Feng, X.; Huang, Y.; Gupta, S.; Paik, U.; Rogers, J. A. Epidermal electronics with advanced capabilities in near-field communication. *Small* **11**, 906-912 (2015).

70. Wang, Z. L. Self-powered nanosensors and nanosystems. *Adv. Mater.* **24**, 280-285 (2012).

71. Maheshwari, V.; Saraf, R. F. High-resolution thin-film device to sense texture by touch. *Science* **312**, 1501-1504 (2006).

72. Bean, K. E. Anisotropic etching of silicon. *IEEE Trans. Electr. Dev.* **25**, 1185-1193 (1978).

73. Huo, F.; Zheng, Z.; Zheng, G.; Giam, L. R.; Zhang, H.; Mirkin, C. A. Polymer pen lithography. *Science* **321**, 1658-1660 (2008).

74. Yin, S. Y.; Zhang, Y. Y.; Kong, J. H.; Zou, C. J.; Li, C. M.; Lu, X. H.; Ma, J.; Boey, F. Y. C.; Chen, X. D. Assembly of graphene sheets into hierarchical structures for high-performance energy storage. *ACS Nano* **5**, 3831-3838 (2011).

75. Yin, S. Y.; Goldovsky, Y.; Herzberg, M.; Liu, L.; Sun, H.; Zhang, Y. Y.; Meng, F. B.; Cao, X. B.; Sun, D. D.; Chen, H. Y.; Kushmaro, A.; Chen, X. D. Functional

free-standing graphene honeycomb films. *Adv. Funct. Mater.* **23**, 2972-2978 (2013).

76. Cao, X.; Qi, D.; Yin, S.; Bu, J.; Li, F.; Goh, C. F.; Zhang, S.; Chen, X. Ambient fabrication of large-area graphene films via a synchronous reduction and assembly strategy. *Adv. Mater.* **25**, 2957-2962 (2013).

77. Weiss, N. O.; Zhou, H. L.; Liao, L.; Liu, Y.; Jiang, S.; Huang, Y.; Duan, X. F. Graphene: An emerging electronic material. *Adv. Mater.* **24**, 5782-5825 (2012).

78. Geim, A. K.; Novoselov, K. S. The rise of graphene. *Nature Mater.* **6**, 183-191 (2007).

79. Bae, S.; Kim, H.; Lee, Y.; Xu, X.; Park, J.-S.; Zheng, Y.; Balakrishnan, J.; Lei, T.; Ri Kim, H.; Song, Y. I.; Kim, Y.-J.; Kim, K. S.; Ozyilmaz, B.; Ahn, J.-H.; Hong, B. H.; Iijima, S. Roll-to-roll production of 30-inch graphene films for transparent electrodes. *Nature Nanotech.* **5**, 574-578 (2010).

80. Kim, R.-H.; Bae, M.-H.; Kim, D. G.; Cheng, H.; Kim, B. H.; Kim, D.-H.; Li, M.; Wu, J.; Du, F.; Kim, H.-S. Stretchable, transparent graphene interconnects for arrays of microscale inorganic light emitting diodes on rubber substrates. *Nano Lett.* **11**, 3881-3886 (2011).

81. Niu, Z. Q.; Zhang, L.; Liu, L.; Zhu, B. W.; Dong, H. B.; Chen, X. D. All-solid-state flexible ultrathin micro-supercapacitors based on graphene. *Adv. Mater.* **25**, 4035-4042 (2013).

82. Sharma, B. K.; Ahn, J. H. Graphene based field effect transistors: Efforts made towards flexible electronics. *Solid-State Electron.* **89**, 177-188 (2013).

83. Huang, X.; Zeng, Z.; Fan, Z.; Liu, J.; Zhang, H. Graphene-based electrodes. *Adv. Mater.* **24**, 5979-6004 (2012).

84. Larisika, M.; Huang, J. F.; Tok, A.; Knoll, W.; Nowak, C. An improved synthesis route to graphene for molecular sensor applications. *Mater. Chem. Phys.* **136**, 304-308 (2012).

85. Yang, Y. H.; Bolling, L.; Priolo, M. A.; Grunlan, J. C. Super gas barrier and selectivity of graphene oxide-polymer multilayer thin films. *Adv. Mater.* **25**, 503-508 (2013).

86. Hu, K.; Gupta, M. K.; Kulkarni, D. D.; Tsukruk, V. V. Ultra-robust graphene oxide-silk fibroin nanocomposite membranes. *Adv. Mater.* **25**, 2301-2307 (2013).

87. Moon, I. K.; Lee, J.; Ruoff, R. S.; Lee, H. Reduced graphene oxide by chemical graphitization. *Nature Commun.* **1**, 73 (2010).

88. Pasternak, T.; Greenlee, M. W. Working memory in primate sensory systems. *Nat. Rev. Neurosci.* **6**, 97-107 (2005).

89. Scheibert, J.; Leurent, S.; Prevost, A.; Debrégeas, G. The role of fingerprints in the coding of tactile information probed with a biomimetic sensor. *Science* **323**, 1503-1506 (2009).

90. Bauer, S. Flexible electronics: Sophisticated skin. *Nature Mater.* **12**, 871-872 (2013).

91. Wong, H. S. P.; Salahuddin, S. Memory leads the way to better computing. *Nature Nanotech.* **10**, 191-194 (2015).

92. Waser, R.; Dittmann, R.; Staikov, G.; Szot, K. Redox-based resistive switching memories - nanoionic mechanisms, prospects, and challenges. *Adv. Mater.* **21**, 2632-2663 (2009).

93. Jo, S. H.; Chang, T.; Ebong, I.; Bhadviya, B. B.; Mazumder, P.; Lu, W. Nanoscale memristor device as synapse in neuromorphic systems. *Nano Lett.* **10**, 1297-1301 (2010).

94. Pickett, M. D.; Medeiros-Ribeiro, G.; Williams, R. S. A scalable neuristor built with mott memristors. *Nature Mater.* **12**, 114-117 (2013).

95. Lu, W. Memristors: Going active. *Nature Mater.* **12**, 93-94 (2013).

96. Wang, H.; Meng, F.; Zhu, B.; Leow, W. R.; Liu, Y.; Chen, X. Resistive switching memory devices based on proteins. *Adv. Mater.* **27**, DOI: 10.1002/adma.201405728 (2015).

97. Wang, H.; Du, Y.; Li, Y.; Zhu, B.; Leow, W. R.; Li, Y.; Pan, J.; Wu, T.; Chen, X. Configurable resistive switching between memory and threshold characteristics for protein-based devices. *Adv. Funct. Mater.* **25**, 3825-3831 (2015).

98. Wang, H.; Meng, F.; Cai, Y.; Zheng, L.; Li, Y.; Liu, Y.; Jiang, Y.; Wang, X.; Chen, X. Sericin for resistance switching device with multilevel nonvolatile memory. *Adv. Mater.* **25**, 5498-5503 (2013).

99. Waser, R.; Aono, M. Nanoionics-based resistive switching memories. *Nature Mater.* **6**, 833-840 (2007).

100. Yang, J. J.; Strukov, D. B.; Stewart, D. R. Memristive devices for computing. *Nature Nanotech.* **8**, 13-24 (2013).

101. Cavallini, M.; Hemmatian, Z.; Riminucci, A.; Prezioso, M.; Morandi, V.; Murgia, M. Regenerable resistive switching in silicon oxide based nanojunctions. *Adv. Mater.* **24**, 1197-1201 (2012).

102. Kim, S.; Son, J. H.; Lee, S. H.; You, B. K.; Park, K.-I.; Lee, H. K.; Byun, M.; Lee, K. J. Flexible crossbar-structured resistive memory arrays on plastic substrates via inorganic-based laser lift-off. *Adv. Mater.* **26**, 7480-7487 (2014).

103. Hwang, S. W.; Park, G.; Cheng, H.; Song, J. K.; Kang, S. K.; Yin, L.; Kim, J. H.; Omenetto, F. G.; Huang, Y.; Lee, K. M.; Rogers, J. A. 25th anniversary article: Materials for high-performance biodegradable semiconductor devices. *Adv. Mater.* **26**, 1992-2000 (2014).

104. Wang, H.; Zhu, B.; Jiang, W.; Yang, Y.; Leow, W. R.; Wang, H.; Chen, X. A mechanically and electrically self-healing supercapacitor. *Adv. Mater.* **26**, 3638-3643 (2014).

105. Keplinger, C.; Sun, J.-Y.; Foo, C. C.; Rothemund, P.; Whitesides, G. M.; Suo, Z. Stretchable, transparent, ionic conductors. *Science* **341**, 984-987 (2013).

106. Sun, J. Y.; Keplinger, C.; Whitesides, G. M.; Suo, Z. Ionic skin. *Adv. Mater.* **26**, 7608-7614 (2014).

107. Kim, J.; Lee, M.; Shim, H. J.; Ghaffari, R.; Cho, H. R.; Son, D.; Jung, Y. H.; Soh, M.; Choi, C.; Jung, S.; Chu, K.; Jeon, D.; Lee, S.-T.; Kim, J. H.; Choi, S. H.; Hyeon, T.; Kim, D.-H. Stretchable silicon nanoribbon electronics for skin prosthesis. *Nature Commun.* **5**, 5747 (2014).

108. Wang, X.; Zhang, H.; Yu, R.; Dong, L.; Peng, D.; Zhang, A.; Zhang, Y.; Liu, H.; Pan, C.; Wang, Z. L. Dynamic pressure mapping of personalized handwriting by a flexible sensor matrix based on the mechanoluminescence process. *Adv. Mater.* **27**, 2324-2331 (2015).

109. Bao, R.; Wang, C.; Dong, L.; Yu, R.; Zhao, K.; Wang, Z. L.; Pan, C. Flexible and controllable piezo-phototronic pressure mapping sensor matrix by zno nw/p-polymer led array. *Adv. Funct. Mater.* **25**, 2884-2891 (2015).

110. Peng, M.; Li, Z.; Liu, C.; Zheng, Q.; Shi, X.; Song, M.; Zhang, Y.; Du, S.; Zhai, J.; Wang, Z. L. High-resolution dynamic pressure sensor array based on piezo-phototronic effect tuned photoluminescence imaging. *ACS Nano* **9**, 3143-3150 (2015).

111. Granqvist, C.-G. Electrochromic materials: Out of a niche. *Nature Mater.* **5**, 89-90 (2006).

112. Granqvist, C. G. Electrochromism and smart window design. *Solid State Ionics* **53–56, Part 1**, 479-489 (1992).

113. Thakur, V. K.; Ding, G.; Ma, J.; Lee, P. S.; Lu, X. Hybrid materials and polymer electrolytes for electrochromic device applications. *Adv. Mater.* **24**, 4071-4096 (2012).

114. Baeck, S. H.; Choi, K. S.; Jaramillo, T. F.; Stucky, G. D.; McFarland, E. W. Enhancement of photocatalytic and electrochromic properties of electrochemically fabricated mesoporous wo3 thin films. *Adv. Mater.* **15**, 1269-1273 (2003).

115. Park, S. Y.; Lee, J. M.; Noh, C.; Son, S. U. Colloidal approach for tungsten oxide nanorod-based electrochromic systems with highly improved response times and color efficiencies. *J. Mater. Chem.* **19**, 7959-7964 (2009).

116. Xie, Z.; Gao, L.; Liang, B.; Wang, X.; Chen, G.; Liu, Z.; Chao, J.; Chen, D.; Shen, G. Fast fabrication of a $WO_3 \cdot 2H_2O$ thin film with improved electrochromic properties. *J. Mater. Chem.* **22**, 19904-19910 (2012).

117. Yan, C.; Kang, W.; Wang, J.; Cui, M.; Wang, X.; Foo, C. Y.; Chee, K. J.; Lee, P. S. Stretchable and wearable electrochromic devices. *ACS Nano* **8**, 316-322 (2014).

118. Ma, W.; Ying, Y.-L.; Qin, L.-X.; Gu, Z.; Zhou, H.; Li, D.-W.; Sutherland, T. C.; Chen, H.-Y.; Long, Y.-T. Investigating electron-transfer processes using a biomimetic hybrid bilayer membrane system. *Nature Protoc.* **8**, 439-450 (2013).